MULTIFUNCTIONAL CONJUGATED POLYMER NANOPARTICLES AS AN ANTICANCER DRUG CARRIER AND A FLUORESCENT PROBE FOR CELL IMAGING

A THESIS
SUBMITTED TO THE DEPARTMENT OF CHEMISTRY
AND THE GRADUATE SCHOOL OF ENGINEERING AND SCIENCE
OF BILKENT UNIVERSITY
IN PARTIAL FULFILLMENT OF THE REQUIREMENTS
FOR THE DEGREE OF
MASTER OF SCIENCE

By
ÖZLEM GEZİCİ
JULY, 2012

I certify that I have read this thesis and in my opinion it is fully adequate, in scope and in quality, as a thesis of the degree of Master of Science.

_____

Assoc. Prof. Dr. Dönüş TUNCEL (Advisor)

I certify that I have read this thesis and in my opinion it is fully adequate, in scope and in quality, as a thesis of the degree of Master of Science.

_____

Prof. Dr. Engin Umut AKKAYA

I certify that I have read this thesis and in my opinion it is fully adequate, in scope and in quality, as a thesis of the degree of Master of Science.

_____

Assoc. Prof. Dr. Rengül ÇETİN-ATALAY

Approved for the Graduate School of Engineering and Science:

_____

Prof. Dr. Levent ONURAL

Director of the Graduate School of Engineering and Science

ABSTRACT

MULTIFUNCTIONAL CONJUGATED POLYMER NANOPARTICLES AS AN ANTICANCER DRUG CARRIER AND A FLUORESCENT PROBE FOR CELL IMAGING

ÖZLEM GEZİCİ

M.S. in Chemistry

Supervisor: Assoc. Prof. Dr. Dönüş TUNCEL

July, 2012

The main motivation of this study is to develop multifunctional nanoparticles which can perform simultaneously the drug delivery and cell imaging tasks. To this end, firstly nanoparticles (Nps) with an average diameter of about 25 nm and based on a green emitting, hydrophobic conjugated polymer, poly[(9,9-bis{propenyl}fluorenyl-2,7-diyl))-co-(1,4-benzo-{2,1,3}-thiodiazole)] (PPFBT) and Nps with an average diameter of about 150 nm and based on a red emitting, hydrophobic conjugated polymer, poly[(9,9-bis{3-azido-propyl}fluorenyl-2,7-divinylene)-co-(1,4-benzo-{2,1,3}-thiodiazole)] (PAPFVBT) were prepared, characterized and their convenience as a fluorescent probe for cell imaging was evaluated via *in vitro* cell assays.

Then, drug loaded nanocapsules in which PPFBT or PAPFVBT acts both as a fluorescent reporter and the main matrix of the nanocapsules accommodating an anti-cancer drug, camptothecin (CPT), were synthesized through a facile, single step reprecipitation method. CPT is a hydrophobic, water-insoluble drug but the encapsulation improved its water-solubility. The CPT loading efficiency in the nanoparticles has been determined to be 100% when a drug to polymer ratio of 1:25 (w/w) was used. Cell viability of Human hepatocellular carcinoma cell line (Huh7) was investigated in the absence and presence of CPT using Sulforhodamine B (SRB) assay. SRB assay results supported further by the fluorescence microscope cell images clearly confirmed that blank and CPT-loaded PPFBT Nps have been taken up by the cells very efficiently and these nanoparticles were accumulated in the cytoplasm. Time and dose dependent SRB assay results indicate that the blank PPFBT Nps are not toxic to the Huh7 cells up to 25 μM. However, even a very low dose of CPT was found to be sufficient to induce the apoptosis of the cells when it was delivered through

nanoparticles. Thus, at the end of 48 h, the half maximal inhibitory concentration (IC_{50}) of free CPT and CPT-loaded PPFBT Nps were calculated to be 0.9 μM and 0.1 μM respectively, corresponding to that CPT-loaded PPFBT Nps are 9 times more effective than free CPT. However, at the end of 72 h, the IC_{50} of free CPT and CPT-loaded PPFBT Nps decreased to 0.1 μM and 0.008 μM, respectively. In this case, CPT-loaded PPFBT Nps are 12.5 times more effective than free CPT in inducing the apoptosis of Huh7 cells. Although the free drug (CPT) reaches IC_{50} of 0.1 μM after 72 h, it is possible to achieve this value with CPT-loaded Nps at the end of 48 h. On the other hand, dose dependent SRB assay results indicate that the blank PAPFVBT Nps are not toxic to the Huh7 cells up to 16 μM. At the end of 72 h, IC_{50} of free CPT and CPT-loaded PAPFVBT Nps were calculated to be 0.03 μM and 0.1 μM respectively, corresponding to that CPT-loaded PAPFVBT Nps are 3.3 times less effective than free CPT. Having bigger size (~150 nm) of PAPFVBT Nps is the main reason of not being effective as PPFBT Nps (~25 nm).

Keywords: Conjugated polymer nanoparticles; drug delivery; fluorescent imaging

ÖZET

ANTİKANSER İLAÇ TAŞIYICI VE HÜCRE GÖRÜNTÜLEME YAPABİLECEK FLÜORESAN KONJUGE POLİMER BAZLI ÇOK FONKSİYONLU NANOPARÇACIKLAR

ÖZLEM GEZİCİ
Kimya, Yüksek Lisans
Tez Yöneticisi: Doç. Dr. Dönüş TUNCEL
Temmuz, 2012

Bu çalışmanın temel motivasyonu aynı anda ilaç taşıma ve hücre görüntüleme görevlerini gerçekleştirebilen çok fonksiyonlu nanoparçacıklar geliştirmektir. Bu amaca yönelik öncelikle, yeşil ışıyan, hidrofobik konjuge polimerden, poli[(9,9-bis{propenil}florenil-2,7-dil))-ko-(1,4-benzo-{2,1,3}-tiyadiazol)] (PPFBT), 25 nm çapında ve kırmızı ışıyan, hidrofobik konjuge polimerden, poli[(9,9-bis{3-azido-propil}florenil-2,7-divinilen)-ko-(1,4-benzo-{2,1,3}-tiyadiazol)] (PAPFVBT), 150 nm çapında nanoparçacıklar hazırlanıp karakterizasyonları yapıldıktan sonra, bunların hücre görüntüleme amaçlı flüoresan probu olarak uygunlukları *in vitro* hücre deneyleriyle değerlendirilmiştir.

Daha sonra, PPFBT veya PAPFVBT polimerlerinin hem flüoresan raportörü olarak davranan hem de bir anti-kanser ilacı olan kamptotesini (CPT) barındıracak ana matrisi oluşturdukları ilaç yüklü nanokapsüller, basit ve tek aşamalı çöktürme yöntemiyle sentezlenmiştir. CPT, hidrofobik ve suda çözünmeyen bir ilaç olmasına rağmen kapsüllemeyle suda çözünürlüğü geliştirilmiştir. Nanoparçacıklara CPT yükleme verimi, ilacın polimere kütlece oranı 1:25 olduğu zaman %100 olarak belirlenmiştir. CPT varlığında ve yokluğunda insan hepatoselüler karsinom hücre hattının (Huh7) hücre canlılığı Sülforodamin B (SRB) testi kullanılarak incelenmiştir. Flüoresan mikroskop hücre görüntüleri ile desteklenen SRB testi sonuçları ile boş ve CPT yüklü PPFBT nanoparçacıklarının hücreler tarafından çok etkili şekilde alındığı ve bu nanoparçacıkların sitoplazmada biriktiği açıkça tespit edilmiştir. Zaman ve doza bağlı SRB testi sonuçları boş PPFBT nanoparçacıklarının 25 μM değerine kadar Huh7 hücreleri için toksik olmadığını göstermiştir. Bununla birlikte, çok düşük dozda

kamptotesinin bile bu nanoparçacıklar kanalıyla sevk edildiğinde hücrelerin apoptozunu teşvik etmek için yeterli olduğu bulunmuştur. Böylece, 48 saat sonunda, serbest CPT ve CPT-yüklü PPFBT nanoparçacıklarının yarı maksimal inhibitör konsantrasyonu (IC_{50}) sırasıyla 0.9 μM ve 0.1 μM olarak hesaplanmış ve CPT-yüklü PPFBT nanoparçacıklarının serbest kamptotesine göre 9 kat daha etkili olduğu belirlenmiştir. Ancak, 72 saat sonunda, serbest CPT ve CPT-yüklü PPFBT nanoparçacıklarının IC_{50} değerleri sırasıyla 0.1 μM ve 0.008 μM miktarlarına düşmüştür. Bu durumda, CPT-yüklü PPFBT nanoparçacıkları Huh7 hücrelerinin apoptozunu indükleyecek şekilde serbest kamptotesine göre 12.5 kat daha etkilidir. Serbest ilacın (CPT) 72 saat sonra 0.1 μM IC_{50} değerine ulaşmasına rağmen, 48 saat sonunda CPT-yüklü nanoparçacıklar ile bu değeri elde etmek mümkündür. Diğer taraftan, doza bağlı SRB testi sonuçları boş PAPFVBT nanoparçacıklarının 16 μM değerine kadar Huh7 hücreleri için toksik olmadığını göstermiştir. 72 saat sonunda, serbest CPT ve CPT-yüklü PAPFVBT nanoparçacıklarının IC_{50} değerleri sırasıyla 0.03 μM ve 0.1 μM olarak hesaplanmış ve CPT-yüklü PAPFVBT nanoparçacıklarının serbest kamptotesine göre 3.3 kat daha az etkili olduğu belirlenmiştir. PAPFVBT nanoparçacıklarının (~ 150 nm) büyük boyuta sahip olması PPFBT nanoparçacıkları (~ 25 nm) kadar etkili olmamasının başlıca nedenidir.

Anahtar Kelimeler: Konjuge polimer nanoparçacıklar; ilaç taşıma; flüoresan görüntüleme.

ACKNOWLEDGEMENT

I wish to express my gratitude to my supervisor Assoc. Prof. Dr. Dönüş Tuncel for her encouragement, trust, guidance, criticism, and motivating support throughout my research. I also would like to thank to the examining committee members, Prof. Dr. Engin Umut Akkaya and Assoc. Prof. Dr. Rengül Çetin Atalay, for their suggestions and comments.

I am grateful to Assoc. Prof. Dr. Rengül Çetin Atalay for the collaboration with us to complete cell culture studies and Ebru Bilget Güven for her careful efforts during these studies.

I would like to express my sincere thanks to my group mates Vusala İbrahimova, Özlem Ünal, Şeyma Ekiz, Meltem Aygüler, Müge Artar, Eda Koçak and my friends from Chemistry Department for their support and friendship.

I am forever grateful to my mother and father, Yüksel and Elyas Gezici for their unconditional love and support during my life. My dear sister, Gizem Gezici and my dear brother, İsa Erdem Gezici, I love you so much and thanks for your unending love that makes me stronger. And, I owe my deepest gratitude to my grandmother and grandfather who have significant contribution in raising me, for the support with their sincere prayers that ensures my success in all my life. I am very lucky to have my family.

And, I am deeply thankful to the most valuable person, Ali Vâlâ Koç, who is the source of my peace with his sincere and unfailing love. You have been my inspiration as I try to complete this work and after that we will be together to make our dreams come true. And, I would like to express my utmost gratitude to Leyla Neşe Koç, Ekrem Koç, Mehvar Ergün Türkkan and Ali Âli Türkkan whose sincerity and encouragement I will never forget. And, I am lucky to be close to the baby star, Ali Selim Türkkan, during this work that playing games with him takes all the stress.

I would like to thank to TÜBİTAK (The Scientific and Technological Research Council of Turkey) for financial support.

ABBREVIATIONS

^{1}H-NMR	Proton-Nuclear Magnetic Resonance
FT-IR	Fourier Transform-Infrared
UV-vis	Ultraviolet-visible
PL	Photoluminescence
GPC	Gel Permeation Chromatography
DLS	Dynamic Light Scattering
TEM	Transmission Electron Microscopy
SEM	Scanning Electron Microscopy
AFM	Atomic Force Microscopy
TOF LC/MS	Time-of-Flight Liquid Chromatography Mass Spectroscopy
$CDCl_3$	Deuterated Chloroform
DMSO-d6	Deuterated Dimethyl sulfoxide
DMF	Dimetylformamide
THF	Tetrahydrofuran
TBAB	Tetra-n-butylammoniumbromide
PPFBT	Poly[(9,9- bis{propenyl}fluorenyl-2,7-diyl))-co-(1,4-benzo-{2,1,3}-thiodiazole)]
PBPFVBT	Poly[(9,9-bis{3-bromo-propyl}fluorenyl-2,7-divinylene)-co-(1,4-benzo-{2,1,3}-thiodiazole)]
PAPFVBT	Poly[(9,9-bis{3-azido-propyl}fluorenyl-2,7-divinylene)-co-(1,4-benzo-{2,1,3}-thiodiazole)]
CPN	Conjugated Polymer Nanoparticle
CPT	Camptothecin
ANT	Anthracene
Huh7	Human hepatocellular carcinoma cell line
DMEM	Dulbecco's Modified Eagle's Medium
ddH_2O	Double-distilled water
SRB	Sulforhodamine B
IC_{50}	The half maximal Inhibitory Concentration

TABLE OF CONTENTS

ABSTRACT ..... **iii**

ÖZET ..... **v**

ACKNOWLEDGEMENT ..... **vii**

ABBREVIATIONS ..... **viii**

LIST OF FIGURES ..... **xii**

LIST OF SCHEMES ..... **xvii**

LIST OF TABLES ..... **xviii**

CHAPTER 1. INTRODUCTION **1**

1.1. Conjugated Polymers **1**

1.1.1. Synthesis Methods of Conjugated Polymers **6**

1.2. Conjugated Polymer Nanoparticles **11**

1.2.1. Preparation of Conjugated Polymer Nanoparticles **11**

1.2.2. Biomedical Applications: Cell Imaging, Drug Delivery, Theranostic **13**

1.3. Some Key Concepts **18**

1.3.1. An anticancer Drug: Camptothecin **18**

1.3.2. Sulforhodamine B (SRB) Cytotoxicity Test **20**

1.3.3. The Half Maximal Inhibitory Concentration (IC_{50}) **21**

1.4. Aim of Thesis **22**

CHAPTER 2. RESULTS AND DISCUSSION **23**

2.1. Synthesis and Characterization of Monomers **24**

2.1.1. Synthesis and Characterization of 2,7-dibromo-9,9-bis(3-bromo-propyl)-9H-fluorene (M1) **24**

2.1.2. Synthesis and Characterization of 9,9-bis-(3-bromo-propyl)-2,7-divinyl-9H-fluorene (M2) **25**

2.1.3. Synthesis and Characterization of 2,7-dibromo-9,9-bis-(propenyl)-9H-fluorene (M3) **30**

2.2. Synthesis and Characterization of Polymers **30**

2.2.1. Synthesis and Characterization of Poly[(9,9- bis{propenyl}fluorenyl-2,7-diyl))-co-(1,4-benzo-{2,1,3}-thiodiazole)] (PPFBT) **30**

2.2.2. Synthesis and Characterization of Poly[(9,9-bis{3-bromo-propyl}fluorenyl-2,7-divinylene)-co-(1,4-benzo-{2,1,3}-thiodiazole)] (PBPFVBT) and Poly[(9,9-bis{3-azido-propyl}fluorenyl-2,7-divinylene)-co-(1,4-benzo-{2,1,3}-thiodiazole)] (PAPFVBT)..... **33**

2.3. Synthesis and Characterization of Blank and Drug Loaded Water Dispersible Conjugated Polymer Nanoparticles (CPNs) **37**

2.3.1. Synthesis and Characterization of Poly[(9,9- bis{propenyl}fluorenyl-2,7-diyl))-co-(1,4-benzo-{2,1,3}-thiodiazole)] (PPFBT) Nanoparticles..... **38**

2.3.1.1. Cell Viability of PPFBT Nanoparticles..... **39**

2.3.2. Synthesis and Characterization Drug Loaded PPFBT Nanoparticles **40**

2.3.2.1. Determination of Loading Efficiency: Synthesis and Characterization of Anthracene(ANT)-Loaded PPFBT Nanoparticles **40**

2.3.2.2. Determination of Drug Loading Efficiency: Synthesis and Characterization of Camptothecin (CPT)-Loaded PPFBT Nanoparticles..... **44**

2.3.2.3. Synthesis and Characterization of Camptothecin (CPT)-Loaded PPFBT Nanoparticles as a Drug Carrier and a Fluorescent Probe for Cell Imaging..... **48**

2.3.3. Synthesis and Characterization of Poly[(9,9-bis{3-azido-propyl}fluorenyl-2,7-divinylene)-co-(1,4-benzo-{2,1,3}-thiodiazole)] (PAPFVBT) Nanoparticles **57**

2.3.3.1. Cell Viability of PAPFVBT Nanoparticles **58**

2.3.4. Synthesis and Characterization of Camptothecin (CPT) - Loaded PAPFVBT Nanoparticles as a Drug Carrier..... **59**

CHAPTER 3. CONCLUSION..... **63**

CHAPTER 4. EXPERIMENTAL **64**

4.1. Synthesis of 2,7-dibromo-9,9-bis(3-bromo-propyl)-9H-fluorene (M1)..... **65**

4.2. Synthesis of 9,9-bis-(3-bromo-propyl)-2,7-divinyl-9H-fluorene (M2)..... **66**

4.3. Synthesis of 2,7-dibromo-9,9-bis-(propenyl)-9H-fluorene (M3)..... **67**

4.4. Synthesis of Poly[(9,9- bis{propenyl}fluorenyl-2,7-diyl))-co-(1,4-benzo-{2,1,3}-thiodiazole)] (PPFBT)..... **67**

4.5. Synthesis of Poly[(9,9-bis{3-bromo-propyl}fluorenyl-2,7-divinylene)-co-(1,4-benzo-{2,1,3}-thiodiazole)] (PBPFVBT)..... **68**

4.6. Synthesis of Poly[(9,9-bis{3-azido-propyl}fluorenyl-2,7-divinylene)-co-(1,4-benzo-{2,1,3}-thiodiazole)] (PAPFVBT) **69**

4.7. Synthesis of PPFBT Nanoparticles **70**

4.8. Synthesis of Drug Loaded PPFBT Nanoparticles **70**

4.9. Sulforhodamine B (SRB) Colorimetric Assay for Cytotoxicity Screening for Blank and Drug Loaded PPFBT Nanoparticles **70**

4.10. Hoechst Staining for Blank and Drug Loaded PPFBT Nanoparticles **71**

4.11. Synthesis of PAPFVBT Nanoparticles **71**

4.12. Synthesis of Drug Loaded PAPFVBT Nanoparticles **71**

4.13. Sulforhodamine B (SRB) Colorimetric Assay for Cytotoxicity Screening for Blank and Drug Loaded PAPFVBT Nanoparticles **72**

REFERENCES **73**

LIST OF FIGURES

Figure 1.1. Simple band picture explaining the difference between an insulator, a semiconductor and a metal. 1

Figure 1.2. Delocalized π-bonds in conjugated polymers. 2

Figure 1.3. The conjugation length determines HOMO/LUMO levels. 2

Figure 1.4. Typical solar cell. a, Polymer bulk-heterojunction.. 3

Figure 1.5. Schematic representation of conjugated polyelectrolytes for imaging, diagnosis and therapy. 4

Figure 1.6. Chemical structures of PFBT and PFVBT and the photographs of the corresponding fluorescent polymer solutions in the absence (up) and presence (bottom) of DNA or BSA with the concentration of 1.2 μM under UV radiation at 365 nm. 5

Figure 1.7. Schematic representation of the photovoltaic cell structure showing the alternating donor (D) and acceptor (A) layers, forming the active material. 5

Figure 1.8. Cartoon representation of step-growth polymerization. 6

Figure 1.9. A general catalytic cycle for cross-coupling. 7

Figure 1.10. Palladium-meeting point for carbon atoms. 8

Figure 1.11. Richard Heck experimented with palladium as a catalyst and linked a short olefin to a ring of carbon atoms. 9

Figure 1.12. Palladium-catalyzed coupling reactions; Suzuki, Heck, Stille and Negishi. 10

Figure 1.13. The preparation of nanoparticles using reprecipitation method. 12

Figure 1.14. The preparation of nanoparticles using miniemulsion method. 12

Figure 1.15. Selected structural and architectural types of drug–polymer conjugates. 13

Figure 1.16. Schematic representation of the anatomical and physiological characteristics of normal and tumor tissue with respect to the vascular permeability and retention of small and large molecules (EPR effect). 15

Figure 1.17. Endocytotic pathway for the cellular uptake of macromolecules and nanocarriers for drug delivery. 16

Figure 1.18. Confocal microscope image of SH-SY5Y neuroblastoma cells treated with MEH-PPV SPNs for 18 h. The SPNs are seen to cluster in the perinuclear region within the cells, suggesting they are in vesicles.....17

Figure 1.19. Physical methods of capsule release.....18

Figure 1.20. (A) Camptothecin. (B) 20*S* chiral centre. (C) Dynamic equilibrium of camptothecin. (D) Camptothecin sodium salt. (E) Topotecan. (F) Irinotecan.. 19

Figure 1.21. Cytotoxicity assays. 20

Figure 1.22. The half maximal inhibitory concentration. 21

Figure 2.1. Schematic illustration of this thesis work.....23

Figure 2.2. ^{1}H-NMR (400 MHz, $CDCl_3$, 25 ^{o}C) spectrum of 2,7-dibromo-9,9-bis(3-bromo-propyl)-9H-fluorene (M1).....25

Figure 2.3. Cartoon representation of the spots on TLC plate under 254 and 366 nm UV light for four fractions (M2-A/B/C/D) of 9,9-bis-(3-bromo-propyl)-2,7-divinyl-9H-fluorene (M2).....27

Figure 2.4. ^{1}H-NMR (400 MHz, $CDCl_3$, 25 ^{o}C) spectra of four fractions (M2-A/B/C/D) of 9,9-bis-(3-bromo-propyl)-2,7-divinyl-9H-fluorene (M2) 28

Figure 2.5. TOF LC/MS results of four fractions (M2-A/B/C/D) of 9,9-bis-(3-bromo-propyl)-2,7-divinyl-9H-fluorene (M2).....29

Figure 2.6. ^{1}H-NMR (400 MHz, $CDCl_3$, 25 ^{o}C) spectrum of poly[(9,9-bis{propenyl}fluorenyl-2,7-diyl))-co-(1,4-benzo-{2,1,3}-thiodiazole)] (PPFBT). 31

Figure 2.7. FT-IR spectrum of poly[(9,9- bis{propenyl}fluorenyl-2,7-diyl))-co-(1,4-benzo-{2,1,3}-thiodiazole)] (PPFBT).....32

Figure 2.8. UV-vis absorption and fluorescence emission spectra of poly[(9,9-bis{propenyl}fluorenyl-2,7-diyl))-co-(1,4-benzo-{2,1,3}-thiodiazole)] (PPFBT) in THF.....32

Figure 2.9. ^{1}H-NMR (400 MHz, $CDCl_3${above} and DMSO-d6{below}, 25 ^{o}C) spectra of poly[(9,9-bis{3-bromo-propyl}fluorenyl-2,7-divinylene)-co-(1,4-benzo-{2,1,3}-thiodiazole)] (PBPFVBT).....34

Figure 2.10. Solvatochromic property of poly[(9,9-bis{3-bromo-propyl}fluorenyl-2,7-divinylene)-co-(1,4-benzo-{2,1,3}-thiodiazole)] (PBPFVBT).....35

Figure 2.11. FT-IR (KBr pellets) spectra of poly[(9,9-bis{3-bromo-propyl}fluorenyl-2,7-divinylene)-co-(1,4-benzo-{2,1,3}-thiodiazole)] (PBPFVBT) and poly[(9,9-bis{3-azido-propyl}fluorenyl-2,7-divinylene)-co-(1,4-benzo-{2,1,3}-thiodiazole)] (PAPFVBT). 36

Figure 2.12. UV-vis absorption and fluorescence emission spectra of poly[(9,9-bis{3-bromo-propyl}fluorenyl-2,7-divinylene)-co-(1,4-benzo-{2,1,3}-thiodiazole)] (PBPFVBT) and poly[(9,9-bis{3-azido-propyl}fluorenyl-2,7-divinylene)-co-(1,4-benzo-{2,1,3}-thiodiazole)] (PAPFVBT)..... 37

Figure 2.13. (a) Size distrubiton histogram from DLS measurement and (b) zeta potential measurement of PPFBT Nanoparticles. 38

Figure 2.14. UV–vis absorption and fluorescence emission spectra of PPFBT in THF ($\lambda_{exc.}$= 447 nm), as film ($\lambda_{exc.}$= 472 nm) and as dispersions of the nanoparticles in water ($\lambda_{exc.}$= 447 nm). 39

Figure 2.15. Percent cell viability results of PPFBT nanoparticles having concentrations of 25, 12.5, 6.25, 3.125, 1.5625 μM after 72 h incubation. 40

Figure 2.16. Size distribution histograms from DLS measurements of (ANT)-loaded PPFBT nanoparticles having the ratios PPFBT to ANT (w:w) 25:1 (a) and 5:1 (c) ; Zeta potential measurements of (ANT)-loaded PPFBT nanoparticles having the ratios PPFBT to ANT (w:w) 25:1 (b) and 5:1 (d). 41

Figure 2.17. The cartoon representation of the synthesis of anthracene (ANT)-loaded PPFBT nanoparticles and the determination of the optimum loading efficiency of the nanoparticles. 42

Figure 2.18. UV-Vis absorption and fluorescence emission spectra of Anthracene (ANT) while increasing its amount (λ_{ex}=350 nm). 43

Figure 2.19. Size distribution histograms from DLS measurements of (CPT)-loaded PPFBT nanoparticles having the ratios PPFBT to CPT (w:w) 25:1 (a) 15:1 (c) and 10:1 (e) ; Zeta potential measurements of (CPT)-loaded PPFBT nanoparticles having the ratios PPFBT to CPT (w:w) 25:1 (b) 15:1 (d) and 10:1 (f). 44

Figure 2.20. The cartoon representation of the synthesis of camptothecine (CPT)-loaded PPFBT nanoparticles and the determination of the optimum drug loading efficiency of the nanoparticles. 45

Figure 2.21. UV-Vis absorption and fluorescence emission spectra of Camptothecin (CPT) while increasing its amount. 46

Figure 2.22. ^{1}H-NMR (400 MHz, DMSO-d6, 25 °C) spectra of the remaining residue of PPFBT nanoparticles and filtrated CPT-loaded PPFBT nanoparticles after evaporation off 47

Figure 2. 23. UV–vis absorption and fluorescence emission spectra of CPT-loaded PPFBT nanoparticles , PPFBT nanoparticles and CPT as dispersions in water (b) $\lambda_{exc.}$= 365 nm (c) $\lambda_{exc.}$= 447 nm. 48

Figure 2.24. Size distribution histograms from DLS measurements of PPFBT nanoparticles and CPT-loaded PPFBT nanoparticles. 49

Figure 2.25. Zeta potential measurements of PPFBT nanoparticles and CPT-loaded PPFBT nanoparticles. 50

Figure 2.26. TEM images of PPFBT nanoparticles (a) and CPT-loaded PPFBT nanoparticles (b). AFM images of PPFBT nanoparticles (c) and CPT-loaded PPFBT nanoparticles (d). 51

Figure 2.27. Fluorescence microscope images of CPT-loaded PPFBT nanoparticles having concentrations of PPFBT as 0.04 mg / mL (a) and 0.75 mg / mL (b); Huh7 cells incubated with PPFBT nanoparticles after 24 h. 52

Figure 2.28. Percent cell death with CPT-loaded PPFBT Nps, PPFBT Nps, CPT and DMSO. 53

Figure 2.29. Huh7 cells plated concomitantly on coverslips and treated identically were Hoechst 33258 stained and examined under a fluorescence microscope after 72 h. 54

Figure 2.30. Huh7 cells plated concomitantly on coverslips and treated identically were Hoechst 33258 stained and examined under a fluorescence microscope after 72 h 55

Figure 2.31. Huh7 cells plated concomitantly on coverslips and treated identically were Hoechst 33258 stained and examined under a fluorescence microscope after 72 h. 56

Figure 2.32. (a) Size distribution histogram from DLS measurement and (b) zeta potential measurement of PAPFVBT Nanoparticles. 57

Figure 2.33. UV–vis absorption and fluorescence emission spectra of PAPFVBT in THF, as film and as dispersions of the nanoparticles in water ($\lambda_{exc.}$= 420 nm). 58

Figure 2.34. Percent cell viability results of PAPFVBT nanoparticles having concentrations of 16, 8, 4, 2, 1 μM after 72 h incubation. 59

Figure 2.35. Size distribution histograms from DLS measurements of PPFBT nanoparticles (a) and CPT-loaded PPFBT nanoparticles (b); SEM images of PPFBT nanoparticles (c) and CPT-loaded PPFBT nanoparticles (d); Zeta potential measurements of PPFBT nanoparticles (e) and CPT-loaded PPFBT nanoparticles (f) 60

Figure 2.36. The image of 96-well plate with SRB dye after 72 h incubation. 61

Figure 2.37. Percent cell death with CPT- loaded PAPFVBT Nps, PAPFVBT Nps, CPT and DMSO. 62

LIST OF SCHEMES

Scheme 2.1. Synthesis of the monomer 2,7-dibromo-9,9-bis(3-bromo-propyl)-9H-fluorene (M1). 24

Scheme 2.2. Synthesis of the monomer 9,9-bis-(3-bromo-propyl)-2,7-divinyl-9H-fluorene (M2) (inset image represents the reaction medium under 366 nm UV light) via Stille Coupling. 26

Scheme 2.3. Synthesis of the monomer 2,7-dibromo-9,9-bis-(propenyl)-9H-fluorene (M3). 30

Scheme 2.4. Synthesis of the polymer poly[(9,9- bis{propenyl}fluorenyl-2,7-diyl))-co-(1,4-benzo-{2,1,3}-thiodiazole)] (PPFBT) via Suzuki coupling. 31

Scheme 2.5. Synthesis of the polymer poly[(9,9-bis{3-bromo-propyl}fluorenyl-2,7-divinylene)-co-(1,4-benzo-{2,1,3}-thiodiazole)] (PBPFVBT) via Heck coupling. 33

Scheme 2.6. Synthesis of the polymer poly[(9,9-bis{3-azido-propyl}fluorenyl-2,7-divinylene)-co-(1,4-benzo-{2,1,3}-thiodiazole)] (PAPFVBT). 35

Scheme 4.1. The structure of 2,7-dibromo-9,9-bis(3-bromo-propyl)-9H-fluorene (M1). 66

Scheme 4.2. The structure of 9,9-bis-(3-bromo-propyl)-2,7-divinyl-9H-fluorene (M2). 66

Scheme 4.3. The structure of 2,7-dibromo-9,9-bis-(propenyl)-9H-fluorene (M3). 67

Scheme 4.4. The structure of poly[(9,9- bis{propenyl}fluorenyl-2,7-diyl))-co-(1,4-benzo-{2,1,3}-thiodiazole)] (PPFBT). 68

Scheme 4.5. The structure of poly[(9,9-bis{3-bromo-propyl}fluorenyl-2,7-divinylene)-co-(1,4-benzo-{2,1,3}-thiodiazole)] (PBPFVBT). 69

Scheme 4.6. The structure of poly[(9,9-bis{3-azido-propyl}fluorenyl-2,7-divinylene)-co-(1,4-benzo-{2,1,3}-thiodiazole)] (PAPFVBT). 69

LIST OF TABLES

Table 1. Size and Zeta potential values of PPFBT nanoparticles and CPT-loaded PPFBT nanoparticles. 49

Table 2. Summary for IC_{50} values of free drug (CPT), CPT-loaded PPFBT and PAPFVBT Nanoparticles. 63

CHAPTER 1. INTRODUCTION

1.1. Conjugated Polymers

Conjugated polymers possess a unique set of properties such as conductivity, photoluminescence, electroluminescence and electrochromism. Therefore, they have been used for optoelectronic applications, such as light-emitting and photovoltaic materials, thin film transistors and chemo/biosensors.[1,2]

In fact, there are two Nobel prizes in chemistry for the research on conjugated polymers. Firstly, the discovery on conducting electricity of "doped" polyacetylene by Professors Alan Heeger, Alan MacDiarmid, and Hideki Shirakawa has been awarded the Nobel Prize for Chemistry in 2000.[3] Secondly, the invention of novel palladium-catalyzed cross couplings that can be used for the synthesis of organic materials and conjugated polymers by Professors Richard F. Heck, Ei-ichi Negishi, and Akira Suzuki has been awarded the Nobel Prize for Chemistry in 2010.[4]

The electronic structure of a material determines the electrical properties. For example, the orbitals of the atoms in metals overlap with the equivalent orbitals of their neighbouring atoms in all directions to form molecular orbitals similar to those of isolated molecules to form an apparently continuous band of energies (Figure 1.1).[3]

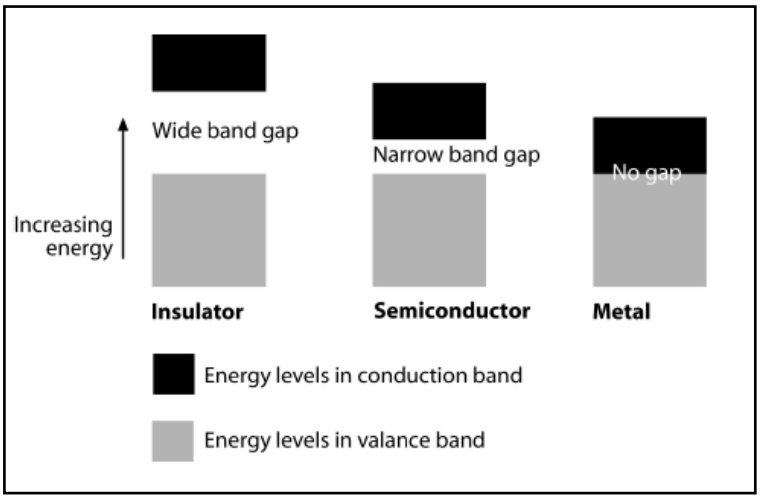

Figure 1.1. Simple band picture explaining the difference between an insulator, a semiconductor and a metal.[3]

Furthermore, the semiconductor like property of conjugated polymers comes from the fact that all conjugated polymers have delocalized π-electrons across all the adjacent aligned p-orbitals meaning that these electrons are not a part of one valence bond (Figure 1.2).[1,5]

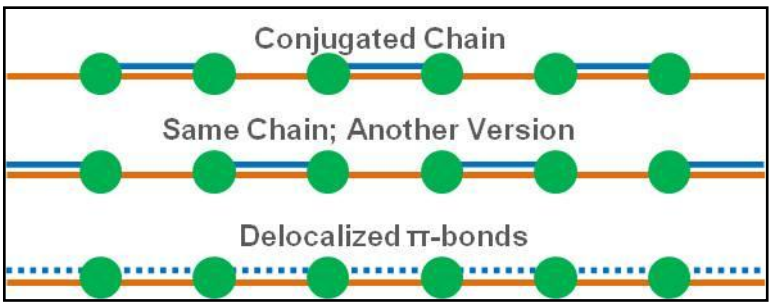

Figure 1.2. Delocalized π-bonds in conjugated polymers.

As shown in Figure 1.3, the conjugation length determines HOMO/LUMO levels. When the conjugation length increases, the HOMO level increases, the LUMO level decreases, so the band gap decreases. Moreover, these levels and the band gap are controlled by type of conjugated system and electron donating/withdrawing groups.[6] While electron donating group increases these energy levels, electron withdrawing groups decreases the levels. The presence of twists in the polymer structure generally decreases the effective conjugation length and therefore increases the band gap.[7]

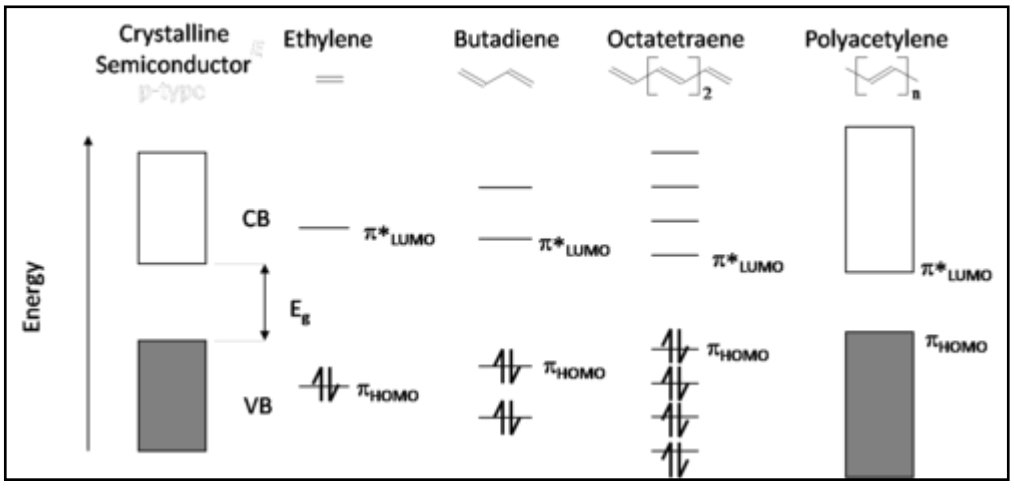

Figure 1.3. The conjugation length determines HOMO/LUMO levels.[7]

The alternative donor-acceptor copolymers provide the expansion of the spectral absorption in which they are synthesized by introducing electron-donating and electron-withdrawing units that finds application in photovoltaic materials.[8-10] Pei *et al.*

synthesized a low band gap donor-acceptor copolymer based on polyfluorene by Heck type of cross coupling polymerization.[11] They introduced a thiophene unit as a conjugated bridge between the electron-donating fluorene unit and electron-accepting benzothiadiazole unit that resulted in a broad absorption and low band gap. This study is an example of tuning the physical properties of copolymers by changing the donor or acceptor units and the linking bridge between them.

Actually, the extension of the absorption and decrease in the band gap are the results of absorption of photons with long wavelengths by the state of internal charge transfer from donor to acceptor inside the copolymer. The most commonly used electron-donating units are thiophene[6], fluorene[11], pyrrole[12] and carbazole[13] while the most commonly used electron-withdrawing units are quinoline[14], quinoxaline[15] and pyridazine[16]. Polyfluorene and its derivatives have been extensively used as a new class of organic semiconductors due their superior optoelectronic properties such as high charge carrier mobility.[17,18] In order to use these semiconductor type of polymers efficiently in sunlight harvesting as organic solar cells, the band gap should be narrow respect to the maximum photon flux of sunlight (~1.7 eV).[19] One way to make narrow is the incorporation of the electron-withdrawing unit into polyfluorene chains to form an alternating donor-acceptor copolymer.[11] A typical solar cell is illustrated in Figure 1.4.

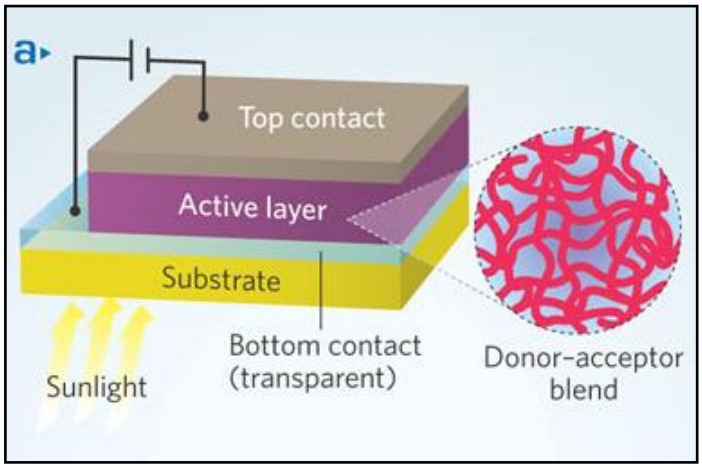

Figure 1.4. Typical solar cell. a, Polymer bulk-heterojunction. The bottom transparent substrate can be glass or flexible plastic, the bottom contact is a transparent conducting oxide (TCO) with a high work function, the active layer is a mixture of donor and acceptor molecules, and the top electrode is a metal with a low work function, such as aluminium. Reprinted with permission from ref. 20 (Copyright 2009, Nature Publishing Group).

Conjugated polyelectrolytes are different from the normal "neutral" conjugated polymers because of the presence of ionic side group attached to the conjugated main chain.[21] As previously discussed, the first common component, π-conjugated backbone, determines the main optical properties such as absorption and emission spectra, so the light-harvesting ability. The second component, charged side-chains, provides water solubility that can interact with biomacromolecules, microorganism, or cells (Figure 1.5). The charged side-chain could be cationic quaternary ammonium groups, sulfonic groups, anionic carboxyl groups, or phosphate groups.[22]

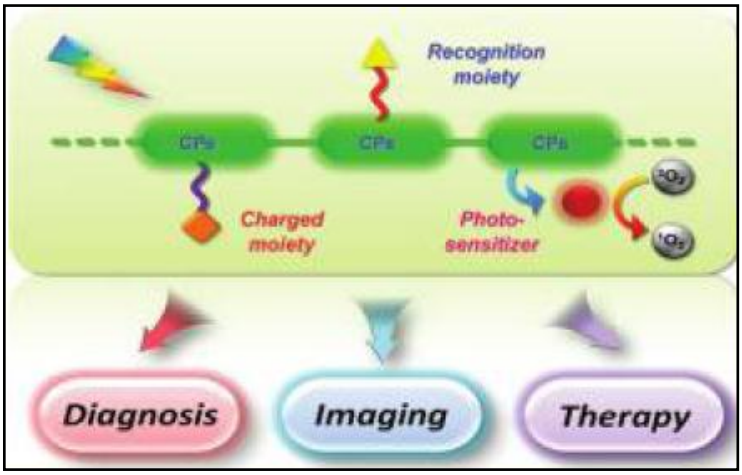

Figure 1.5. Schematic representation of conjugated polyelectrolytes for imaging, diagnosis and therapy. Reprinted with permission from ref. 22 (Copyright 2012, American Chemical Society).

Pu *et al.* designed two multicolor light-up probes from two cationic conjugated polymers for biomolecular quantification (Figure 1.6).[23] The idea was the enhancement of fluorescence, which is weak in aqueous media because of the charge-transfer electronic states of the polymers, by increasing the hydrophobicity of polymeric environment through complexation with biomolecules. Both cationic polymers showed an increase in fluorescence turn-on responses toward bovine serum albumine (BVA) and DNA resulting in biomolecule-dependent light-up signatures. The larger light-up response was shown by the polymer with vinyl linkages along its backbone because of the stronger charge-tranfer character.[24]

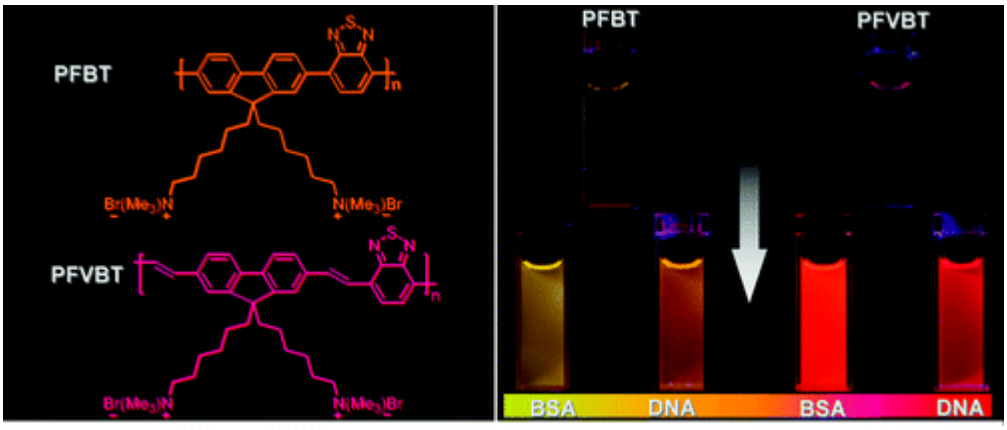

Figure 1.6. Chemical structures of PFBT and PFVBT and the photographs of the corresponding fluorescent polymer solutions in the absence (up) and presence (bottom) of DNA or BSA with the concentration of 1.2 μM under UV radiation at 365 nm. Reprinted with permission from ref. 23 (Copyright 2012, American Chemical Society).

Although, the unique properties of conjugated polyelectrolytes provide many new opportunities for the use in biological applications[25,26], they can be used in the fabrication of polymer light-emitting diodes (PLEDs)[21] besides the use of neutral conjugated polymers for PLEDs[27]. However, the incorporation of ionic side chains increases the solubility in water and polar organic solvents, so more environmentally friendly producing opportunities are provided.[5] Furthermore, Mwaura *et al.* demonstrated the fabrication of active materials for organic photovoltaic cells from two conjugated polyelectrolytes in which anionic sulfonate solubilizing groups were used as the electron donors and cationic methanofullerene was used as the electron acceptor (Figure 1.7).[28]

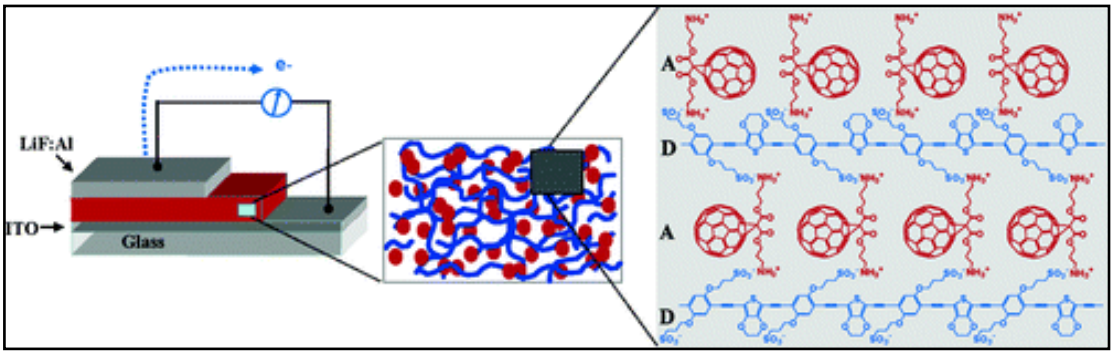

Figure 1.7. Schematic representation of the photovoltaic cell structure showing the alternating donor (D) and acceptor (A) layers, forming the active material. Reprinted with permission from ref. 28 (Copyright 2005, American Chemical Society).

1.1.1. Synthesis Methods of Conjugated Polymers

Although superior properties of conjugated polymers, the synthetic methods make tricky the control over molecular weight and polydispersity, in other words the uniformity of the sample weights[7]. Actually, the polymerization reactions go through step-growth mechanism in which bifunctional or multifunctional monomers react to form first dimers, then trimers, then longer oligomers and eventually long chain polymers (Figure 1.8). As a result of step-gowth polymerization, broad molecular weights are obtained that the molecular weight is dependent on the purity of the monomer. Therefore, there could be a batch-to-batch variability, so the variation of optoelectronic properties.

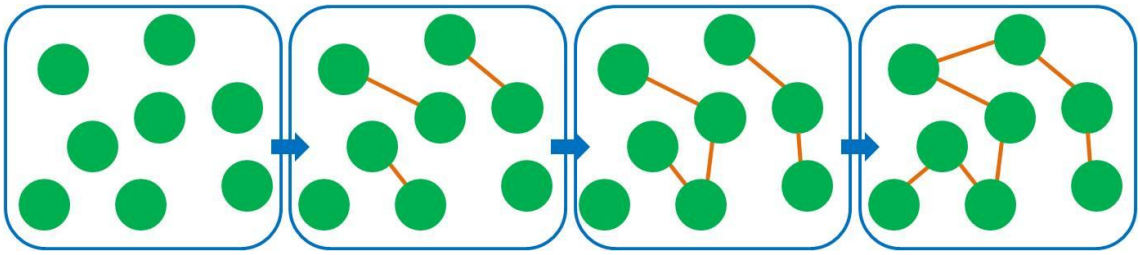

Figure 1.8. Cartoon representation of step-growth polymerization.

The common synthetic methodology is the cross-coupling reactions via different organometallic reagents. There are many examples in the history such as the reaction of organomagnesium reagents with aryl or alkenyl halides catalyzed by Ni(II) complexes, the cross-coupling of Grignard reagents with 1-halo-1-alkenes catalyzed by Fe(III) complexes.[29] Moreover, many other organometallic reagents such as organolithiums, organostannans, 1-alkenylcopper and organosilicon compounds have proven to be highly useful as nucleophiles for the cross-coupling reactions.[29]

The cross-coupling reactions of organometallics have a general catalytic cycle, shown in Figure 1.9. It mainly involves three sequences which are oxidative addition, then transmetalation, followed by reductive elimination. Most of the cross-coupling reactions catalyzed by Ni(0) and Pd(0) are relied on this common catalytic cycle.[29]

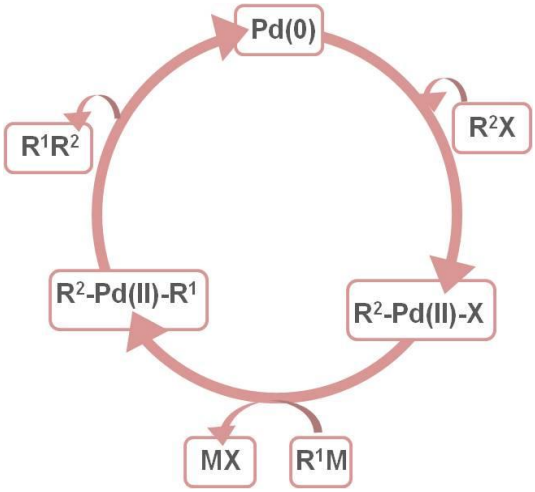

Figure 1.9. A general catalytic cycle for cross-coupling. Adopted from ref. 29.

As it is said before, the development of methods for novel palladium-catalyzed cross couplings, i.e. the formation of carbon-carbon bonds by Professors Richard F. Heck, Ei-ichi Negishi, and Akira Suzuki has been awarded the Nobel Prize for Chemistry in 2010. It is very important to synthesize carbon-carbon bonds for obtaining organic materials, complex molecules and conjugated polymers, so the research on this subject throughout the history has been awarded the Nobel Prizes in Chemistry; the Grignard reaction (1912), the Diels-Alder reaction (1950), the Wittig reaction (1979) and olefin metathesis to Y.Chauvin, R. H. Grubbs and R. R. Schrock (2005).[4]

The wide range of Pd(0) catalysts or precursors can be used for cross-coupling reaction. The most commonly used one is $Pd(PPh_3)_4$, however $PdCl_2(PPh_3)_2$ and $Pd(OAc)_2$ with PPh_3 or other phosphine ligands are also efficiently used. These precursors are stable to air and readily reduced to active Pd(0) complexes by organometallics or phosphine ligands.[29] In principle, palladium is like a meeting point for carbon atoms, that is depicted in Figure 1.10. Through the formation of metal-carbon bonds, two molecules are assembled on the metal. As a result of the proximity of carbon atoms, they couple to form new carbon-carbon single bond.[30]

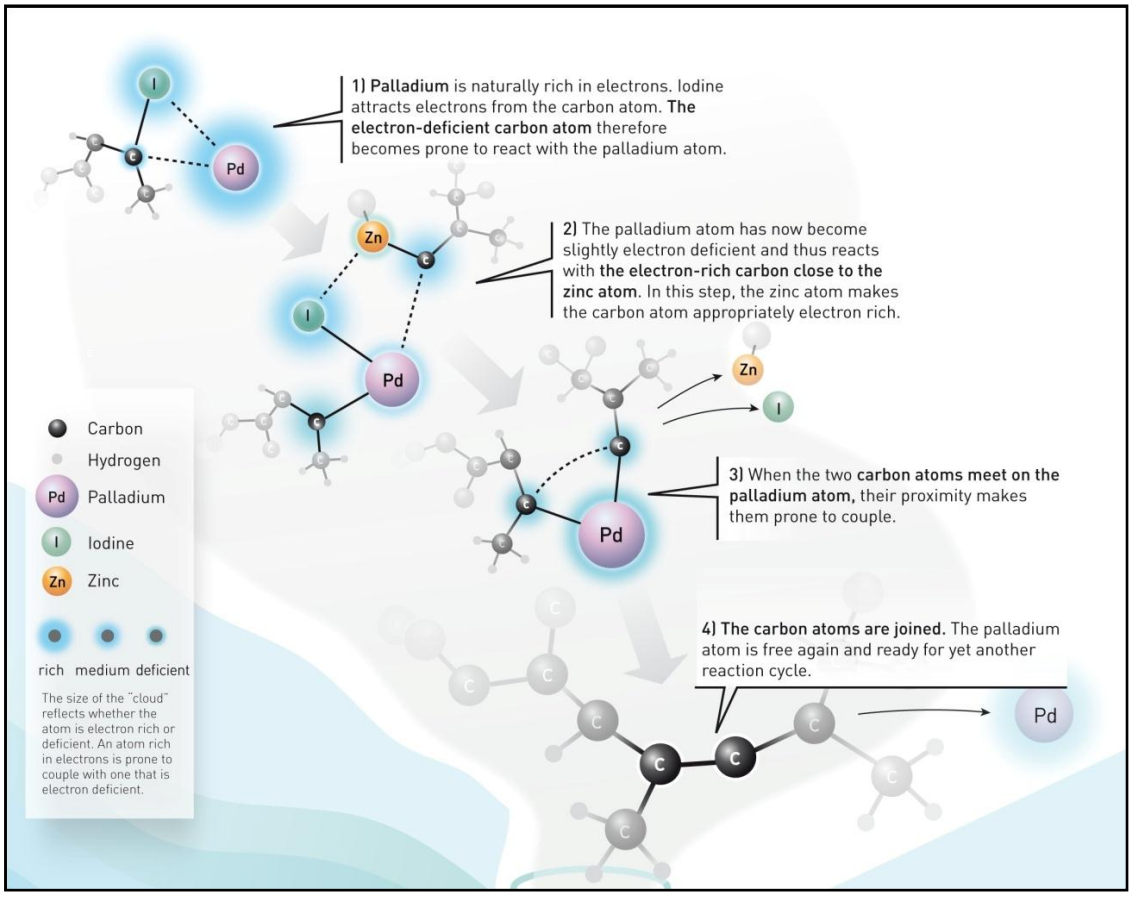

Figure 1.10. Palladium-meeting point for carbon atoms. (Scientists have re-created discodermolide in a test tube. In one of the critical steps of that procedure, they used Negishi's variant of the palladium-catalyzed cross coupling).[30]

One of the basic types of reactivity in palladium-driven catalytic cycles is the Heck-type reactivity. In first place, Heck chemistry was adding in situ-generated methly- and phenylpalladium halides to olefins in which organopalladium compound was generated from an organomercury compound and Pd(II) salt. The overall reaction was not catalytic without any additives because of the formation of Pd(0) at the end. Then, Heck developed this situation by adding $CuCl_2$ to reoxidize Pd(0). However, he made a significant modification in 1972 that organopalladium complex is generated from an organohalide and Pd(0) in a so-called oxidative addition.[4] This reaction is illustrated in Figure 1.11 that gives styrene as product. Heck reaction presents a simple way to obtain olefins, dienes, other unsaturated compounds with different substituents, and conjugated polymers.[31,32]

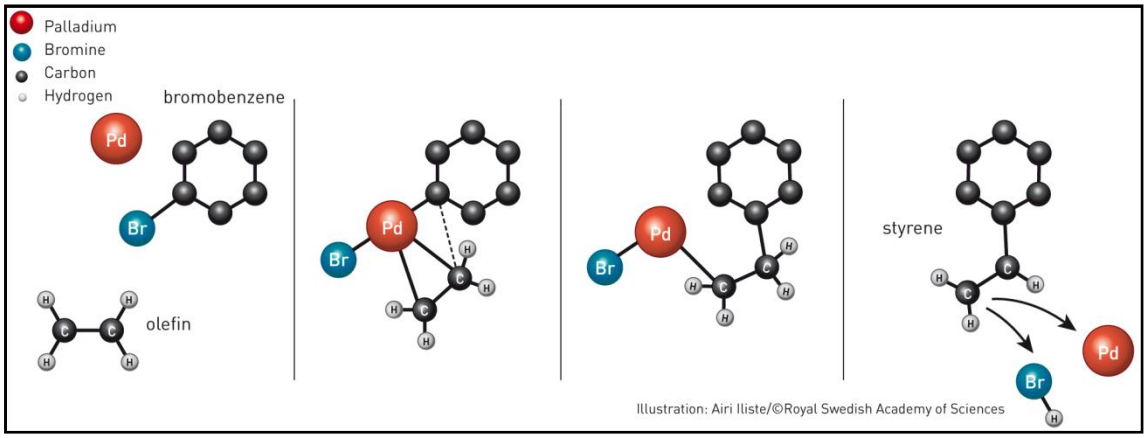

Figure 1.11. Richard Heck experimented with palladium as a catalyst and linked a short olefin to a ring of carbon atoms. When the two meet on the palladium atom they react with each other. The result of the reaction is styrene, a fundamental component of the plastic polystyrene.[30]

Negishi's studies were concentrated on the use of more chemoselective organometallic compounds in the palladium catalyzed couplings with organohalides. Firstly, he got successful results by using organozirconium or organoaluminium, followed by the trials with less reactive organometallic species. However, his biggest development was introducing organozinc compounds as coupling partners in 1977.[4] Figure 1.10 shows the artificially synthesis of discodermolide by Negishi's type palladium-catalyzed cross coupling.

In 1979, Suzuki presented the use of organoboron compounds in palladium-catalyzed cross coupling. As compared to previous ones, boron is the mildest activator and even less toxic.[4] Moreover, the convenience of organoboron compounds comes from being thermally stable and inert to water and oxygen, so allowing their handling without special precautions.[29] The organoboron reagents in the presence of a base become coupling partners in palladium catalyzed cross couplings to vinyl, aryl and alkyl halides in Suzuki reaction.[4]

The other type of coupling catalyzed by palladium was developed by John Kenneth Stille in 1977. It is the cross-coupling of organotin compounds with an organic electrophile, i.e. organohalide, via the catalyzation of palladium. This novel method is stereospecific and regioselective in which results in high yields of product.[33]

The mechanisms of commonly employed palladium-catalyzed coupling reactions for the synthesis of conjugated polymers are shown in Figure 1.12; Suzuki, Heck, Stille and Negishi.

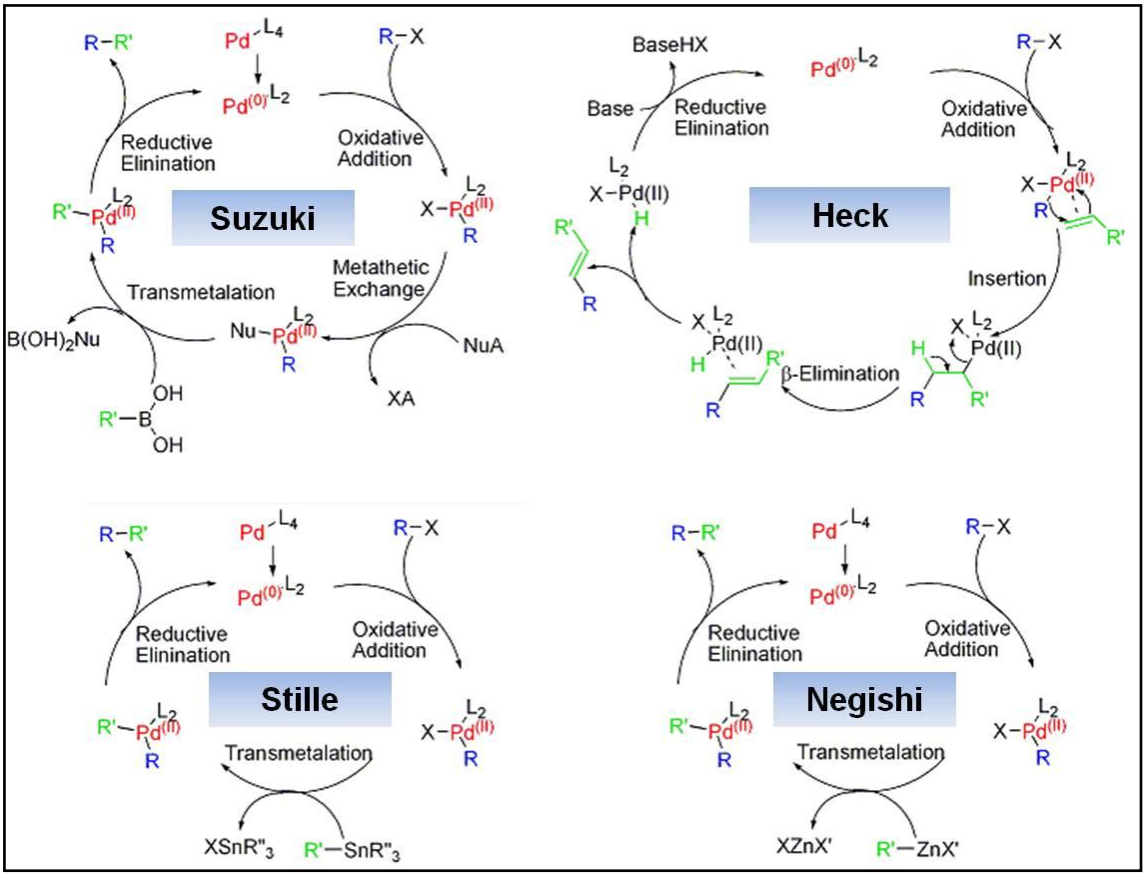

Figure 1.12. Palladium-catalyzed coupling reactions; Suzuki, Heck, Stille and Negishi.[34]

These mechanisms start with the common step, oxidative addition, in which the active Pd(0) catalyst react with the organohalide resulting in the change of oxidation state of palladium to Pd(II) to form organopalladium compound.[4] This step is often rate-determining step in the catalytic cycle that the relative reactivity decreases in the order of I > OTf > Br >> Cl.[29] In the second common step called transmetallation, the organic group on organometallic compound is transferred to palladium. However, Suzuki mechanism has special case in which the boronic acid must be activated, e.g. with base that facilitates transmetallation. By this transmetallation step, the assembly of two organic groups on palladium is achieved by palladium-carbon bonds. In the last step, two organic groups couple to give a new carbon-carbon single bond. Before this step, there is an extra migratory insertion step in Heck coupling that the organic group on

palladium shifts to one of the carbons of the co-ordinated olefin while palladium shifts to the other carbon of the olefin to generate carbon-carbon bond. Finally, the release of the formed organic compound occur via reductive elimination in all type of reactions that proceeds through the reduction of Pd(II) to Pd(0).[4,29,31-33]

1.2. Conjugated Polymer Nanoparticles

Nanoparticles are widely used for biological applications such as cell imaging.[35-38] However, the most important property for an imaging agent is its photostability that most of organic dyes suffer from photobleaching. To overcome this problem, quantum dots (QDs) have been synthesized that they have much greater photostability and brightness.[39] However, they are cytotoxic since they leach harmful metals.[40] The use of water dispersible conjugated polymer nanoparticles (CPNs) for cellular imaging providing more photostability, high fluorescence brightness and lower toxicity has been much increased in the recent years.[41-47] Moreover, they can be synthesized easily with a desired emission wavelength and functionalities from a number of different polymers.[48-52] These features make them very attractive for photonics[53-55] and biomedical applications.[41-47,56-60]

1.2.1. Preparation of Conjugated Polymer Nanoparticles

Conjugated polymer nanoparticles (CPNs) are generally prepared by two methods; reprecipitation and miniemulsion.[61-63]

The reprecipitation method presented in Figure 1.13 is used to dissolve the hydrophobic conjugated polymer in a good (miscible) solvent such as THF or acetonitrile. The obtained solution is then poured into a large excess of poor solvents, generally water. The formation of nanoparticles driven by hydrophobic interaction is accelerated by vigorously stirring and ultrasonication. The water dispersible nanoparticles are obtained after the evaporation of the organic solvents. The spherical morphology is the result of avoiding the contact of polymer chains with water to get minimum interaction. Unlike the miniemulsion method, this process does not involve additives, such as surfactants, and the common nanoparticle size is in the range of 5−150 nm in diameter, that depends on the concentration of polymer solution and molecular weight of the polymer. This method has been applied to a wide variety of conjugated polymers that are soluble in organic solvents.[46,48,64]

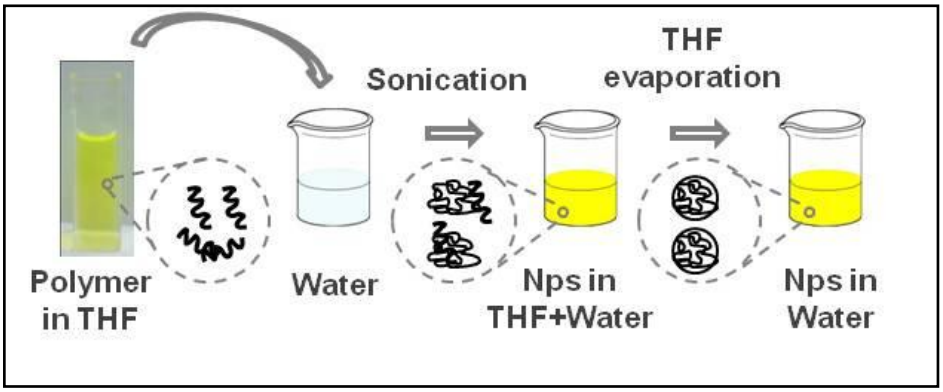

Figure 1.13. The preparation of nanoparticles using reprecipitation method.

The miniemulsion method is illustrated in Figure 1.14 that starts with dissolving the conjugated polymer in an apolar organic solvent (water immiscible). Then, the polymer solution is transferred into an aqueous solution of an appropriate surfactant to avoid undesirable coalescence of emulsion droplets. Under the aid of ultrasonication, the resulting mixture is drastically stirred to form stable miniemulsions composed of polymer droplets. After the evaporation of organic solvent, CPNs are obtained as stable dispersion in water. The size range of the resulting CPNs is in between 30 nm and 500 nm that is dependent on the concentration of polymer solution.

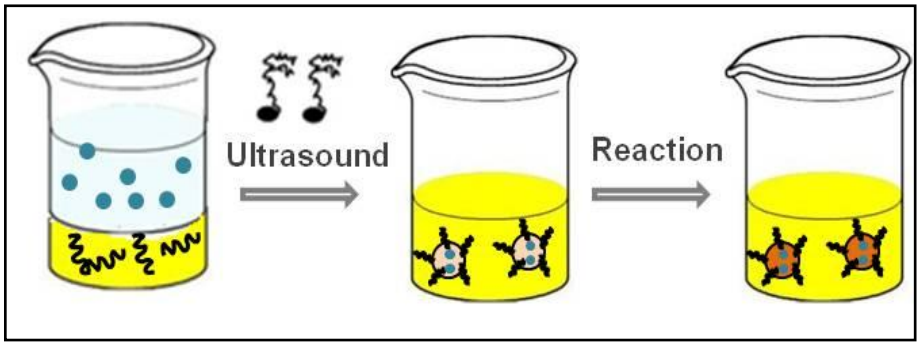

Figure 1.14. The preparation of nanoparticles using miniemulsion method.

Landfester and co-workers reported the deposition of the layers of conjugated semiconducting polymers from aqueous dispersions with controllable particle sizes in the range of 70-250 nm prepared by the miniemulsion method.[65] Using this method, Baier et al. demonstrated the preparation of poly-(arylene diethynylene) nanoparticles by stepwise polymerization of the corresponding monomers under Glaser coupling conditions, then resulted in the tunable emission colors of CPNs by controlling intramolecular energy transfer.[66]

1.2.2. Biomedical Applications: Cell Imaging, Drug Delivery, Theranostic

The diagnosis and therapy of life threatening diseases, such as cancer, present serious challenges. In this context, the development of non-invasive methods and materials for early cancer diagnosis and efficient drug delivery are highly sought after. The usage of nanomaterials for drug delivery is increased as a result of their high therapeutic efficacy while having lower systematic side effects.[67,68] Various nanostructured-materials in different geometries are designed and synthesized from inorganic nanoparticles, polymers, lipids and dendrimers to be used as contrast agents, therapeutics, and delivery vehicles.[69- 73] Especially, bioconjugated fluorescent polymeric nanoparticles are widely employed in imaging and targeted delivery.[74-76]

For the preparation of bioconjugates, many kinds of synthetic polymers with structural and architectural variations have been recently investigated.[77] These types are monofunctional or polyfunctional linear, starlike and dendritic architectures, depicted in Figure 1.15.

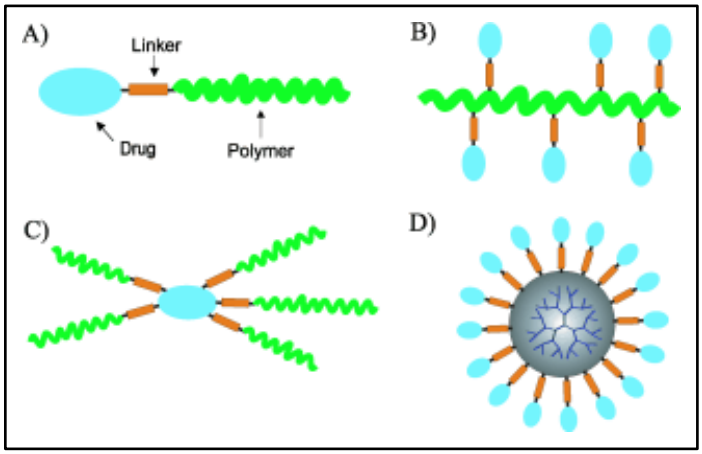

Figure 1.15. Selected structural and architectural types of drug–polymer conjugates. Reprinted with permission from ref. 77 (Copyright 2006 WILEY-VCH Verlag GmbH & Co. KGaA).

Way et al. developed conjugated polymer nanoparticles conjugated with biorecognition molecule, Herceptin, in dendritic-like architecture.[74] While Herceptin-conjugated fluorescent nanoparticles were seen on the HER2-overexpressig cancer cells but not on the HER2 basal cells, they could suppress the growth of HER2-overexpressig cancer cells. Therefore, these nanoparticles were suitable probes for targeted therapy and imaging of HER2-overexpressing cancer cells. Nanoparticles have also been prepared

by *Feng et al.* for drug delivery through the electrostatic assembly of cationic polyfluorene based conjugated polymer with doxorubicin conjugated anionic poly(L-glutamic acid) in polyfunctional linear fashion.[78] This complex system could deliver doxorubicin to targeted cancer cells while imaging the cells by monitoring doxorubicin release based on fluorescence "turn-on" signal of the cationic polyfluorene based conjugated polymer.

Actually, there is an increase in the use of these kinds of theranostic medicine in which the diagnosis and therapeutic agents are incorporated into one system to be delivered to the cells effectively while following the whole process through appropriate techniques with the help of the contrast agents incorporated in the system.[79,80] However, there are no reports on the facile synthesis of drug-loaded conjugated polymer nanoparticles through reprecipitation method using only one type polymer and their dual use simultaneously for the drug delivery and the imaging.

The theranostic nanomedicine has many advantages over conventional chemotherapy because of a number of reasons. In the latter treatment, the drugs may not approach the target easily or be cleared off from the body in a very short time and as a result the treatment may require the usage of higher doses of drugs; in turn, this may cause unwanted side effects. The nanomedicine has the potential to enable preferential delivery of drugs to tumor due to the enhanced permeability and retention (EPR) effect is depicted schematically in Figure 1.16, in which the vasculature in tumors is leaky to certain sizes of molecules (e.g. liposomes, nanoparticles, and macromolecular drugs) by allowing these molecules to accumulate in tumor tissues more than normal tissues.[77,81,82] There are two main factors that influence the EPR effect and tumor targeting. Firstly, the physicochemical properties of nanoparticles such as the size and surface charge of particles influence the their tumor accumulation and pharmacokinetic behaviors. Secondly, the tumor properties such as cancer type, stage of disease, tumor size affect the tumor targeting properties of nanoparticles.[83]

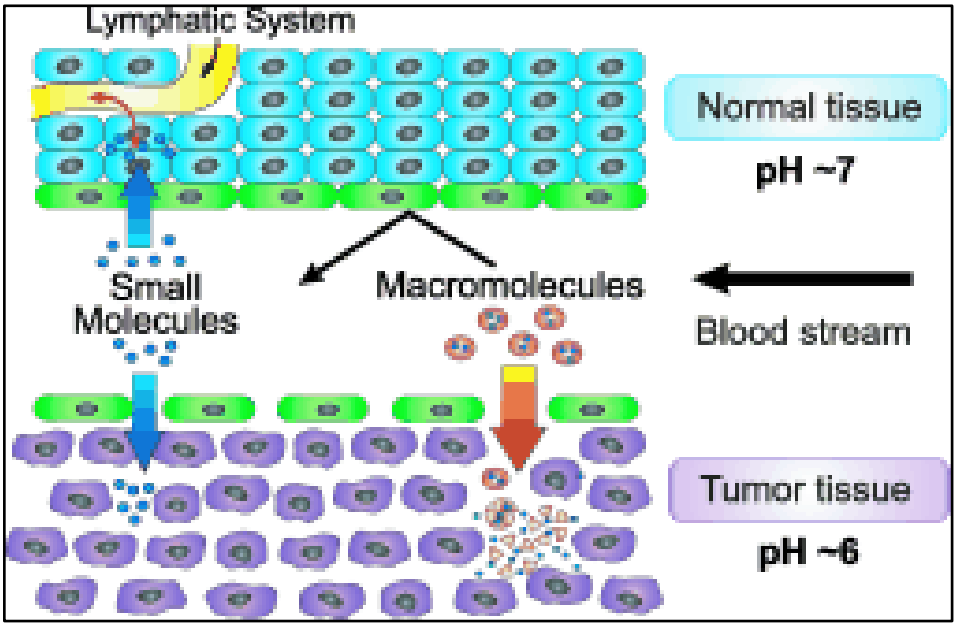

Figure 1.16. Schematic representation of the anatomical and physiological characteristics of normal and tumor tissue with respect to the vascular permeability and retention of small and large molecules (EPR effect). Reprinted with permission from ref. 77 (Copyright 2006 WILEY-VCH Verlag GmbH & Co. KGaA).

The cellular uptake and cytotoxicity studies of CPNs based on various conjugated polymers have been reported and these studies clearly demonstrated that CPNs were taken up efficiently by the cells through endocytosis even in a very short incubation time.[46] Generally, cellular uptake of macromolecules is achieved through receptor-mediated endocytosis, adsorptive endocytosis, or fluid-phase endocytosis, that is illustrated in Figure 1.17. There is significant drop in the pH value that takes place from pH 7.2-7.4 in the extracellular space to pH 6.5–5.0 in the endosomes and to around pH 4.0 in primary and secondary lysosomes. Therefore, it is needed to be sufficiently stable of drug–polymer conjugates or complexes in the blood stream before releasing the drug at the site of action. The polymer-drug conjugates can be released in the body by reduction, or in a pH-dependent manner.[77] Scherman and coworkers demonstrated the synthesis of a supramolecular double hydrophilic block copolymer held together by cucurbit[8]uril ternary complexation and its subsequent self-assembly into micelles.[84] They encapsulated the the chemotherapeutic drug doxorubicin by this system, then investigated the controlled release of the drug through multiple external triggers including temperature, pH and the addition of a competitive guest.

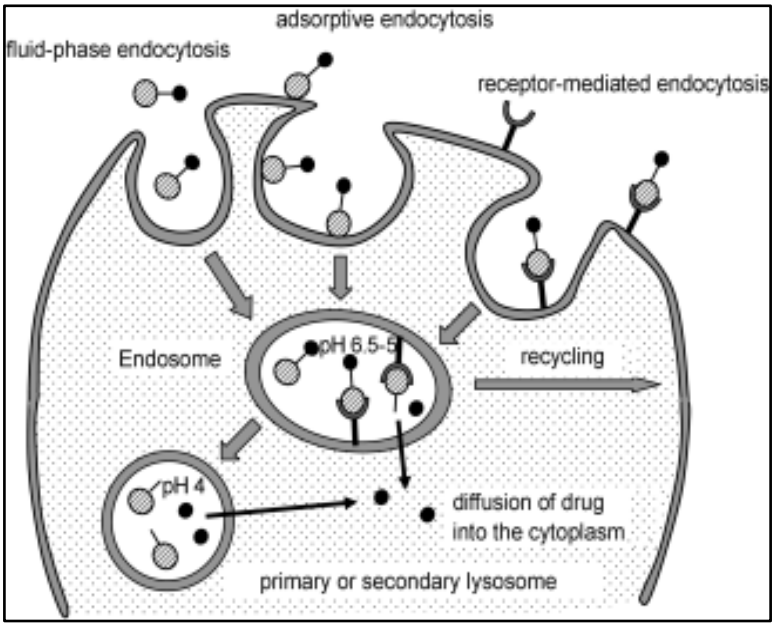

Figure 1.17. Endocytotic pathway for the cellular uptake of macromolecules and nanocarriers for drug delivery. Reprinted with permission from ref. 77 (Copyright 2006 WILEY-VCH Verlag GmbH & Co. KGaA).

Howes et al. demonstrated the synthesis of conjugated polymer nanoparticles encapsulated by phospholipid micelles that could be used as an imaging agent in biomedical applications.[57] These nanoparticles were firstly used for simple cell imaging experiment that the significance of the result shown in Figure 1.18 comes from their deduction on the uptake through endocytosis by observing vesicles of the nanoparticles. If nanoparticles were not taken by endocytosis, they expected to observe a uniform distribution throughout the cytoplasm. Fernando et al. also suggested the endocytic mechanism for the uptake of nanoparticles by observing the intracellular fluorescence contained in vesicles.[46]

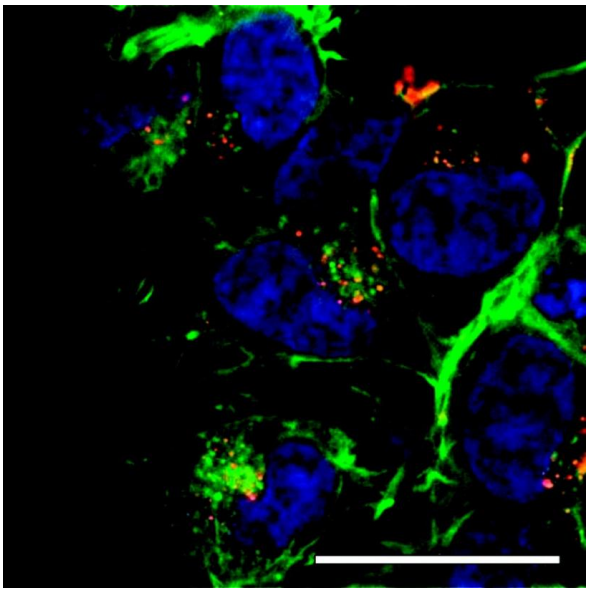

Figure 1.18. Confocal microscope image of SH-SY5Y neuroblastoma cells treated with MEH-PPV SPNs for 18 h. The SPNs are seen to cluster in the perinuclear region within the cells, suggesting they are in vesicles. The scale bar represents 25 μm. Reprinted with permission from ref. 57 (Copyright 2010, American Chemical Society).

It can be seen in the examples up to this point that for drug-loaded polymer nanoparticles, the polymer can form the capsule which hosts the drug molecules inside it. However, the controlled release of the contents is important as the encapsulation of the drug. In the release of capsule contents, stimuli-responsive phenomenon, i.e. triggering plays a key role by causing the change in capsule shell. The mechanisms of chemical reactions in polymeric shell wall include triggering by chemical, light, biological, magnetic, thermal and electric stimuli. Moreover, there are physical methods for the release of capsule content that are shown in Figure 1.19. Firstly, the shell wall can rupture by the increase in internal pressure that results in burst. Secondly, the shell wall can melt upon temperature increase. Thirdly, core materials are released by the change in porosity of the shell wall resulting from a phase transition of a shell wall polymer. Diblock copolymer or a mixture of two polymers is needed for this method in order to shrink of one polymer while the other one remaining physically intact to create the pores upon heating the capsule. Finally, the release can occur through thermomechanical degradation of the shell. When mechanical triggering such as exposure to magnetic or electrical fields is applied, the nanoparticles start to oscillate repeatedly that results in heating and tearing of the shell walls, so the release of core materials.[85]

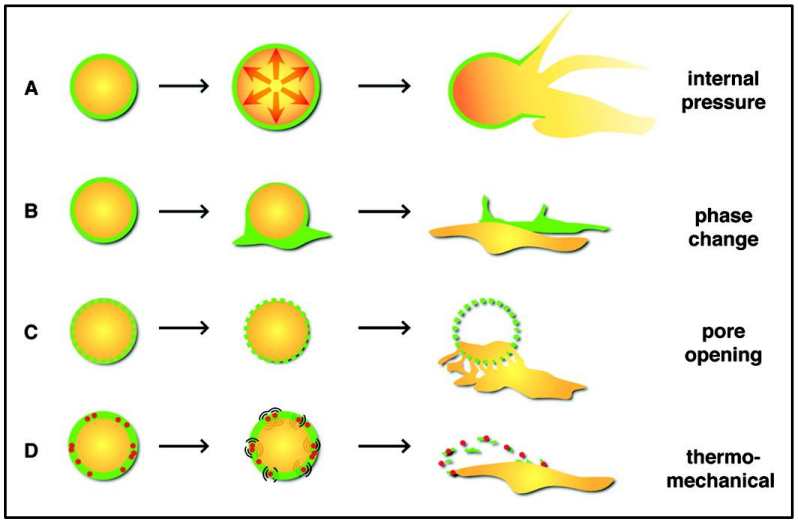

Figure 1.19. Physical methods of capsule release: (A) shell wall rupture by an increase in internal pressure, (B) melting of the polymer shell wall, (C) change in porosity of the shell wall resulting from a phase transition of a shell wall polymer, and (D) disintegration of the shell wall utilizing nanoparticles that oscillate in response to an external trigger. Reprinted with permission from ref. 85 (Copyright 2011, American Chemical Society).

1.3. Some Key Concepts

1.3.1. An anticancer Drug: Camptothecin

Camptothecin (CPT) is a quinoline alkoloid-based chemotherapy drug for the treatment of a broad range of cancers, including human lung, ovarian, breast, pancreas and stomach cancers. This anticancer agent kills the cells by converting DNA topoisomerase I into a DNA-damaging agent. In a mechanistical look, CPT firstly stabilizes a topisomerase I-induced single-strand break in the phosphodiester backbone of DNA, so preventing subsequent religation of the broken single strand. During the replication, when the DNA replication fork encounters the cleavable complex, it results in an irreversible double-strand break, so in an apoptosis. As shown in Figure 1.20, CPT has a five-ring structure. The 20*S* chiral carbon is importatnt for its activity while there is a dynamic equilibrium between the closed ring lactone and open-ring carboxylic acid forms. In order to be active (cytotoxic), CPT should be in the form of closed ring lactone.[86-88]

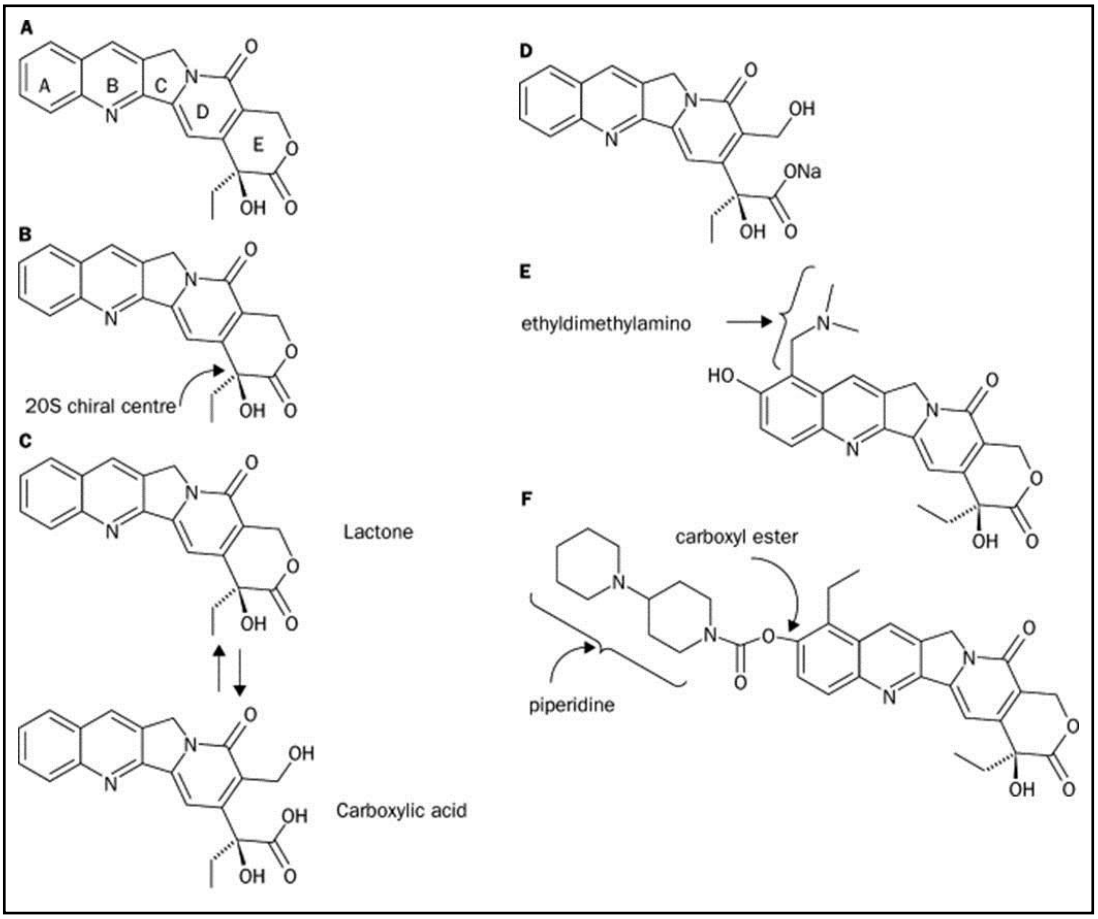

Figure 1.20. (A) Camptothecin. (B) 20*S* chiral centre. (C) Dynamic equilibrium of camptothecin. (D) Camptothecin sodium salt. (E) Topotecan. (F) Irinotecan. Reprinted with permission from ref. 86 (Copyright 2003, Elsevier).

CPT has poor water solubility and its inactive carboxylic acid form is favoured by neutral and alkaline pH. Moreover, this inactive form of CPT promptly binds to human serum albumin which hinders its cellular uptake.[86-88] However, CPT-based drugs, e.g., topotecan and irinotecan (Figure 1.20. E and F), are currently approved for use in humans despite their adverse side effects due to the solubilizing groups attached to CPT backbone. In addition to structurally modified water soluble analogues, special drug delivery systems are needed to increase the anticancer efficacy of CPT. The one way is to make substitution on 20-OH of CPT that can substantially reduce the tendency for lactone ring opening.[88,89] Botella *et al.* developed a drug delivery system through the attachment of CPT onto silica nanoparticles through an ester bond with 20-hydroxy moiety to stabilize the lactone ring.[83] Feng *et al.* used click chemistry as a coupling method to conjugate CPT and folic acid onto the Janus-type dendrimer-like poly(ethylene oxide)s.[90]

Moreover, the encapsulation of CPT by polymeric nanoparticles without any conjugation is an another method to overcome the identified shortcomings of CPT.[91] Schneider *et al.* generated biodegradable CPT-loaded polymer microspheres by using hydrodynamic flow.[92] In this study, the cell viability results showed its toxic effects indicating that the encapsulated CPT stayed in its lactone form. Other research on the encapsulation of CPT was done by Wang *et al.* that they used block copolymer nanoparticles as encapsulating matrix.[93] According to this study, the encapsulated CPT was more effective compared to free drug in inducing apoptotic responses in the cultured bone metastatic prostate cancer cells.

1.3.2. Sulforhodamine B (SRB) Cytotoxicity Test

It is important to choose a suitable cytotoxicity assay depending on the supposed cell death mechanism.[94] As shown in Figure 1.21, the assays are based on different modes of detection like MTT metabolism, LDH release, neutral red uptake and the ATP content of treated cells. Keepers and co-workers compared SRB protein stain assay with the tetrazolium (MTT) colorimetric assay for in vitro chemosensitivity testing of various human tumour cell lines.[95] They found that the SRB assay provided a better linearity with cell number and a higher sensitivity, and its staining was not cell-line dependent.

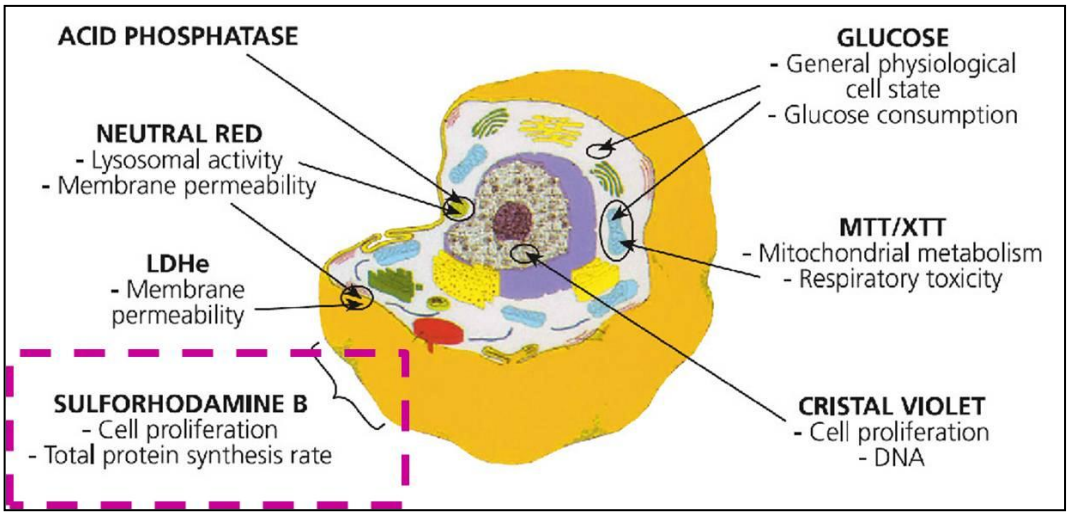

Figure 1.21. Cytotoxicity assays.[96]

In principle, SRB assay is based on the measurement of cellular protein content for cell density determination.The dye sulforhodamine B binds electrostatically and pH dependently on cellular protein whose basic amino acid residues were fixed by trichloroacetic acid. This binding occurs under mild acidic conditions, however solubilization for the measurement occur under mild basic conditions by extracting the dye from cells. There is a linear relationship between the results of the SRB assay and the cell number and cellular protein. The SRB assay is a nondestructive method by having a colorimetric end point and it is indefinitely stable. As a result of these practical properties, the SRB assay is appropriate and sensitive to measure drug-induced cytotoxicity.[97-100]

1.3.3. The Half Maximal Inhibitory Concentration (IC_{50})

It is extremely important to measure accurately the concentration of the inhibitor by half which is required for the inhibition of biological or biochemical function. The half maximal inhibitory concentration (IC_{50}) is a quantitative measure of the effectiveness of this inhibiton.[101] The concept of IC_{50} is shown in Figure 1.22.

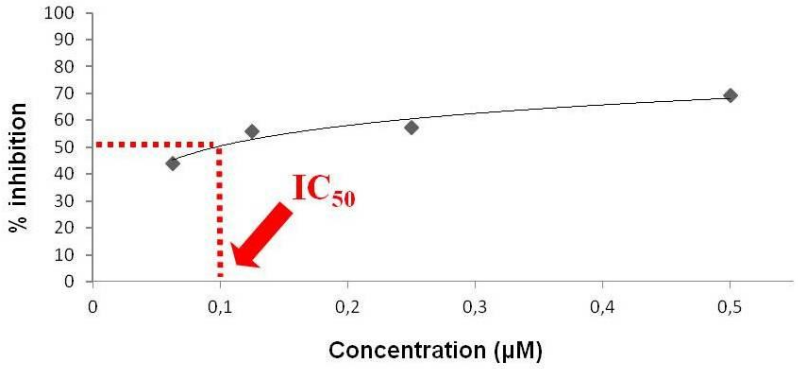

Figure 1.22. The half maximal inhibitory concentration.

In the comparison on toxic properties, IC_{50} values are very important parameter in which smaller values are the indication of superior inhibiting activity, i.e., less amount is needed to inhibit the same function by half. The drug delivery system through the attachment of CPT onto silica nanoparticles through an ester bond with 20-OH moiety developed by Botella *et al.* has similar IC_{50} values with the naked drug.[83] On the other hand, Aryal *et al.* observed superior therapeutic effect in the cytotoxicity of dual-drug (CPT and DOX) carrying nanoparticles compared with their cocktail mixtures.[102]

1.4. Aim of Thesis

Here it is aimed to synthesize water dispersible, multifunctional nanoparticles which can perform simultaneously the drug delivery and cell imaging tasks.

Firstly, previously synthesized[103], a green emitting, hydrophobic conjugated polymer, poly[(9,9-bis{propenyl}fluorenyl-2,7-diyl))-co-(1,4-benzo-{2,1,3}-thiodiazole)] (PPFBT) was used to prepare water dispersible nanoparticles. PPFBT Nps were characterized and their cytotoxicity and suitability as a fluorescent marker for cell imaging was evaluated *in vitro* cell assays. Then, drug loaded nanocapsules in which PPFBT act both as a fluorescent reporter and the main matrix of the nanocapsules accommodating an anticancer drug, camptothecin (CPT), were synthesized through a facile, single step reprecipitation method. Actually, to address the solubility problem of CPT is highly desirable and one of the objectives of this work is to achieve this through encapsulation. To determine the encapsulation efficiency, anthracene (ANT) was used besides using CPT. The optimum drug loading capacity of the nanoparticles was determined using various ratios of ANT to PPFBT, then CPT to PPFBT. Cell viability of Human hepatocellular carcinoma cell line (Huh7) was investigated in the absence and presence of CPT using Sulforhodamine B (SRB) assay. Moreover, Huh7 cells incubated with PPFBT Nps in the absence and presence of CPT plated concomitantly on coverslips and treated identically were Hoechst 33258 stained and examined under a fluorescence microscope.

Secondly, a red emitting, hydrophobic conjugated polymer, poly[(9,9-bis{3-bromo-propyl}fluorenyl-2,7-divinylene)-co-(1,4-benzo-{2,1,3}-thiodiazole)] (PBPFVBT) was synthesized by incorporating vinyl bonds between fluorene segments and benzothiadiazole units within the polymer to get red-shift in the fluorescence. Red emitting conjugated polymers have lower energy that make them better for biomedical applications such as drug delivery without tissue damage. To eliminate toxic effects, bromine group of PBPFVBT converted into azide group resulting in poly[(9,9-bis{3-azido-propyl}fluorenyl-2,7-divinylene)-co-(1,4-benzo-{2,1,3}-thiodiazole)] (PAPFVBT). PAPFVBT Nps were characterized and their cytotoxicity was evaluated *in vitro* cell assays. Then, drug loaded nanocapsules in which PAPFVBT act as the main matrix of the nanocapsules accommodating CPT were synthesized. Cell viability of Huh7 cells was investigated in the absence and presence of CPT using SRB assay.

CHAPTER 2. RESULTS AND DISCUSSION

This chapter has mainly two parts. The first part consists of the discussion on the synthesis and the characterization results of the monomers and polymers. In the second part, the synthesis and characterization of blank and drug loaded nanoparticles are discussed followed by cell culture studies.

This work demonstrates a novel strategy for combination of drug delivery with cell imaging without any further need for conventional dyes. The contents of this work is illustrated in Figure 2.1. This drug delivery system is much more simple and efficient just by using one kind of polymeric capsule that drug loaded nanoparticles showed superior efficacy over free drug.

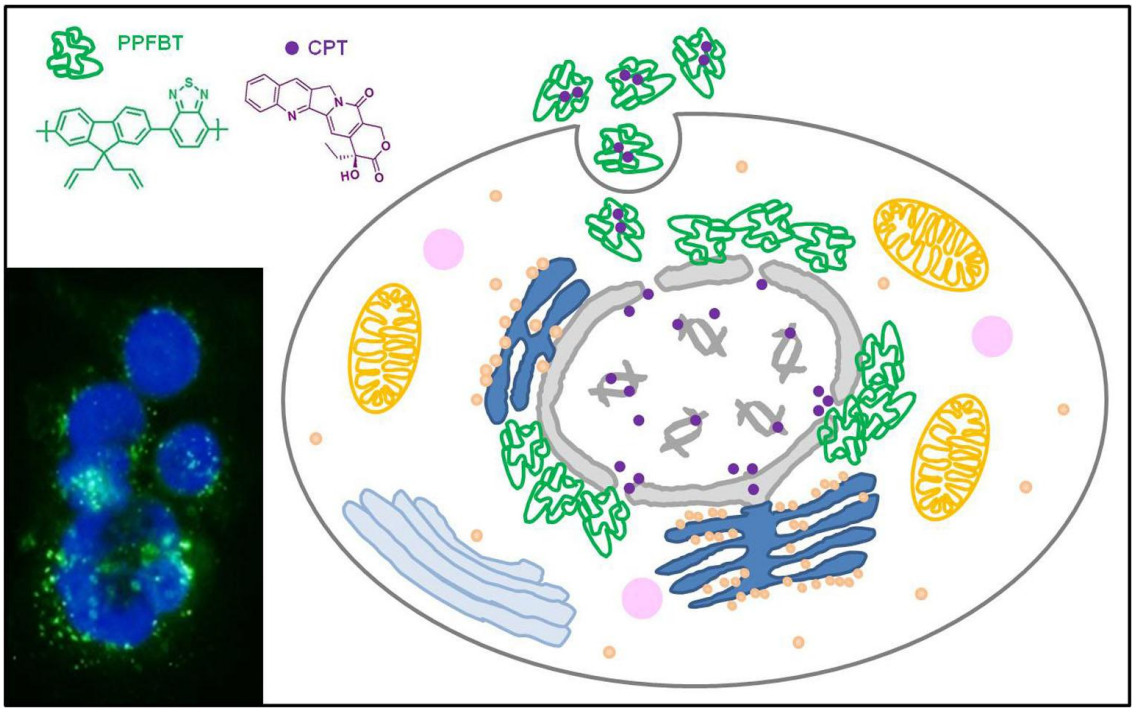

Figure 2.1. Schematic illustration of this thesis work.

2.1. Synthesis and Characterization of Monomers

2.1.1. Synthesis and Characterization of 2,7-dibromo-9,9-bis(3-bromo-propyl)-9H-fluorene (M1)

2,7-dibromo-9,9-bis(3-bromo-propyl)-9H-fluorene (M1) was synthesized from 2,7-dibromofluorene and 1,3-dibromopropane according to Scheme 2.1. 50% (w/w) NaOH solution provided very strong basic condition utilizing the abstraction of weakly acidic C9-H. To get the desired monomer, both protons at C9 should be removed. Then, 1,3-dibromopropane reacted with the resulting anion by adding to 9-position through nucleophilic substitution reaction. Although the reaction was exothermic, the temperature was kept at room temperature by using ice bath to prevent the formation of side products through elimination. The isolation and purification of the product was done by work-up with extraction (diethyl ether, distilled water, 2 N HCl) followed by column chromatography (cyclohexane as the eluent). The monomer M1 in white powders was obtained with 33% yield.

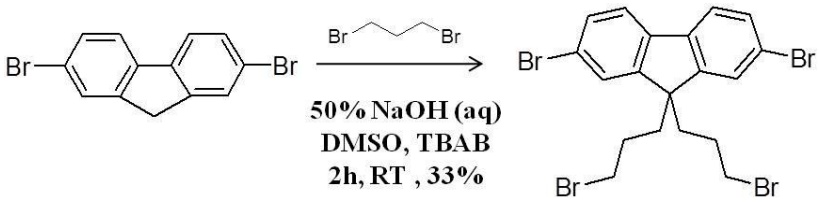

Scheme 2.1. Synthesis of the monomer 2,7-dibromo-9,9-bis(3-bromo-propyl)-9H-fluorene **(M1)**.

The structural characterization of the monomer M1 was done by ^{1}H-NMR spectroscopy shown in Figure 2.2. The signals at 1.6 and 7.3 ppm belong to solvent $CDCl_3$. Then, there are four groups of peaks available in the ^{1}H NMR spectrum centered around 1.17, 2.17, 3.14 and 7.5 ppm. It is known that the area under each peak is obtained from integration of the signal and is proportional to the number of hydrogen nuclei. The integration of each peak at 1.17, 2.17 and 3.14 ppm to 7.5 ppm is nearly 2:3. The multiplet at 1.17 ppm labelled as (a) integrates for four protons of methylene next to aromatic ring. The triplet at 2.17 ppm labelled as (b) integrates for four protons of methylene near to the electron-withdrawing bromine group. The multiplet at 3.14 ppm labelled as (c) integrates for four protons of methylene next to the electron-withdrawing bromine group. The multiplet at around 7.5 ppm labeled as (d), (e) and (f) integrates for six protons of aromatic ring.

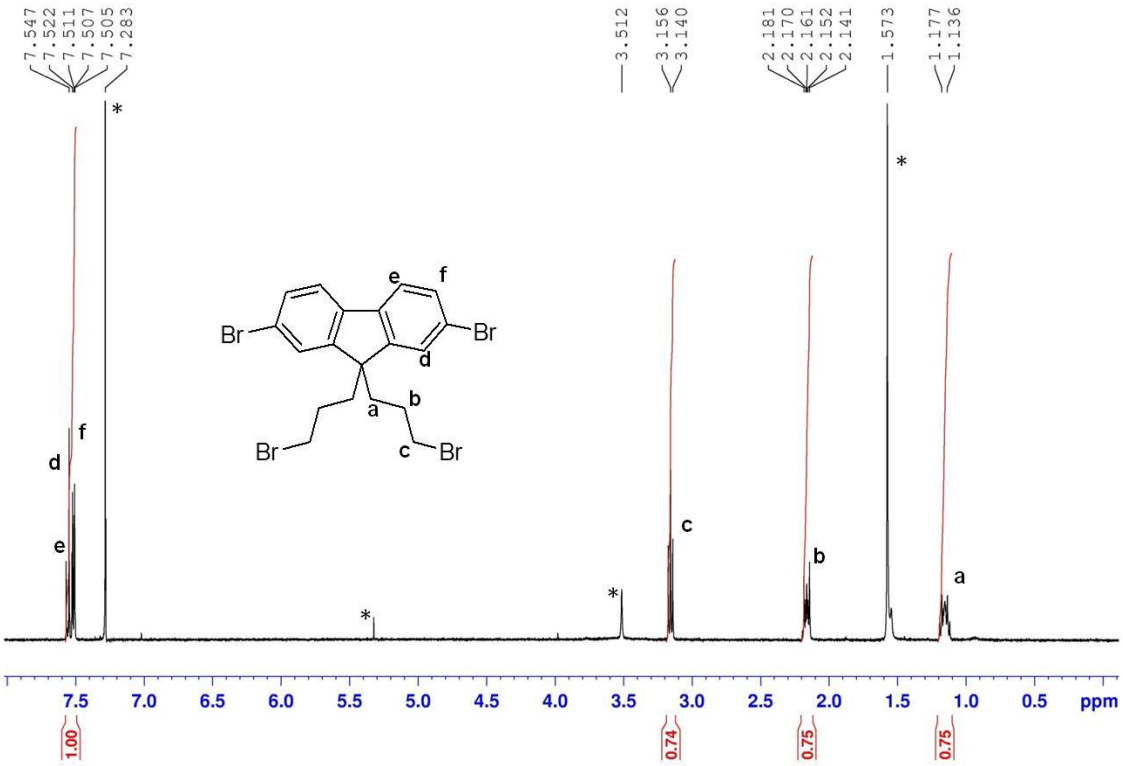

Figure 2.2. ^{1}H-NMR (400 MHz, $CDCl_3$, 25 ^{o}C) spectrum of 2,7-dibromo-9,9-bis(3-bromo-propyl)-9H-fluorene **(M1)** *Denotes for impurities in the solvent.

2.1.2. Synthesis and Characterization of 9,9-bis-(3-bromo-propyl)-2,7-divinyl-9H-fluorene (M2)

9,9-bis-(3-bromo-propyl)-2,7-divinyl-9H-fluorene (M2) was obtained through the synthetic route in Scheme 2.2. The monomer M2 was synthesized via Stille coupling by heating the mixture of 2,7-dibromo-9,9-bis(3-bromo-propyl)-9H-fluorene (M1) and tributylvinyltin in toluene using $PdCl_2(PPh_3)_2$/2,6-di-tert-butylphenol as catalyst at 100 ^{o}C for 24 h. Then, the reaction mixture was treated with 10% (w/w) NaF for further 12 h at room temperature. The isolation and purification of the product was done by work-up with extraction (diethyl ether and distilled water) followed by column chromatography (cyclohexane/chloroform, 8/2, as the eluent). For further purification, the monomer solution in chloroform was precipitated into cold methanol to provide white-yellowish powder in 30% yield.

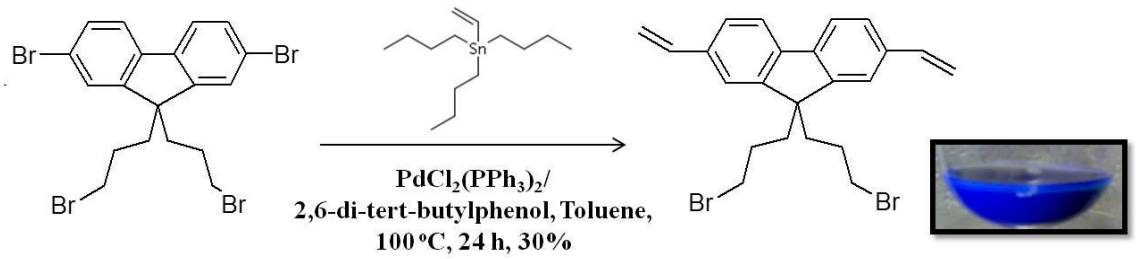

Scheme 2.2. Synthesis of the monomer 9,9-bis-(3-bromo-propyl)-2,7-divinyl-9H-fluorene **(M2)** (inset image represents the reaction medium under 366 nm UV light) via Stille Coupling.

The polymerization reactions in this work go through step-growth mechanism in which bifunctional or multifunctional monomers react to form first dimers, then trimers, then longer oligomers and eventually long chain polymers. Actually, stoichiometry of functional monomers is crucial to get longer polymers. Therefore, the purification of monomers becomes very important to achieve longer chain polymers. As usual, the monomer M2 was purified through column chromatography and checked with thin layer chromatography (TLC) under UV light. At the end of column chromatography, four fractions labelled as M2-A, M2-B, M2-C and M2-D were collected respectively. As shown in Figure 2.3., the one spot on TLC plate under 254 nm UV light belongs to the desired di-substituted monomer, however an additional spot appeared when switched to 366 nm UV light. Although, there are two spots under 366 nm UV light, the below one overlaps with the one under 254 nm light. Therefore, above spot belongs to a different molecule whose structure is very close to the monomer M2. These four fractions were characterized by ^{1}H-NMR spectroscopy and TOF LC/MS, then it was found out that this second spot belongs to mono-substituted monomer. The amount of this molecule decreases in the fractions M2-A to M2-C, then it finishes in M2-D that consists of only the desired monomer M2.

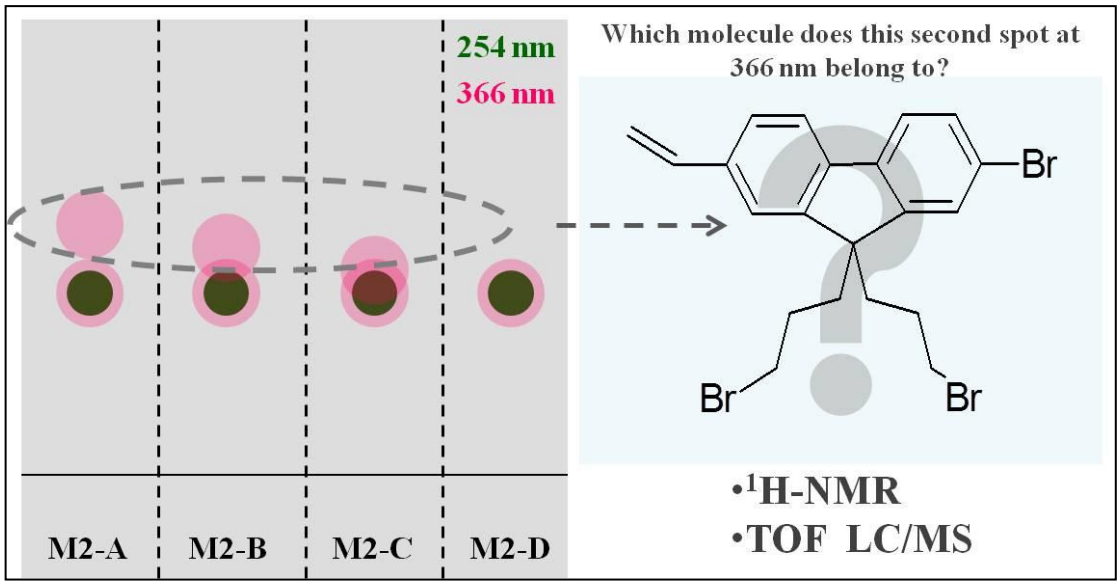

Figure 2.3. Cartoon representation of the spots on TLC plate under 254 and 366 nm UV light for four fractions (M2-A/B/C/D) of 9,9-bis-(3-bromo-propyl)-2,7-divinyl-9H-fluorene **(M2)**.

The comparative ^{1}H-NMR spectra of four fractions is shown in Figure 2.4. The ^{1}H-NMR spectra are very similar to each other except the case in the aromatic region. Although there are small differences in the intensities of the peaks for vinyl and alkyl protons, the easily noticable difference is observed at aromatic region. The intensities of the peaks around 7.5-7.6 ppm gradually decrease through the fraction M2-A to M2-C, then almost dissappear in the spectrum of M2-D. The aromatic protons of fluorene and benzothiadiazole segments are observed as multiplets at 7.4-7.7 ppm. The peaks as multiplets at 6.8, 5.8 and 5.3 ppm are referred to the vinyl protons. The triplet at 3.18 ppm exhibits the presence of deshielded -CH_2 protons due to the presence of electronegative bromine in close proximity. Moreover, the triplet at 2.2 ppm for the protons of methylene near to bromine group and the multiplet at 1.1 ppm for the protons of methylene next to aromatic ring.

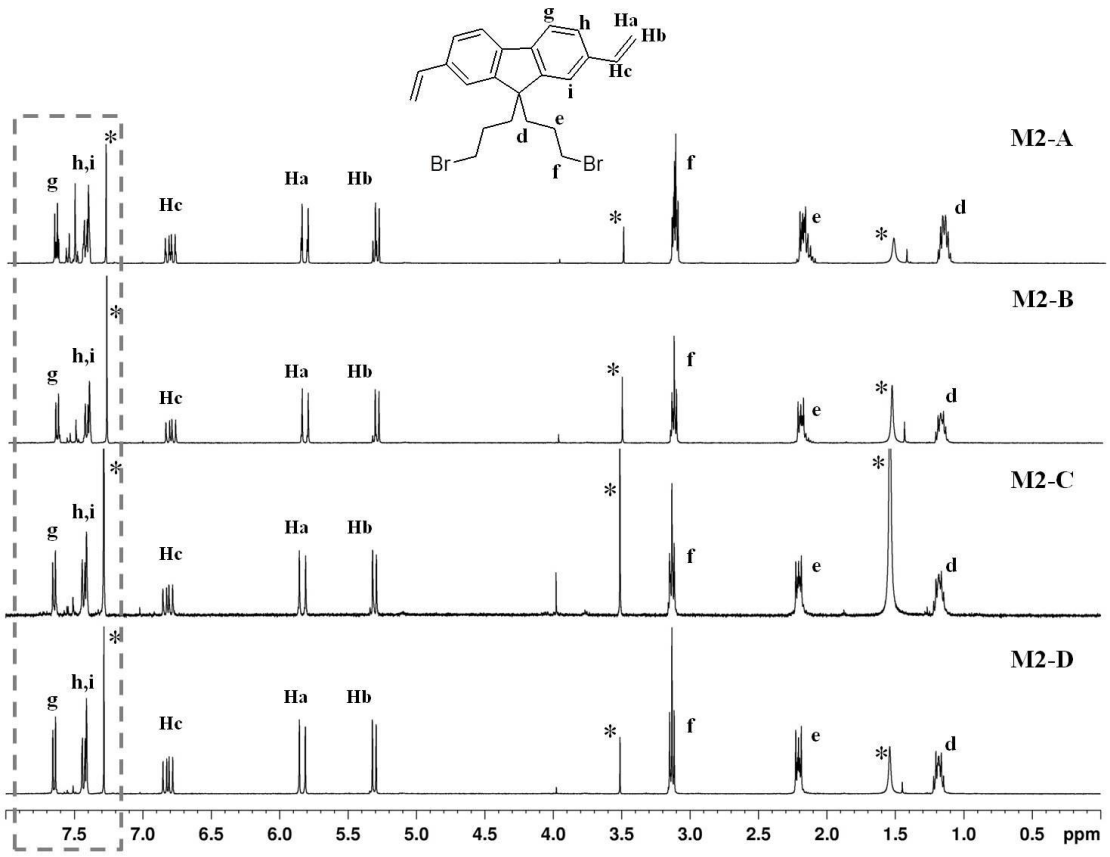

Figure 2.4. ^{1}H-NMR (400 MHz, $CDCl_3$, 25 ^{o}C) spectra of four fractions (M2-A/B/C/D) of 9,9-bis-(3-bromo-propyl)-2,7-divinyl-9H-fluorene **(M2)** *Denotes for impurities in the solvent**.**

TOF LC/MS results shown in Figure 2.5 confirm the arguments in ^{1}H-NMR characterization. . The intensities of the peaks corresponding the mono-subtituted monomer gradually decrease through the fraction M2-A to M2-C, then almost dissappear in M2-D. As a result, M2-D consists of only the desired monomer M2 and has been used for the polymerization reactions.

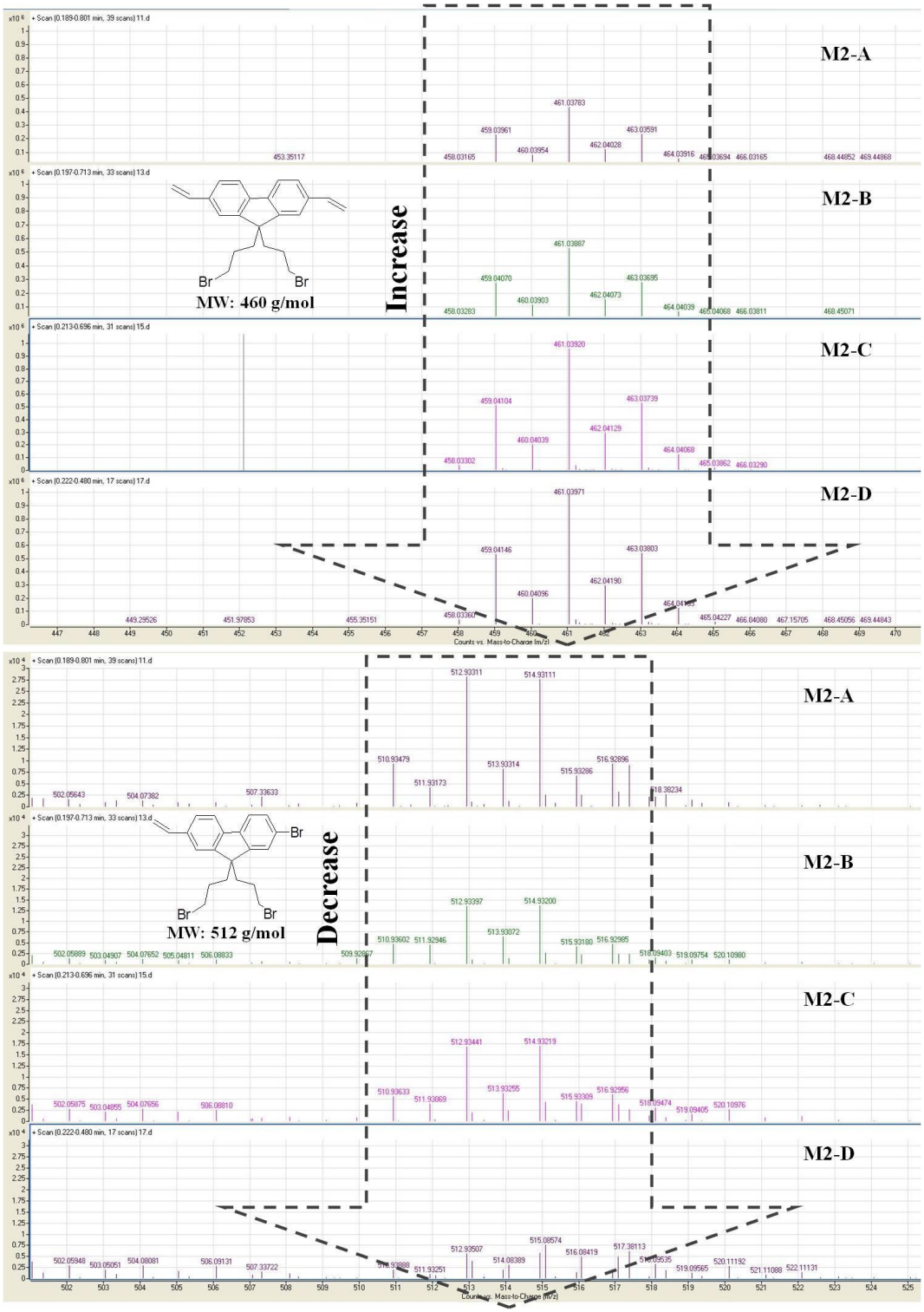

Figure 2.5. TOF LC/MS results of four fractions (M2-A/B/C/D) of 9,9-bis-(3-bromo-propyl)-2,7-divinyl-9H-fluorene **(M2)** (y-axis scale is same for all)**.**

2.1.3. Synthesis and Characterization of 2,7-dibromo-9,9-bis-(propenyl)-9H-fluorene (M3)

2,7-dibromo-9,9-bis(propenyl)-9H-fluorene (M3) was previously synthesized[103] from 2,7-dibromofluorene and allybromide according to Scheme 2.3. As same with the procedure of the monomer M1, 50% (w/w) NaOH solution provided very strong basic condition utilizing the abstraction of weakly acidic C9-H. Then, excess allybromide reacted with the resulting anion by adding to 9-position through nucleophilic substitution reaction. After the isolation and purification of the product, the monomer M3 was obtained with 89% yield.

^{1}H-NMR (400 MHz, $CDCl_3$, δ ppm): 7.52 (m, 6H), 5.21 (m, 2H), 4.89 (m, 4H), 2.68 (t, 4H).

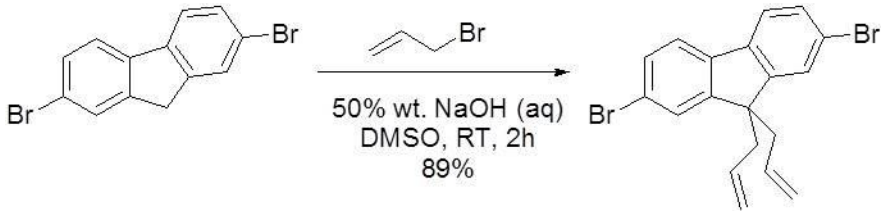

Scheme 2.3. Synthesis of the monomer 2,7-dibromo-9,9-bis-(propenyl)-9H-fluorene **(M3)**.

2.2. Synthesis and Characterization of Polymers

2.2.1. Synthesis and Characterization of Poly[(9,9- bis{propenyl}fluorenyl-2,7-diyl))-co-(1,4-benzo-{2,1,3}-thiodiazole)] (PPFBT)

The polymer PPFBT was previously synthesized[103] using Suzuki coupling reaction of 2, 7-dibromo-9,9-bis-(propenyl)-9H-fluorene and 1,2,3-benzothiadiazole-4,7-bis (boronic acid pinocol ester) as shown in Scheme 2.4. The polymer was purified by the precipitation of the polymer solution in THF into cold methanol to provide orange powder in 60% yield.

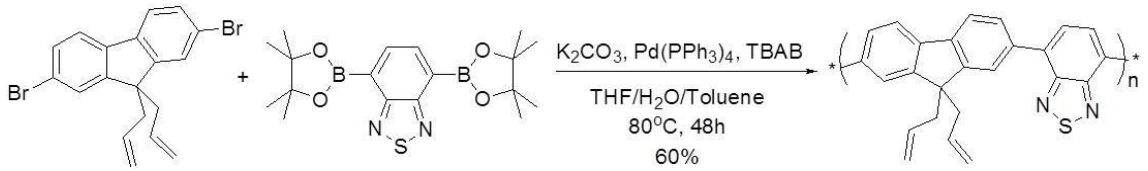

Scheme 2.4. Synthesis of the polymer poly[(9,9- bis{propenyl}fluorenyl-2,7-diyl))-co-(1,4-benzo-{2,1,3}-thiodiazole)] **(PPFBT)** via Suzuki coupling**.**

PPFBT was characterized by ^{1}H-NMR, UV-Vis, Fluorescence and FT-IR spectroscopies. ^{1}H-NMR spectrum of PPFBT is shown in Figure 2.6. Signals observed at around 7.8-8.2 ppm as multiplets are for the aromatic protons of fluorene and benzothiodiazole units. The multiplets at 5.5 ppm and 4.8-5.1 ppm are assigned to the alkenyl protons of allyl group and the signal at 2.8 ppm is due to the –CH_2 protons of allyl group.

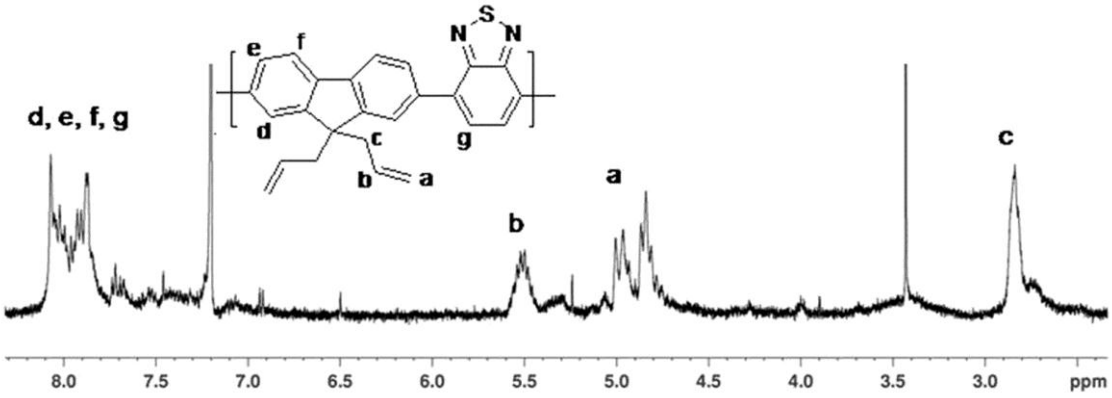

Figure 2.6. ^{1}H-NMR (400 MHz, $CDCl_3$, 25 ^{o}C) spectrum of poly[(9,9-bis{propenyl}fluorenyl-2,7-diyl))-co-(1,4-benzo-{2,1,3}-thiodiazole)] **(PPFBT)**.

FT-IR spectrum of the polymer PPFBT is shown in Figure 2.7. FT-IR spectrum shows a peak at 3074 cm^{-1} for Ph-*H* stretching and characteristic peak of R-CH=CH_2 was observed at 910 cm^{-1} due to out- of - plane C-H bendings**.** Peaks are observed at 1461 cm^{-1}, 2918 cm^{-1} and 1609 cm^{-1} for –C=N stretching in benzothiadiazole moiety and aliphatic –C-H stretching, C=C stretching of benzene rings, respectively.

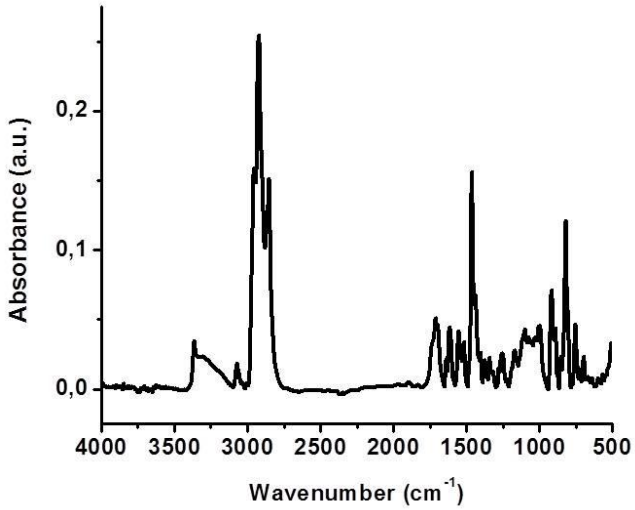

Figure 2.7. FT-IR spectrum of poly[(9,9- bis{propenyl}fluorenyl-2,7-diyl))-co-(1,4-benzo-{2,1,3}-thiodiazole)] **(PPFBT).**

UV-Vis absorption and fluorescence emission properties of the polymer PPFBT in THF are shown in the spectra in Figure 2.8. The maximums of absorption band at 317 and 447 nm and the maximum of fluorescence emission band at 537 nm were observed that it is in the range of green in the visible light.

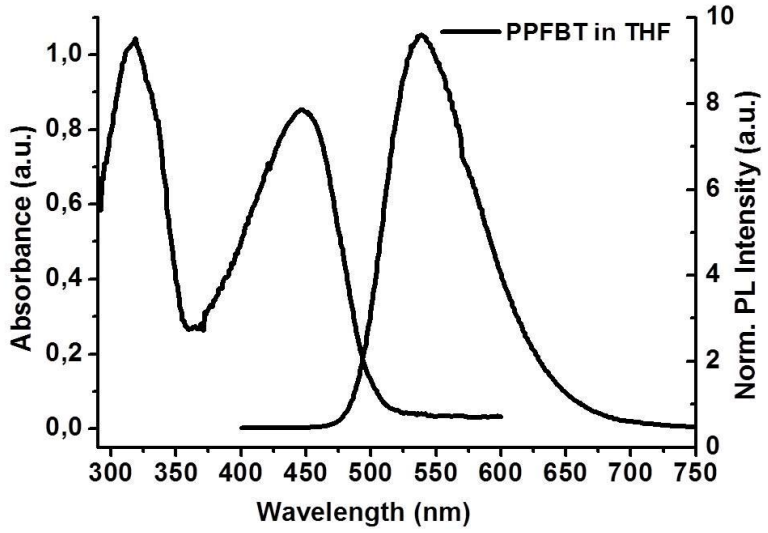

Figure 2.8. UV-vis absorption and fluorescence emission spectra of poly[(9,9-bis{propenyl}fluorenyl-2,7-diyl))-co-(1,4-benzo-{2,1,3}-thiodiazole)] **(PPFBT)** in THF (λ_{ex}=447 nm).

2.2.2. Synthesis and Characterization of Poly[(9,9-bis{3-bromo-propyl}fluorenyl-2,7-divinylene)-co-(1,4-benzo-{2,1,3}-thiodiazole)] (PBPFVBT) and Poly[(9,9-bis{3-azido-propyl}fluorenyl-2,7-divinylene)-co-(1,4-benzo-{2,1,3}-thiodiazole)] (PAPFVBT)

The polymer, poly[(9,9-bis{3-bromo-propyl}fluorenyl-2,7-divinylene)-co-(1,4-benzo-{2,1,3}-thiodiazole)] (PBPFVBT) was synthesized through Heck coupling polymerization shown in Scheme 2.5. In fact, Heck polymerization needs a reaction medium with very basic organic solvent like triethylamine (TEA). However, the reaction temperature is very high (100 ^{o}C) that causes to form insoluble byproducts by the reaction of the monomers with alkyl bromides with basic organic solvent. Therefore, K_2CO_3 was used instead of such basic organic solvent to provide basic reaction medium. By incorporating vinyl bonds within the fluorene and benzothiadiazole segments, red-shift in the fluorescence was obtained via Heck polymerization that PBPFVBT was synthesized by heating the mixture of 9,9-bis-(3-bromo-propyl)-2,7-divinyl-9H-fluorene (M2) and 4,7-dibromo-2,1,3-benzothiadiazole in K_2CO_3/water/DMF using $Pd(OAc)_2$/ PPh_3 as catalyst at 100 ^{o}C for 14 h. The polymer was purified by the precipitation of the polymer solution in THF into cold methanol to provide red powder in 52% yield.

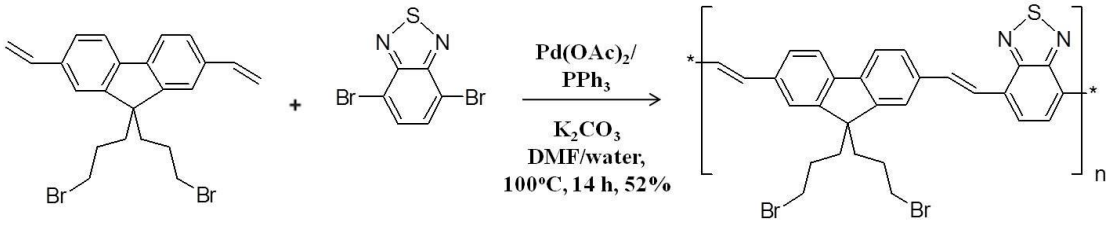

Scheme 2.5. Synthesis of the polymer poly[(9,9-bis{3-bromo-propyl}fluorenyl-2,7-divinylene)-co-(1,4-benzo-{2,1,3}-thiodiazole)] **(PBPFVBT)** via Heck coupling.

PBPFVBT was characterized by ^{1}H-NMR, UV-Vis, Fluorescence and FT-IR spectroscopies.

^{1}H-NMR spectra of PBPFVBT are shown in Figure 2.6. The polymer is soluble in $CDCl_3$ and DMSO-d6, so the spectra in both solvents are given. Some shifts are observed due to solvent effect. The multiplet at 7.5-8.2 ppm are accounting for the aromatic protons of both fluorene and benzothiadiazole segments. The triplet at 3.4 ppm reveals the presence of deshielded -CH_2 protons due to the presence of electronegative bromine in close proximity. The weak peaks as multiplets at 6.8, 5.8 and 5.2 ppm are referred to the resonance of vinyl protons of fluorenylvinylene end groups of PBPFVBT. The polymer is in *trans* configuration since there is no peak at around 6.5 ppm correspondig to resonance peak of *cis* vinyl protons. For biosensor applications, it is beneficial to have *trans* configuration since in additon to providing electron delocalization along the backbone, backbone planarization is achieved that result in red shift of absorption and emission maxima compared to *cis* configuration[23]. Furthermore, there are multiplets observed at 2.1 and 0.9 ppm for the other protons on the alkyl chain constituting the side chain.

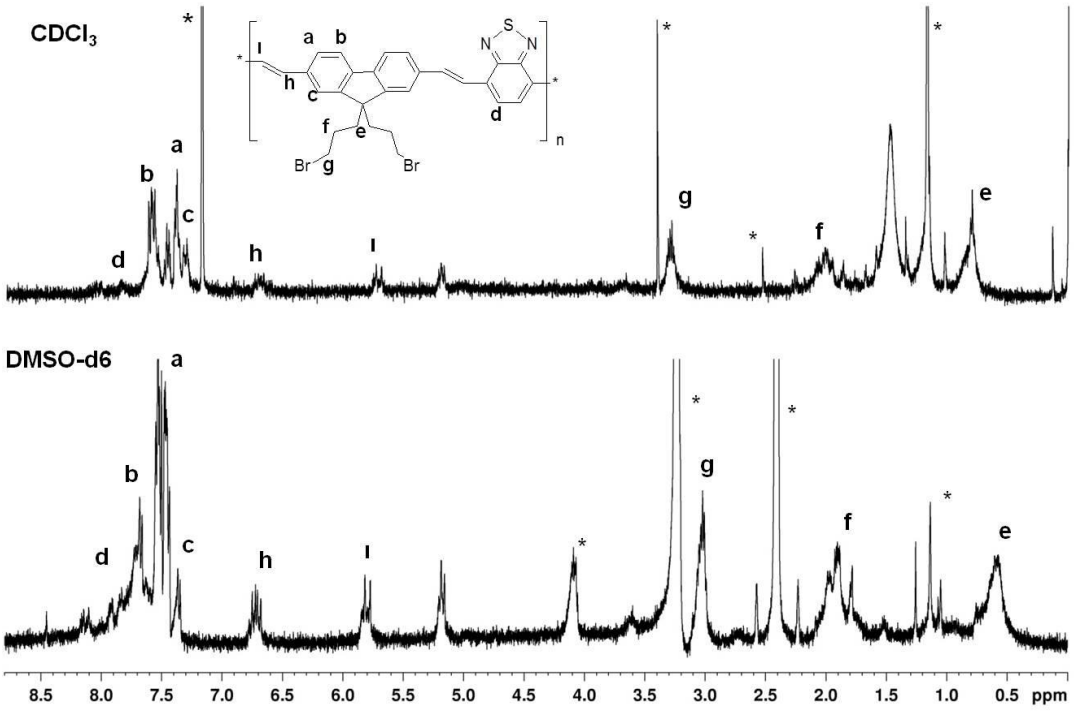

Figure 2.9. ^{1}H-NMR (400 MHz, $CDCl_3${above} and DMSO-d6{below}, 25 ^oC) spectra of poly[(9,9-bis{3-bromo-propyl}fluorenyl-2,7-divinylene)-co-(1,4-benzo-{2,1,3}-thiodiazole)] **(PBPFVBT).**

When the polymer PBPFVBT is dissolved in various solvents having different polarities, a change in color is observed that indicates it solvatochromic property shown in Figure 2.10. PBPFVBT was dissolved in THF, $CHCl_3$, DMF and DMSO in order of increasing polarity that results in red shift. Actually, the polymer has different polarity when it is in ground or excited states, so the stabilization of these states is different when the solvent polarity is changing[104]. Therefore, a change in the energy gap between ground and excited states is observed, such that the gap is decreasing when the solvent polarity is increased.

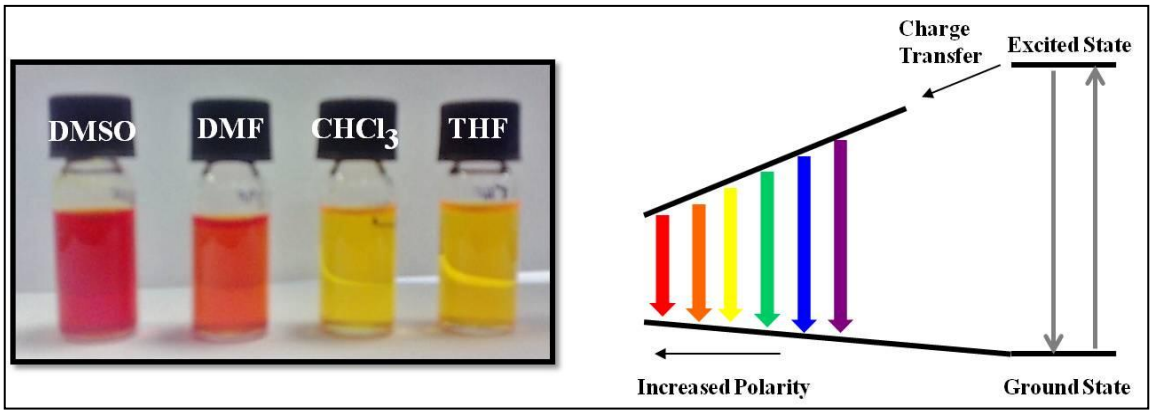

Figure 2.10. Solvatochromic property of poly[(9,9-bis{3-bromo-propyl}fluorenyl-2,7-divinylene)-co-(1,4-benzo-{2,1,3}-thiodiazole)] **(PBPFVBT).**

To eliminate toxic effects for cell culture studies, bromine group of PBPFVBT converted into azide group resulting in poly[(9,9-bis{3-azido-propyl}fluorenyl-2,7-divinylene)-co-(1,4-benzo-{2,1,3}-thiodiazole)] (PAPFVBT). PAPFVBT was synthesized in 83% yield by heating the mixture of PBPFVBT and NaN_3 in DMF using at 60 ^oC for 24 h via nucleophilic substitution reaction.

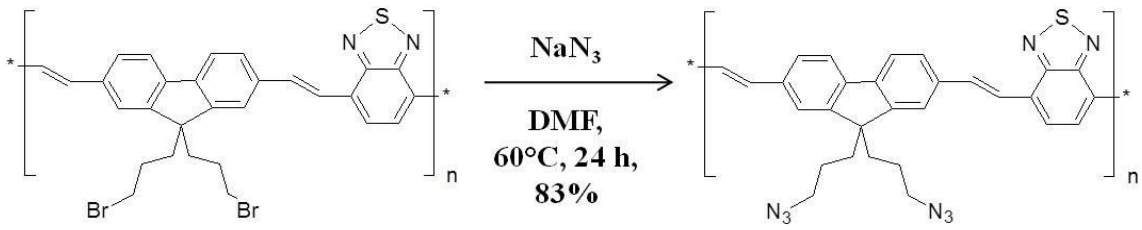

Scheme 2.6. Synthesis of the polymer poly[(9,9-bis{3-azido-propyl}fluorenyl-2,7-divinylene)-co-(1,4-benzo-{2,1,3}-thiodiazole)] **(PAPFVBT)**.

PAPFVBT was characterized by UV-Vis, Fluorescence and FT-IR spectroscopies. In Figure 2.11., the FT-IR spectra of PBPFVBT and PAPFVBT are depicted which they are very similar to each other except for the stretching band of azide at 2020 cm^{-1} confirming the successful functionalization. The aromatic C=C bonds are observed at 1620 cm^{-1}, while a strong peak at 1431 cm^{-1} corresponds to the C-C stretching of the aromatic fluorene backbone of the polymer. The presence of aliphatic C-H stretching is indicated by the peak at 2961 cm^{-1}. C-Br stretching is observed at 822 cm^{-1}. Although NMR spectroscopy is most useful for determining the structure of molecules that provides much more information than F-TIR, FT-IR is very useful to identify functional groups. That's why azide functionalization was proved by FT-IR.

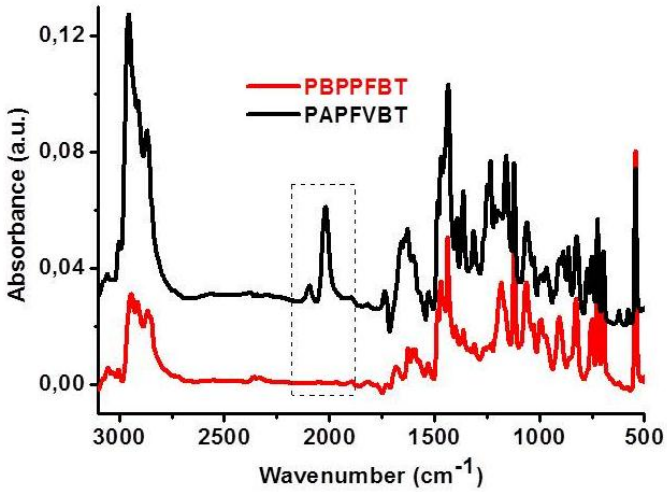

Figure 2.11. FT-IR (KBr pellets) spectra of poly[(9,9-bis{3-bromo-propyl}fluorenyl-2,7-divinylene)-co-(1,4-benzo-{2,1,3}-thiodiazole)] **(PBPFVBT)** and poly[(9,9-bis{3-azido-propyl}fluorenyl-2,7-divinylene)-co-(1,4-benzo-{2,1,3}-thiodiazole)] **(PAPFVBT).**

Optical characterization of the polymers PBPFVBT and PAPFVBT was performed bu UV-Vis and fluorescence spectroscopies. For both polymers, there is a broad absorption band having maxima at 340 and 420 nm. However, 30 nm blue-shift is observed in the emission maximum of azide funtionalized polymer compared to the emission maximum (575 nm) of the polymer with bromine group.

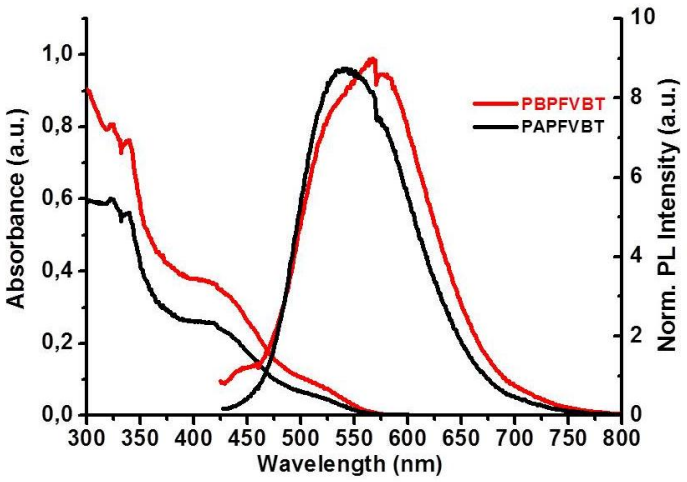

Figure 2.12. UV-vis absorption and fluorescence emission spectra of poly[(9,9-bis{3-bromo-propyl}fluorenyl-2,7-divinylene)-co-(1,4-benzo-{2,1,3}-thiodiazole)] **(PBPFVBT)** and poly[(9,9-bis{3-azido-propyl}fluorenyl-2,7-divinylene)-co-(1,4-benzo-{2,1,3}-thiodiazole)] **(PAPFVBT)** (λ_{ex}=420 nm)**.**

2.3. Synthesis and Characterization of Blank and Drug Loaded Water Dispersible Conjugated Polymer Nanoparticles (CPNs)

Blank and drug loaded conjugated polymer nanoparticles were prepared through a simple reprecipitation method in which the polymer or the mixture of drug and polymer solution in THF (a good solvent) was injected into a large excess of water (a poor solvent) while sonicating. After the removal of THF under reduced pressure, stable nanoparticles in spherical shape were obtained. The main driving forces for the encapsulation of drug by the polymer to form drug-loaded nanoparticles were probably the hydrophobic effect and π-π interaction between aromatic polymer backbone and aromatic rings of drug.

The characterization of nanoparticles was done by the help of DLS and Zeta Potential measurements to determine their sizes and stability, UV-vis and Fluorescence Spectroscopies to investigate their optical properties, SEM, TEM and AFM to assign their morphology.

2.3.1. Synthesis and Characterization of Poly[(9,9- bis{propenyl}fluorenyl-2,7-diyl))-co-(1,4-benzo-{2,1,3}-thiodiazole)] (PPFBT) Nanoparticles

Firstly, the polymer PPFBT was dissolved in THF. The resulting solution was sonicated for 30 min and then injected rapidly into autoclaved double distilled water . It was stirred with sonication for further 30 min. THF was removed under reduced pressure. The resulting nanoparticle solution was concentrated by evaporating its water under reduced pressure. The size of nanoparticles and the zeta potential values were measured as 21.49 nm and -37.6 mV, shown in Figure 2.13.

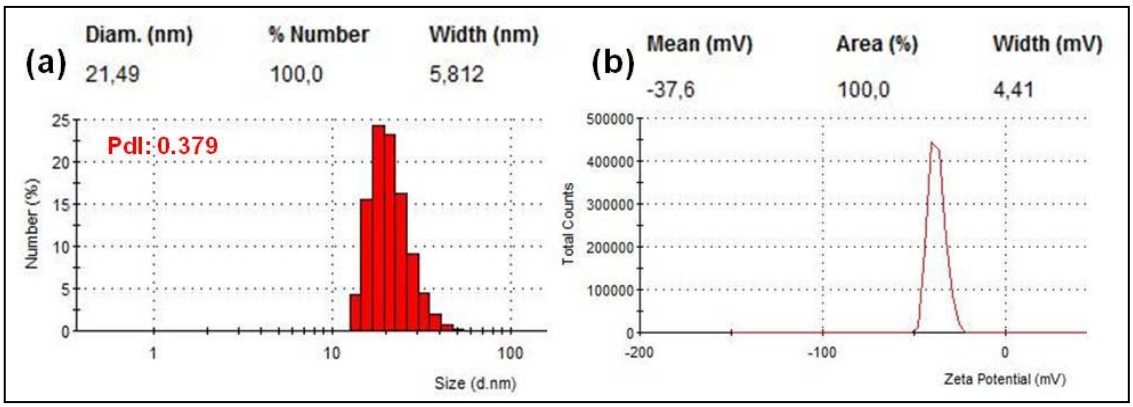

Figure 2.13. (a) Size distrubiton histogram from DLS measurement and **(b)** zeta potential measurement of **PPFBT** Nanoparticles.

Optical characterization of PPFBT nanoparticles was investigated with UV-Vis and fluorescence spectroscopies and compared with the polymer in THF and in solid state (Figure 2.14). Maximum absorption peaks were observed at 317, 447 nm for polymer in THF; these are almost the same for nanoparticle dispersion in water but approximately 10 and 25 nm red shifted for the film of the polymer. However, when nanoparticle dispersion in water were excited with 447 nm light, green-yellow emission band at 550 nm was observed which was 13 nm red shifted compared to the emission band of the polymer in THF. If the emission wavelengths of nanoparticles in water compared with the emission wavelength of the polymer film, it can be seen that only there is 8 nm difference between them (550 nm for nanoparticle dispersion in water and 558 nm for the polymer film) indicating that optical properties of nanoparticles in water resembles to polymer's solid state properties. The quantum yield of the polymer in THF is 70%, while it becomes 26% when nanoparticle formation in water[103].

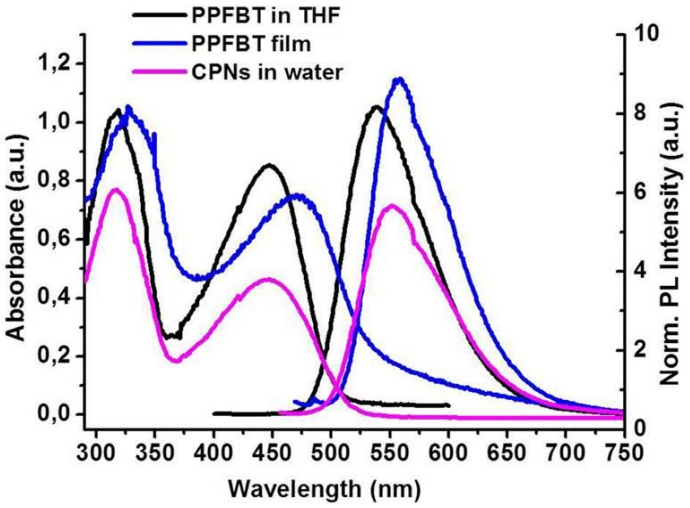

Figure 2.14. UV–vis absorption and fluorescence emission spectra of **PPFBT** in THF ($\lambda_{exc.}$= 447 nm), as film ($\lambda_{exc.}$= 472 nm) and as dispersions of the nanoparticles in water ($\lambda_{exc.}$= 447 nm).

The red shift of emission maximum for CPNs compared to polymer in THF shows the aggregation of polymer chains upon nanoparticle formation in water. As a result of aggregation, the overlap of π-orbitals increases, then followed by π-electrons delocalization across the chains. The lower band gaps, observed by red shift, are the sign of this delocalization[41,50-52]. Similarly, the red shift of emission maximum for the solid state of polymer is the result of tight packing of polymer chains[44].

2.3.1.1. Cell Viability of PPFBT Nanoparticles

Dose dependent *in vitro* cytotoxicity test of the blank PPFBT nanoparticles (~22 nm) against Huh7 cells were performed through SRB assay and the results were plotted as in Figure 2.15. The cytotoxicity assay of the blank nanoparticles indicates that they are not toxic to the Huh7 cells up to 25 μM at the end of 72 h. Therefore, their convenience for further studies on cell imaging and the drug delivery is proven.

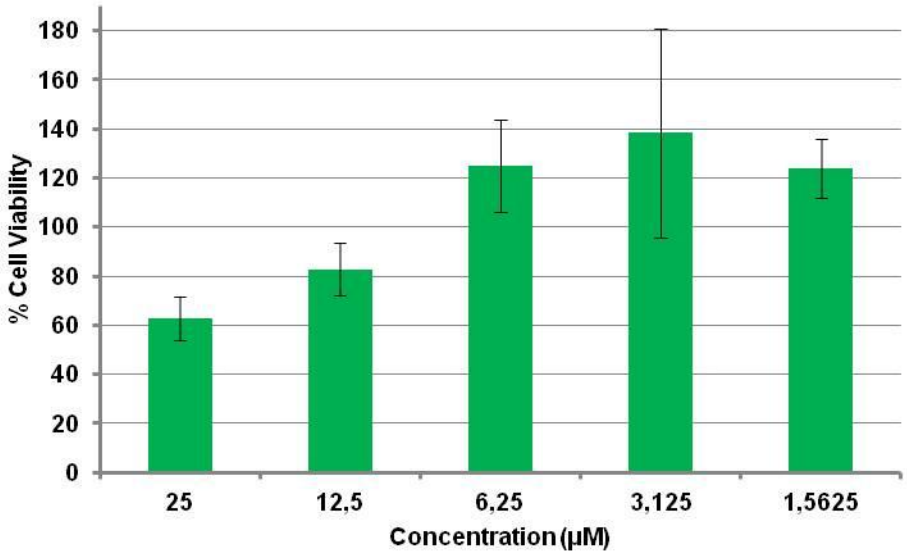

Figure 2.15. Percent cell viability results of **PPFBT** nanoparticles having concentrations of 25, 12.5, 6.25, 3.125, 1.5625 µM after 72 h incubation.

2.3.2. Synthesis and Characterization Drug Loaded PPFBT Nanoparticles

2.3.2.1. Determination of Loading Efficiency: Synthesis and Characterization of Anthracene(ANT)-Loaded PPFBT Nanoparticles

Anthracene was chosen for having aromatic rings like Camptothecin in order to be a positive control in the determination of drug loading efficiency. PPFBT and ANT were dissolved in THF and the resulting solution was injected into rapidly stirring water. After the removal of THF, ANT-loaded nanoparticles were obtained. In order to determine the optimum loading capacity of nanoparticles, the ratios of PPFBT to ANT (w:w) 25:1 and 5:1 were used during the nanoparticle preparation. In each case, after the nanoparticle formation, the dispersion was filtered through to remove the unencapsulated ANT. The size of nanoparticles and the zeta potential values were measured as 21.00 nm and -38.2 mV for the one with the ratio of 25:1, as 21.52 nm and -41.9 mV for the one with the ratio of 5:1, shown in Figure 2.16.

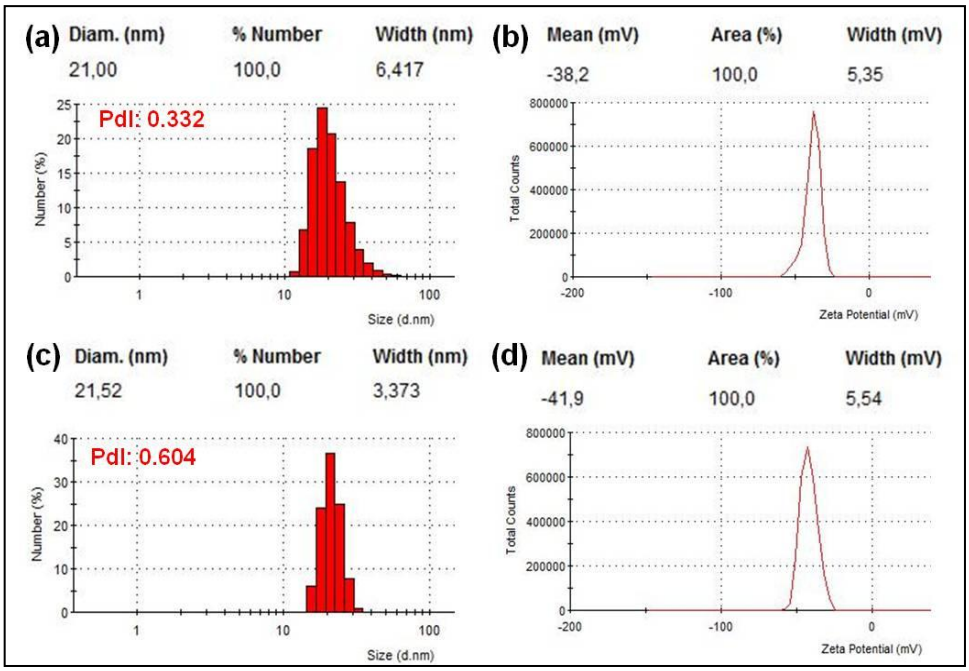

Figure 2.16. Size distribution histograms from DLS measurements of (ANT)-loaded PPFBT nanoparticles having the ratios PPFBT to ANT (w:w) 25:1 **(a)** and 5:1 **(c)** ; Zeta potential measurements of (ANT)-loaded PPFBT nanoparticles having the ratios PPFBT to ANT (w:w) 25:1 **(b)** and 5:1 **(d).**

The synthesis of anthracene (ANT)-loaded PPFBT nanoparticles and the determination of the optimum loading efficiency of the nanoparticles are illustrated in Figure 2.17. In the first step, UV-vis and PL spectra of PPFBT to ANT in various ratios dissolved in THF were recorded. These spectra were compared with the spectra of only ANT in THF and only PPFBT in THF. Some parts of the absorption peaks of ANT and PPFBT overlap, so the presence of ANT in the mixtures can be seen as shoulders on the peaks of PPFBT. The intensity of the shoulders increases when the amount of ANT increases (such as the one with the ratio of 5:1). However, the emission peaks of each ANT and PPFBT can be easily distinguishable in the mixtures. As expected, the intensity of ANT decreases when its portion in the mixture decreases. In the second step, the solutions prepared in the first step were injected into water. Then, THF was removed and the dispersion was filtered through filter papers. The residue on the filter paper was dissolved in THF and analyzed via UV-vis and fluorescence spectroscopy by following the absorption and emission maxima of ANT. As it can be seen from both of the absorption and PL spectra, the residue of the dispersion with 5:1 ratio consists of only unencapsulated ANT while all of the ANT is encapsulated in the one with 25:1 ratio.

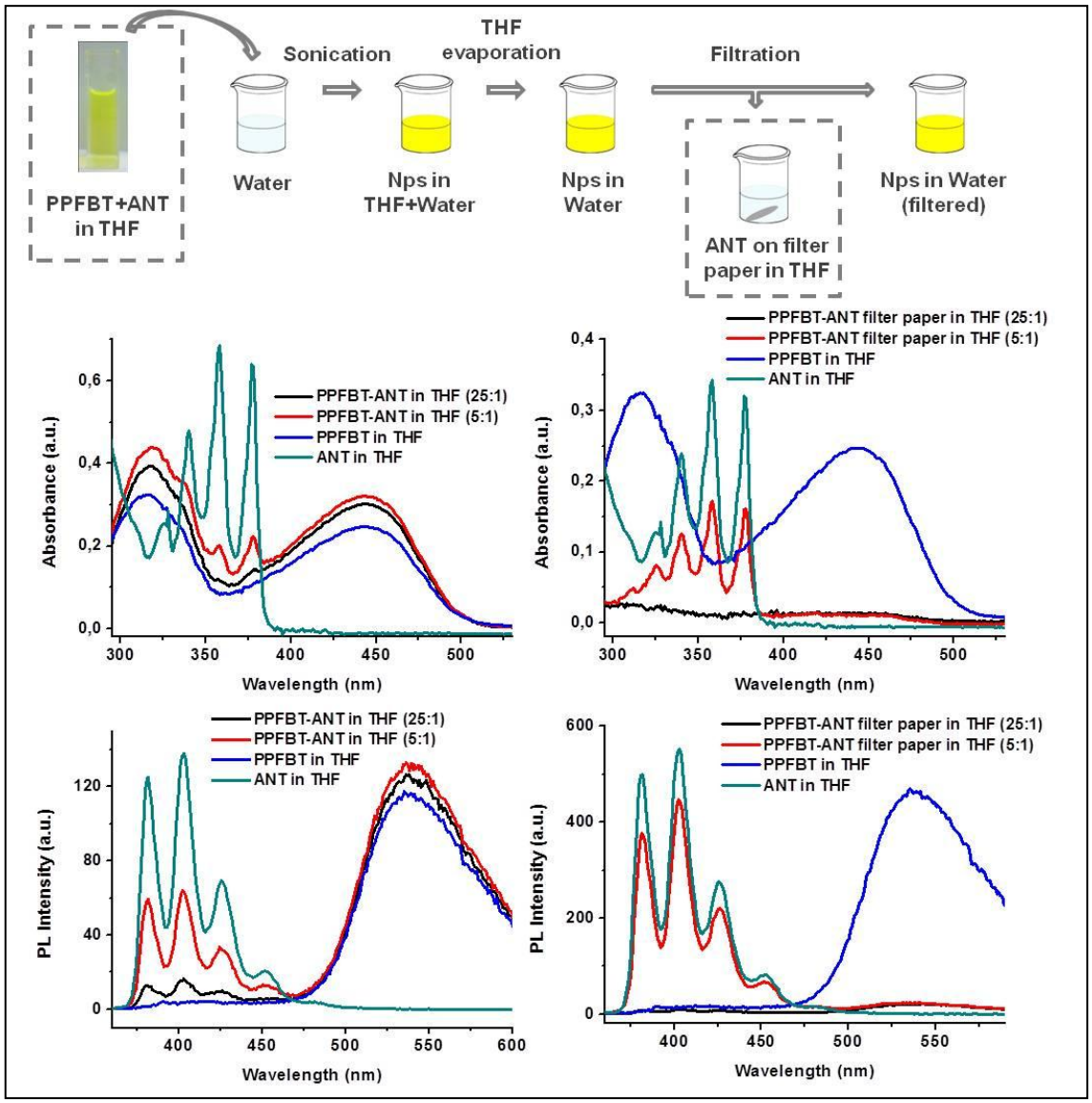

Figure 2.17. The cartoon representation of the synthesis of anthracene (ANT)-loaded PPFBT nanoparticles and the determination of the optimum loading efficiency of the nanoparticles. UV-Vis absorption and fluorescence emission spectra of PPFBT to ANT in various ratios dissolved in THF and the precipitate on the filter papers dissolved in THF ($\lambda_{exc.}$= 350 nm).

Moreover, the amount of unencapsulated ANT was determined via the calculation of the area under fluorescence emission curves. In Figure 2.18, firstly UV-Vis absorption and fluorescence emission spectra of ANT with increasing its amount were recorded, then a calibration curve called fit curve was obtained from the area of fluorescence emission curves (between 370 and 462 nm) versus the amount of ANT. The absorption curves could not be used for this purpose because of overlapping of the absorption peaks of ANT and PPFBT. Secondly, the area under the emission curves of the residue on the filter papers were calculated and then the resulting values were put in the linear equation of fit curve to find out the amount of unencapsulated ANT, so then the encapsulated portion. The mole of encapsulated ANT to the mole of polymer was found as 8% and 4% for the dispersions with 5:1 and 25:1 ratios, respectively. Although the capacity of encapsulation is up to 8%, it is guaranteed to encapsulate all by preparing the dispersions with the quantities resulting 4%. Finally, the loading efficiency was determined by the weight percent of encapsulated ANT to initally added ANT through nanoparticle formation so it was determined to be 100% when PPFBT to ANT ratio was 25:1.

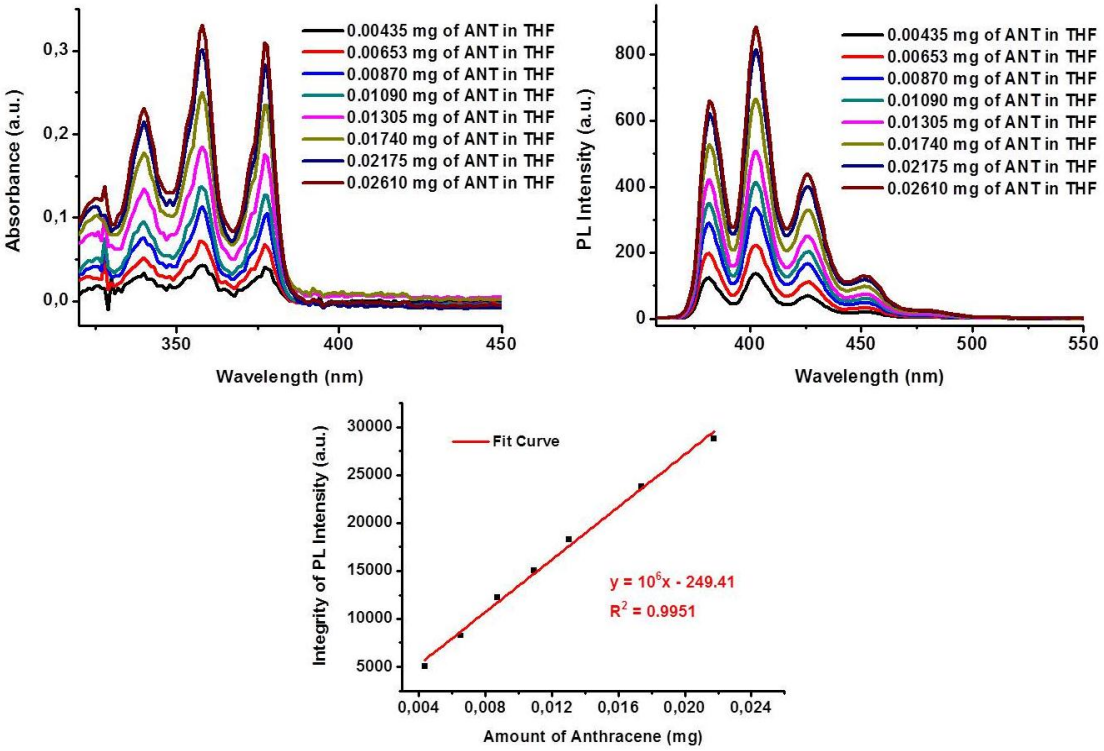

Figure 2.18. UV-Vis absorption and fluorescence emission spectra of Anthracene (ANT) while increasing its amount (λ_{ex}=350 nm). The below fit curve represents the area of fluorescence emission curves (between 370 and 462 nm) vs. the amount of ANT.

2.3.2.2. Determination of Drug Loading Efficiency: Synthesis and Characterization of Camptothecin (CPT)-Loaded PPFBT Nanoparticles

A similar approach to the work on ANT loading was followed to determine the drug loading efficiency by encapsulating CPT. PPFBT and CPT were dissolved in THF and the resulting solution was injected into rapidly stirring water. After the removal of THF, drug-loaded nanoparticles were obtained. This time, the ratios of PPFBT to CPT (w:w) 25:1, 15:1 and 10:1 were used during the nanoparticle preparation. In Figure 2.19, the size and the zeta potential values of nanoparticles were measured as 24.69, 23.33, 23.78 nm and -33.1, -46.19/-18.0, -39.7/-59.1 for the ones with the ratio of 25:1, 15:1 and 10:1, respectively.

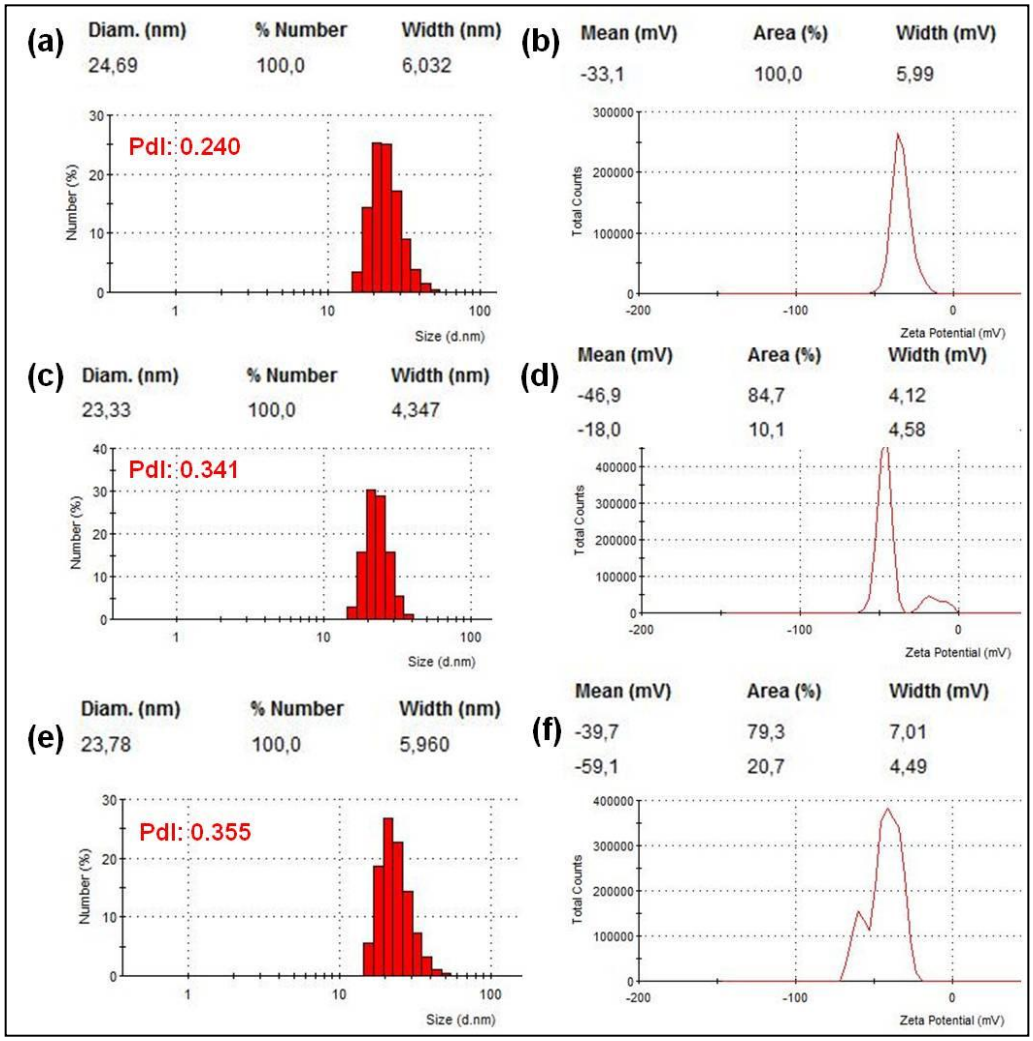

Figure 2.19. Size distribution histograms from DLS measurements of (CPT)-loaded PPFBT nanoparticles having the ratios PPFBT to CPT (w:w) 25:1 **(a)** 15:1 **(c)** and 10:1 **(e)** ; Zeta potential measurements of (CPT)-loaded PPFBT nanoparticles having the ratios PPFBT to CPT (w:w) 25:1 **(b)** 15:1 **(d)** and 10:1 **(f).**

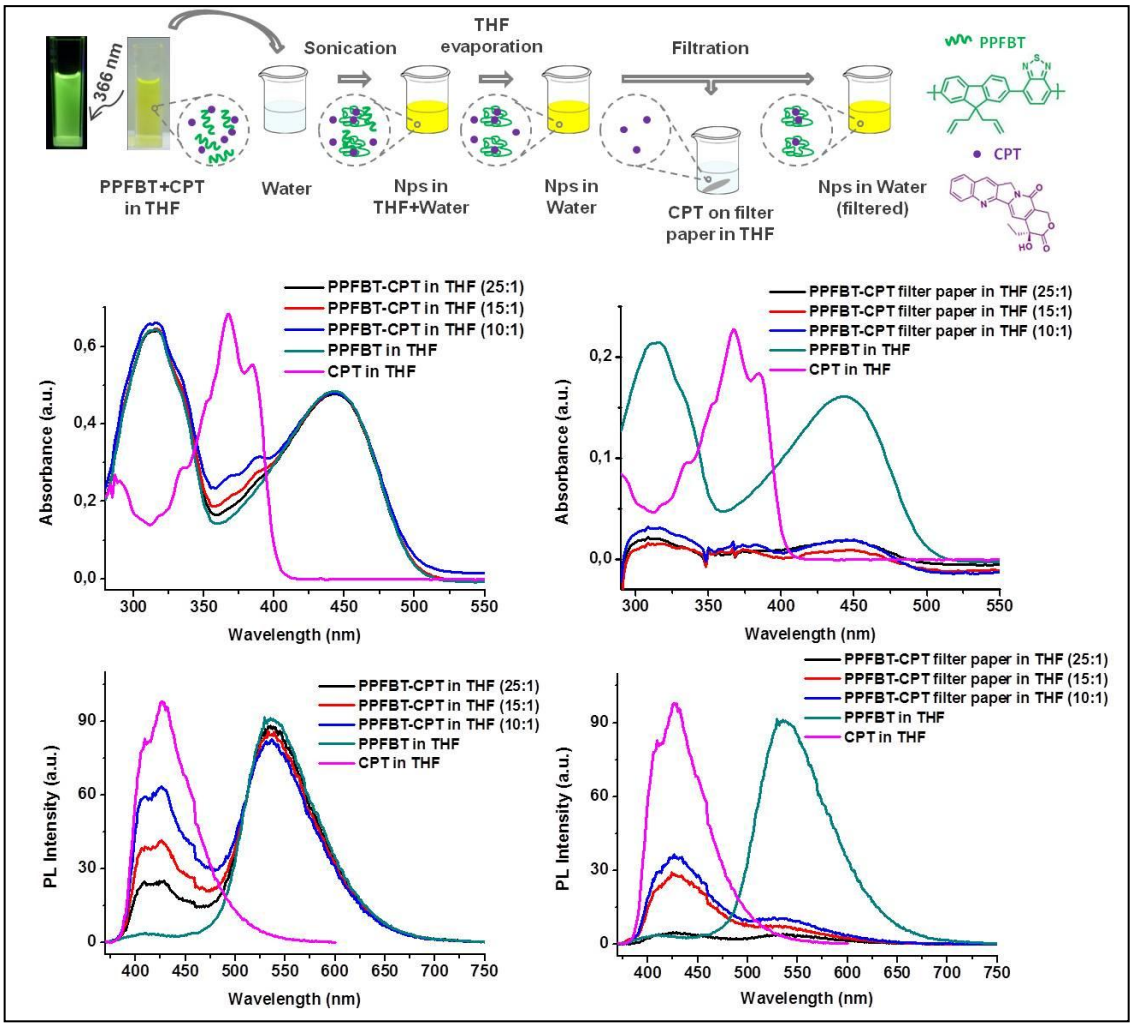

Figure 2.20. The cartoon representation of the synthesis of camptothecine (CPT)-loaded PPFBT nanoparticles and the determination of the optimum drug loading efficiency of the nanoparticles. UV-Vis absorption and fluorescence emission spectra of PPFBT to CPT in various ratios dissolved in THF and the precipitate on the filter papers dissolved in THF ($\lambda_{exc.}$= 365 nm).

The synthesis of CPT-loaded PPFBT nanoparticles and the determination of the optimum loading efficiency of the nanoparticles are illustrated in Figure 2.20. In the first step, UV-vis and PL spectra of PPFBT to CPT in various ratios dissolved in THF were recorded. These spectra were compared with the spectra of only CPT in THF and only PPFBT in THF. Like in the case of ANT, some parts of the absorption peaks of CPT and PPFBT overlap , so the presence of CPT in the mixtures can be seen as shoulders on the peaks of PPFBT. The intensity of the shoulders increases when the amount of CPT increases through 25:1 to 10:1 ratios. Although, there is small overlap in the end of CPT emission peak and the start of PPFBT emission peak, the emission

bands of each one can be easily distinguishable in the mixtures. As expected, the intensity increases when the amount of CPT increases through 25:1 to 10:1 ratios. In the second step, the solutions prepared in the first step were injected into water. Then, THF was removed and the dispersion was filtered through filter papers. The residue on the filter paper was dissolved in THF and analyzed via UV-vis and fluorescence spectroscopy by following the absorption and emission maxima of CPT. As it can be seen from the PL spectra, all of the drug was encapsulated in the dispersion with 25:1 ratio.

In Figure 2.21, UV-Vis absorption and fluorescence emission spectra of CPT with increasing its amount are recorded, then fit curve was obtained from the area of fluorescence emission curves versus the amount of CPT. Secondly, the area under the emission curves of the residue on the filter papers were calculated and then the resulting values were put in the linear equation of fit curve to find out the amount of unencapsulated drug, so then the encapsulated portion. The mole of encapsulated CPT to the mole of polymer was found as 11%, 7% and 4% for the dispersions with 10:1, 15:1 and 25:1 ratios, respectively. Actually, it is highly possible to encapsulate all of the drug by preparing the dispersions with the quantities resulting 4%.

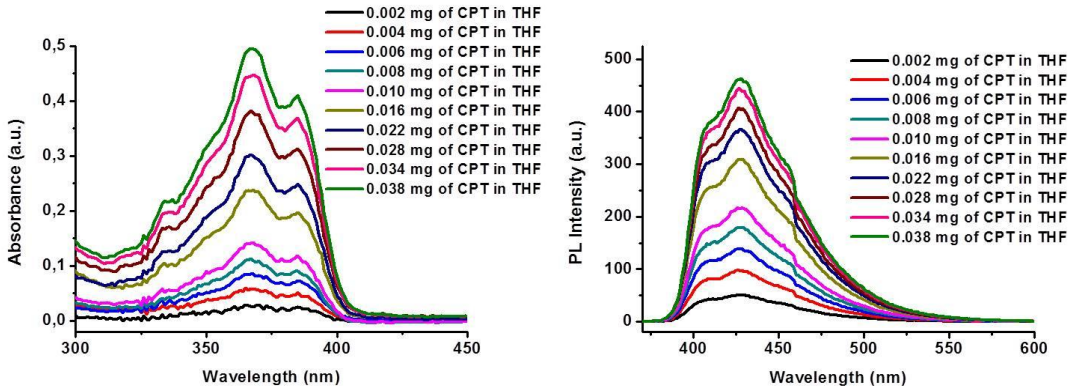

Figure 2.21. UV-Vis absorption and fluorescence emission spectra of Camptothecin (CPT) while increasing its amount (λ_{ex}=365 nm).

The CPT loading efficiency in the nanoparticles was determined to be 100% when a polymer to drug ratio of 25:1 was used. This was also supported by an additional experiment in which the water of the CPT-loaded nanoparticles after filtration was evaporated off and the remaining residue was dissolved in DMSO-d6 and analyzed by ^{1}H-NMR spectroscopy shown in Figure 2.22. As the main difference between these spectra, the CPT peaks at positions (h), (i), (j), (k) and (l) can be clearly observed in the spectrum of drug loaded nanoparticle dispersion (above).

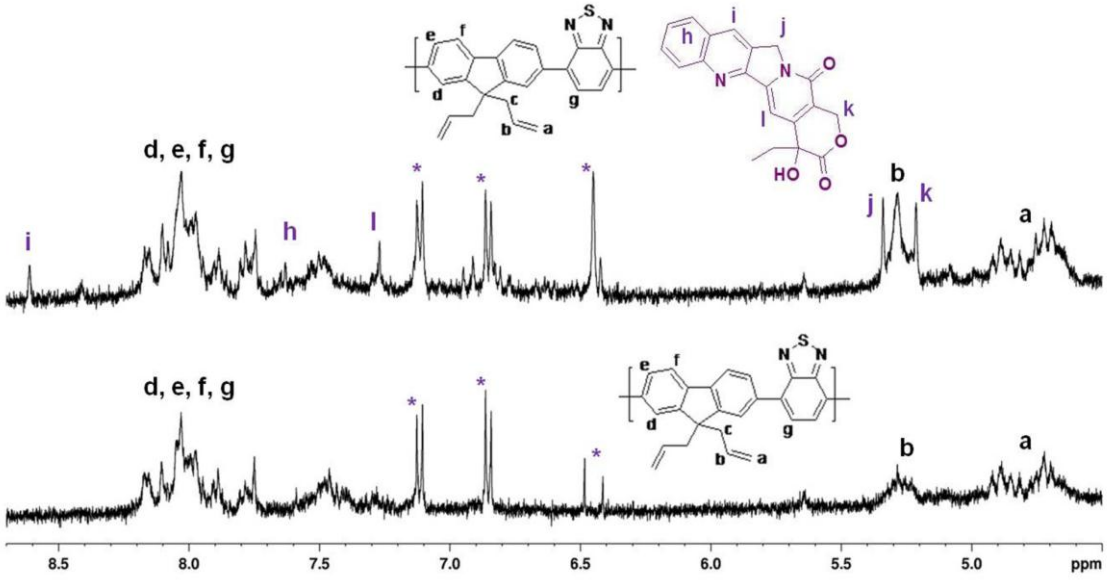

Figure 2.22. ^{1}H-NMR (400 MHz, DMSO-d6, 25 °C) spectra of the remaining residue of PPFBT nanoparticles and filtrated CPT-loaded PPFBT nanoparticles after evaporation off (*denotes for impurities).

Optical characterization of the nanoparticles with drug to polymer ratio of 25:1 was done by UV-Vis and fluorescence emission spectroscopies. In Figure 2.23, the absorption and emission spectra of nanoparticle dispersion in water were compared with the spectra of only CPT in water and only blank nanoparticles in water. Aqueous CPT has absorption maximum at 365 nm, and blank nanoparticles has absorption maxima at 317 and 447 nm (Figure 2.23.(a)). When they are excited at 447 nm (Figure 2.23 (c)), the emission maxima of the nanoparticle dispersion is observed at around 537 nm, however the emission peak of CPT could not be observed. When they are excited at 365 nm (Figure 2.23 (b)), the emission maxima of CPT is observed at around 426 nm, but this time the emission peak of the nanoparticle dispersion dissappears.

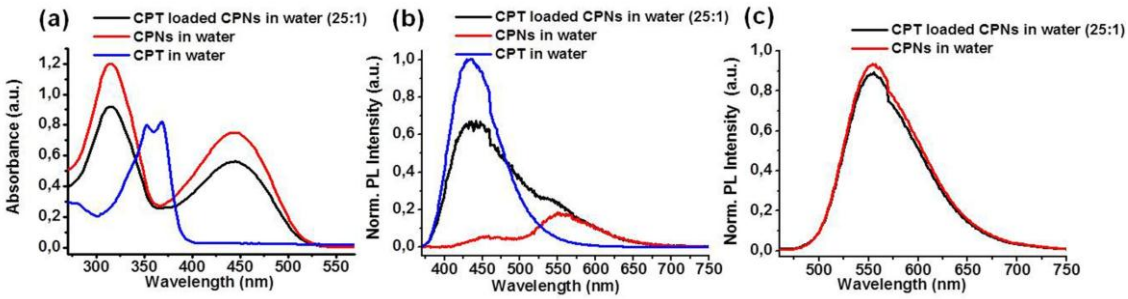

Figure 2.23. UV–vis absorption and fluorescence emission spectra of CPT-loaded PPFBT nanoparticles , PPFBT nanoparticles and CPT as dispersions in water (b) $\lambda_{exc.}$= 365 nm (c) $\lambda_{exc.}$= 447 nm.

2.3.2.3. Synthesis and Characterization of Camptothecin (CPT)-Loaded PPFBT Nanoparticles as a Drug Carrier and a Fluorescent Probe for Cell Imaging

After the CPT loading efficiency in the nanoparticles was determined to be 100% when a polymer to drug ratio of 25:1 was used, the synthetic conditions were kept constant for drug loaded nanoparticles that would be used for cell studies. The syntheses of blank and CPT-loaded nanoparticles were repeated three times. Their size were determined by dynamic light scattering (DLS) measurements (Figure 2.24) and the averages of three different DLS measurements were calculated as 25.50±0.76 nm for blank nanoparticles and 24.38±1.37 nm for drug loaded nanoparticles by dynamic light scattering measurements (Table 1). The morphologies of blank nanoparticles and CPT loaded nanoparticles were revealed by TEM and AFM (Figure 2.26) imaging techniques. The zeta potential values were measured as -51.17±2.16 and -29.80±6.52 mV for blank nanoparticles and -40.70±4.82 mV for CPT loaded nanoparticles (Figure 2.25 and Table 1), which indicate the formation of stable nanoparticle dispersion caused by the repulsion between the nanoparticles. As can be seen from the DLS measurements, no significant changes were observed in their diameters, indicating that the structural integrity of nanoparticles were not affected when they are loaded with drug.

		Batch 1	Batch 2	Batch 3	Average	St.Deviation	
PPFBT Np	Size	24.68	25.65	26.18	25.50	0.76	**25.50 ±0.76**
	Zeta Potential	-52.7	-52.1	-48.7	-51.17	2.16	**-51.17±2.16**
		-22.6	-35.3	-31.5	-29.80	6.52	**-29.80±6.52**
PPFBT-CPT Np	Size	22.86	25.52	24.77	24.38	1.37	**24.38 ±1.37**
	Zeta Potential	-36.3	-45.5	-38.4	-40.07	4.82	**-40.07±4.82**

Table 1. Size and Zeta potential values of PPFBT nanoparticles and CPT-loaded PPFBT nanoparticles.

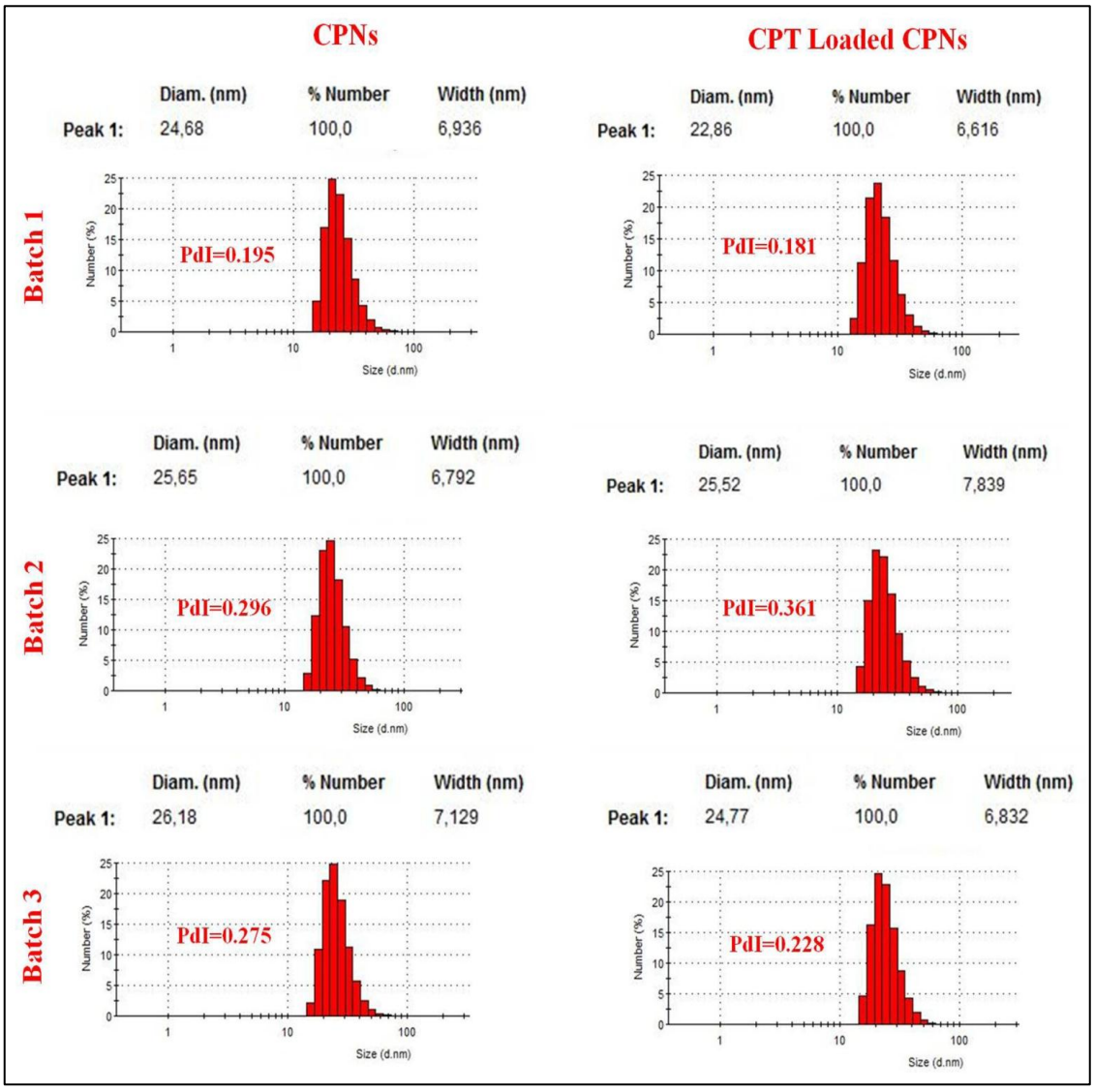

Figure 2.24. Size distribution histograms from DLS measurements of PPFBT nanoparticles and CPT-loaded PPFBT nanoparticles.

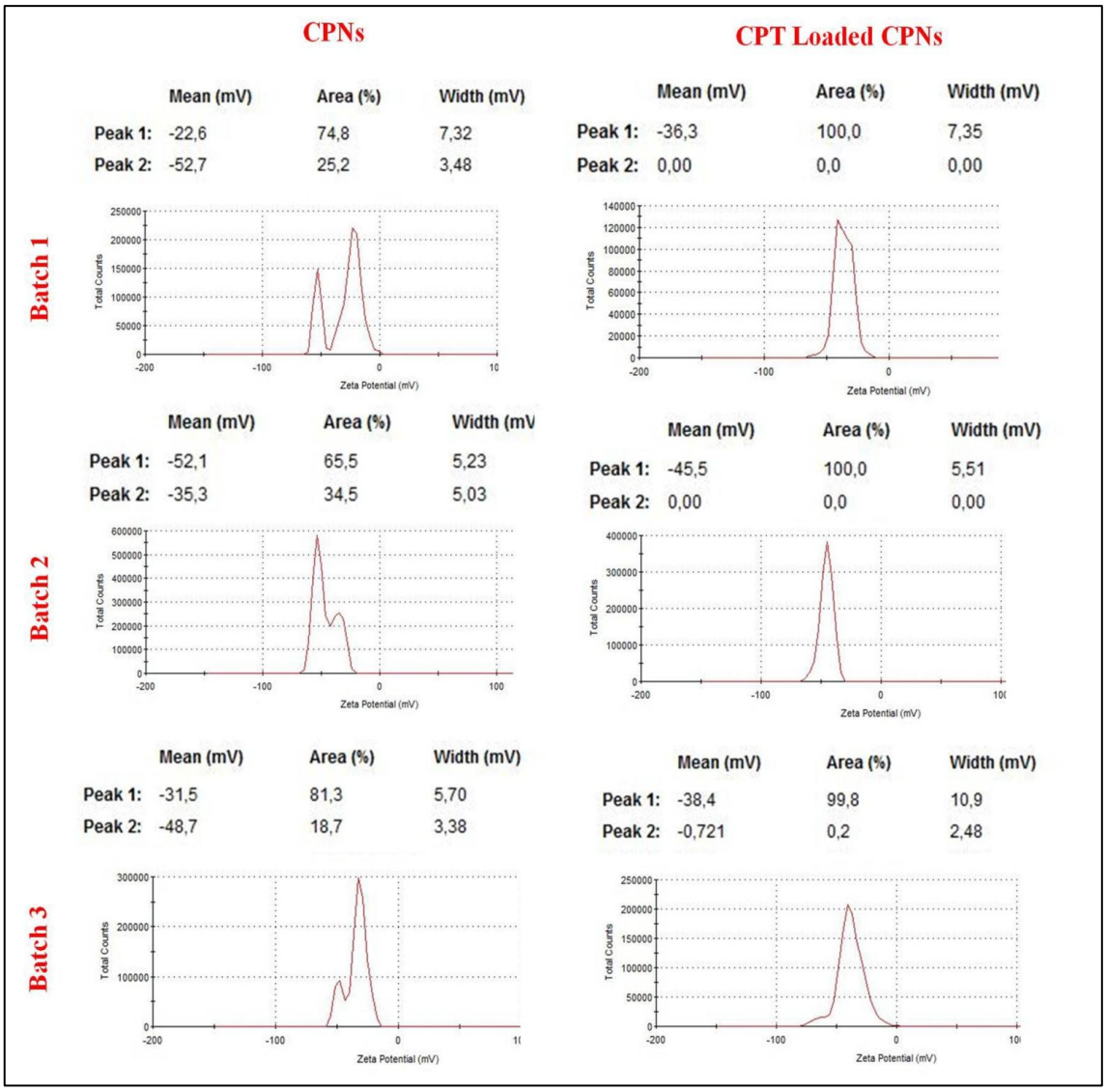

Figure 2.25. Zeta potential measurements of PPFBT nanoparticles and CPT-loaded PPFBT nanoparticles**.**

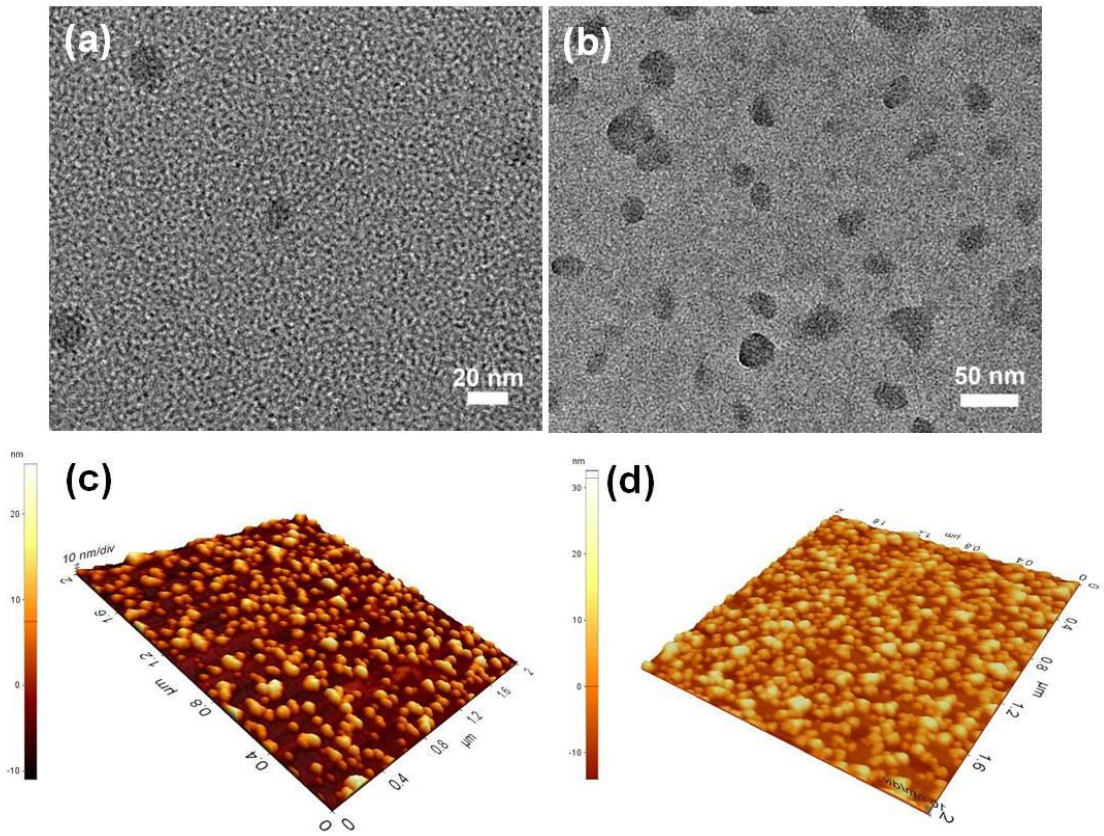

Figure 2.26. TEM images of PPFBT nanoparticles **(a)** and CPT-loaded PPFBT nanoparticles **(b).** AFM images of PPFBT nanoparticles **(c)** and CPT-loaded PPFBT nanoparticles **(d).**

Fluorescence microscope images of CPT-loaded PPFBT nanoparticles and Huh7 cells incubated with blank and (CPT)-loaded PPFBT nanoparticles are shown in Figure 2.27. The bright green CPN emission is the evidence for the efficent cellular uptake of these small nanoparticles, even for very short incubation time (24 h). These nanoparticles were accumulated in cytoplasm and around the nucleus.

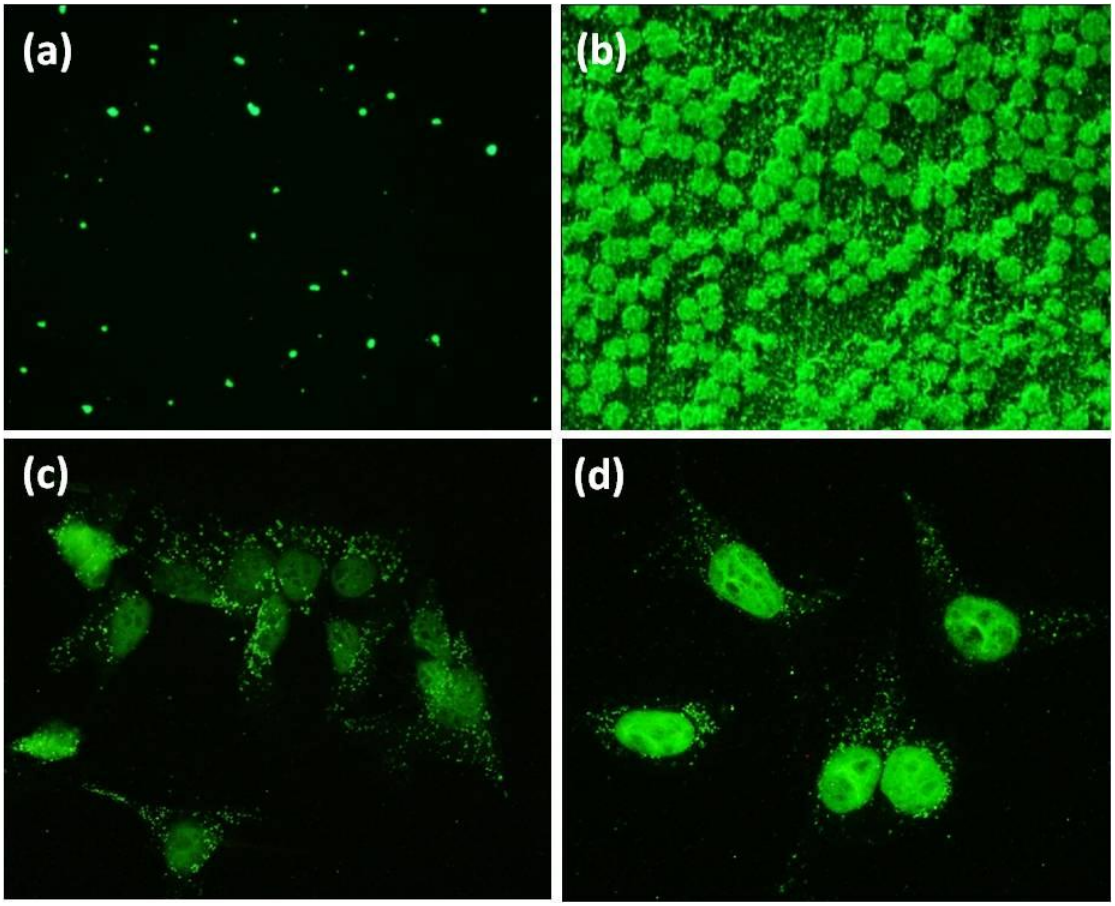

Figure 2.27. Fluorescence microscope images (40x) of CPT-loaded PPFBT nanoparticles having concentrations of PPFBT as 0.04 mg / mL **(a)** and 0.75 mg / mL **(b)**; Huh7 cells incubated with PPFBT nanoparticles ([PPFBT]=25 μM) **(c)** and (CPT)-loaded PPFBT nanoparticles ([PPFBT]=6.25 μM, [CPT]=0.25 μM) **(d)** after 24 h.

Time and dose dependent *in vitro* cytotoxicity tests of the blank CPNs, CPT loaded CPNs and free CPT against Huh7 cells were performed through SRB assay and the results were plotted as in Figure 2.28 a and b. In this experimental set-up, free CPT was used as a positive control and DMSO and blank CPNs were used as negative controls to CPT loaded CPNs. At the end of 48 h, the IC_{50} of free CPT and CPT loaded CPNs were calculated to be 0.9 μM and 0.1 μM respectively, corresponding to that CPT loaded CPNs are 9 times more effective than free CPT. However, at the end of 72 h, the IC_{50} of free CPT and CPT-loaded CPNs decreased to 0.1 μM and 0.008 μM, respectively. In this case, CPT-loaded CPNs are 12.5 times more effective than free CPT in inducing the apoptosis of Huh7 cells. Although the free drug (CPT) reaches IC_{50} of 0.1 μM after 72 h, it is possible to achieve this value with CPT-loaded CPNs at the end of 48 h.

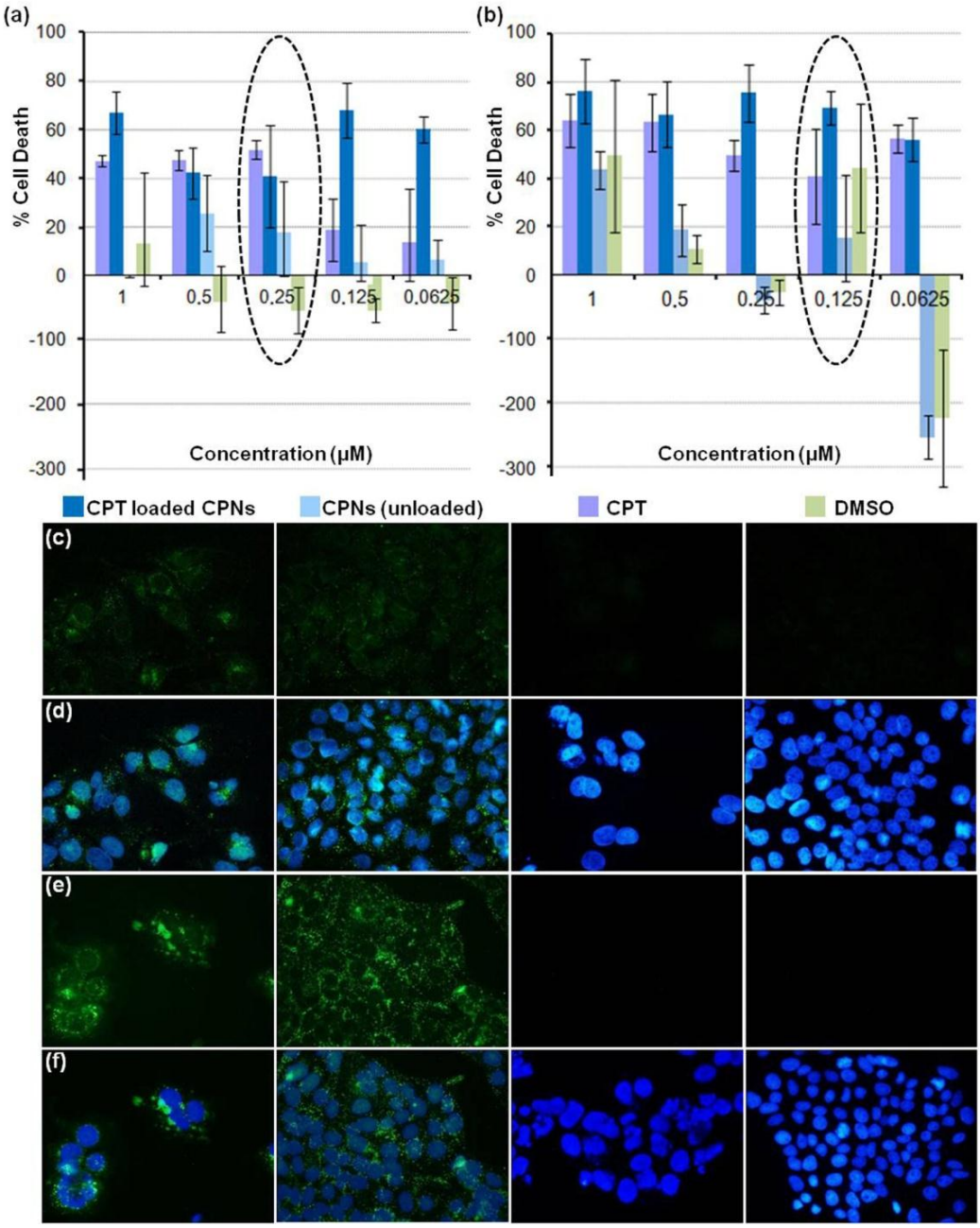

Figure 2.28. Percent cell death with CPT-loaded PPFBT Nps, PPFBT Nps, CPT and DMSO. Huh7 cells were inoculated in 24-well plates. All molecules and their DMSO controls were administered to the cells in triplicates with five different concentrations: 1, 0.5, 0.25, 0.125, and 0.0625 μM. After 48h (a) and 72h (b) of incubation, SRB assays were generated and the cell death percentages were calculated in comparison with DMSO-treated wells. Huh7 cells plated concomitantly on coverslips and treated identically were Hoechst 33258 stained and examined under a fluorescence microscope (40x) only for labelled (dashed oval) conditions (c and d for a) and (e and f for b).

SRB assay results clearly confirm that CPT-loaded nanoparticles have been taken up by the cells and unloaded their payload very efficiently. With this delivery system, even very low dose of CPT is found to be sufficient to induce the apoptosis of Huh7 cells; this is certainly a very desirable goal in the chemotherapy. The cellular uptake of the blank CPNs and CPT-loaded CPNs were analyzed by fluorescence microscope (using Huh7 cells) in Figure 2.28. only for dashed oval conditions. More microscope images on dose dependent study of DMSO-only, CPT-only, Np-only and CPT-loaded Nps treated cells are given in Figure 2.29, Figure 2.30 and Figure 2.31. These nanoparticles were accumulated in the cytoplasm and around the nucleus suggesting that the uptake might be achieved via endocytosis. Especially, CPT-loaded CPNs seem to be densely populated around the destroyed nucleus as well as within the nucleus when it was fragmented through apoptosis.

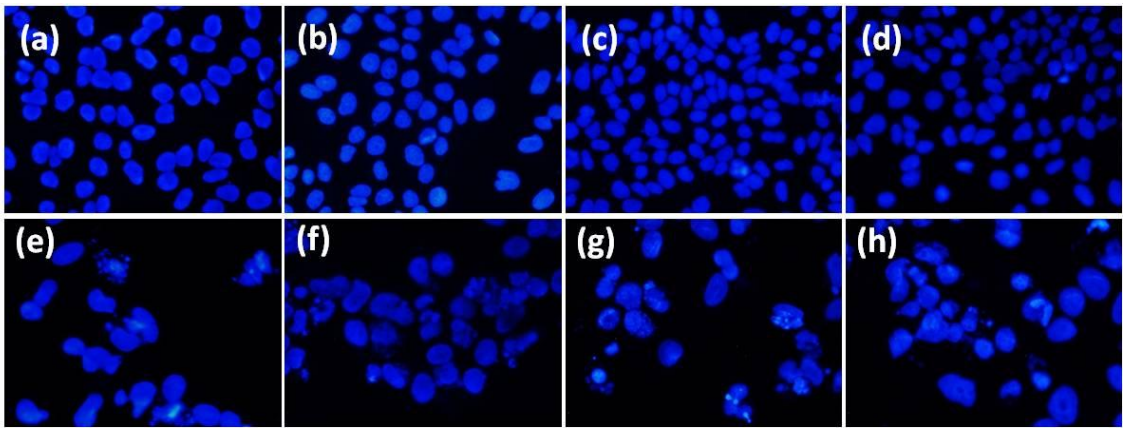

Figure 2.29. Huh7 cells plated concomitantly on coverslips and treated identically were Hoechst 33258 stained and examined under a fluorescence microscope (40x) after 72 h incubation with DMSO-only **(a-d)** and 0.5 μM **(e)** 0.25 μM **(f)** 0.125 μM **(g)** 0.0625 μM **(h)** CPT-only which were used as controls in serial dilutions.

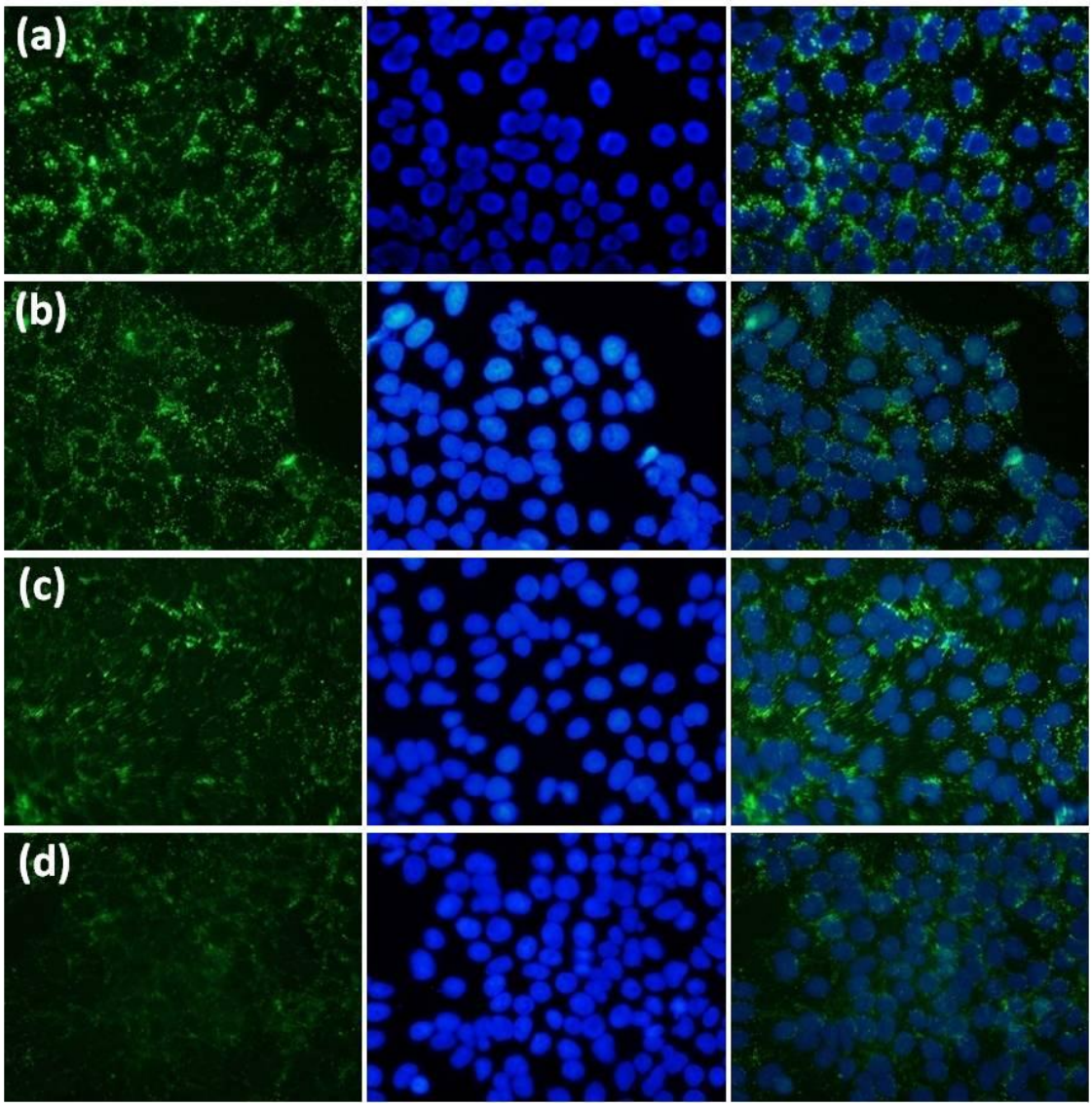

Figure 2.30. Huh7 cells plated concomitantly on coverslips and treated identically were Hoechst 33258 stained and examined under a fluorescence microscope (40x) after 72 h incubation with 12.5 μM **(a)** 6.25 μM **(b)** 3.125 μM **(c)** 1.5625 μM **(d)** PPFBT nanoparticles.

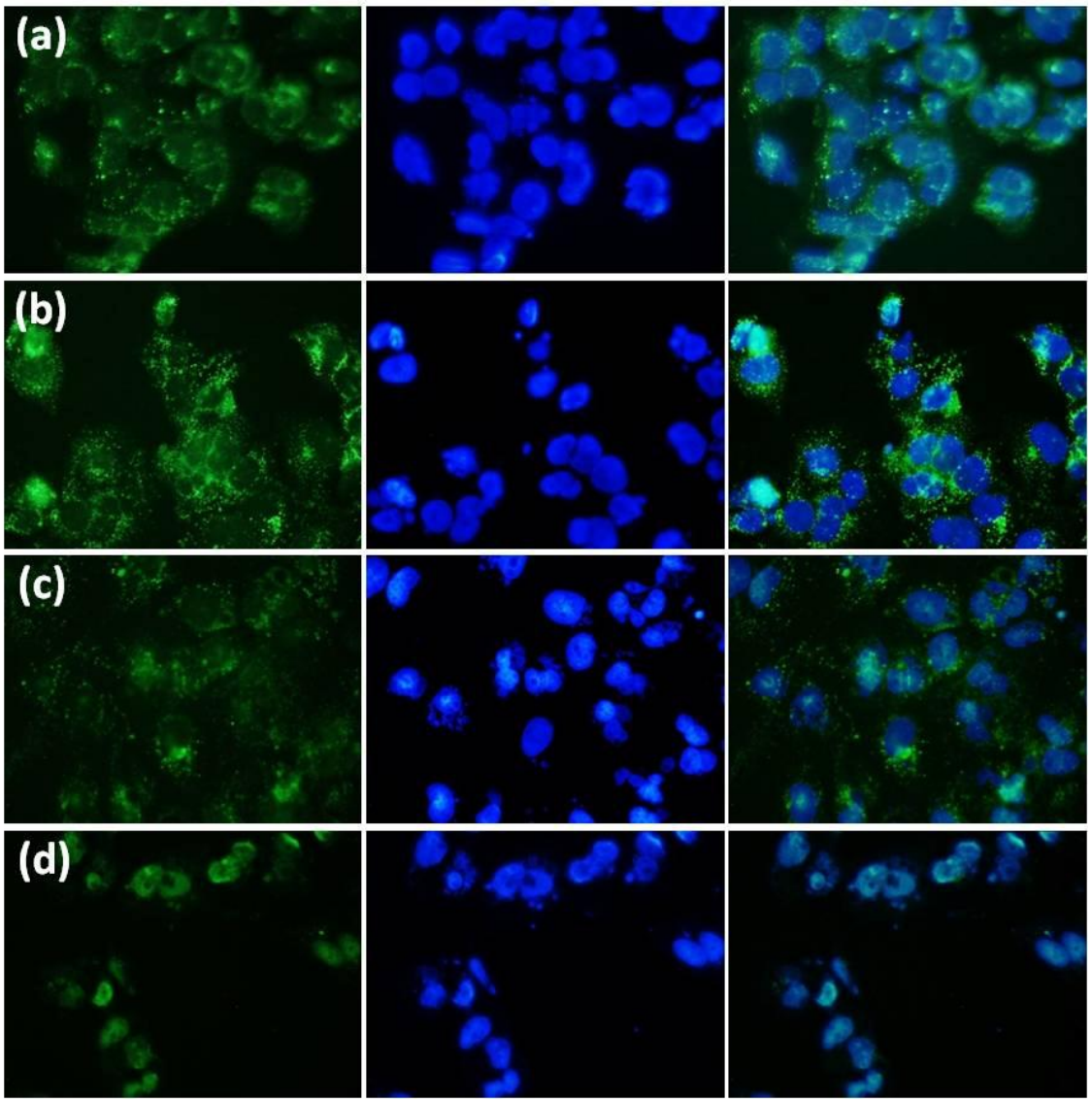

Figure 2.31. Huh7 cells plated concomitantly on coverslips and treated identically were Hoechst 33258 stained and examined under a fluorescence microscope (40x) after 72 h incubation with [CPT]=0.5 μM, [PPFBT]=12.5 μM **(a)** [CPT]=0.25 μM, [PPFBT]=6.25 μM **(b)** [CPT]=0.125 μM, [PPFBT]=3.125 μM **(c)** [CPT]=0.0625 μM, [PPFBT]=1.5625 μM **(d)** CPT-loaded PPFBT nanoparticles.

The high efficacy of this approach can be attributed to a number of factors. Amongst them, the drug-loaded nanoparticles have potential to avoid multidrug resistance mechanisms (MRMs) when they enter cells via endocytosis[105]. MRMs operate through the transmembrane drug efflux pumps effect involving cell-surface proteins such as glycoproteins which can prevent small drugs to enter the cells. CPT is a water insoluble drug molecule which dissolves in organic solvents (e.g. DMSO) or in the acidified water. None of them are desirable because for the former, DMSO has toxic effects to the cells and, for the latter, CPT molecules are hydrolyzed in the acidic aqueous media, and in turn, this causes their inhibitory activities to be diminished. However, the encapsulation renders the water solubility of CPT molecules and provides stability to preserve their full activity.

2.3.3. Synthesis and Characterization of Poly[(9,9-bis{3-azido-propyl}fluorenyl-2,7-divinylene)-co-(1,4-benzo-{2,1,3}-thiodiazole)] (PAPFVBT) Nanoparticles

Firstly, the polymer PAPFVBT was dissolved in THF. The resulting solution was sonicated for 30 min and then injected rapidly into autoclaved double distilled water . It was stirred with sonication for further 30 min. THF was removed under reduced pressure. The resulting nanoparticle solution was concentrated by evaporating its water under reduced pressure. The size of nanoparticles and the zeta potential values were measured as 146.5 nm and -35 mV, shown in Figure 2.32.

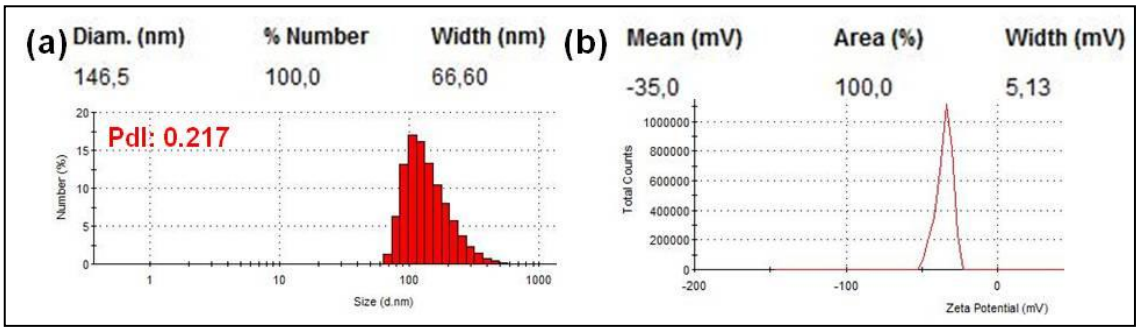

Figure 2.32. (a) Size distribution histogram from DLS measurement and **(b)** zeta potential measurement of **PAPFVBT** Nanoparticles**.**

Optical characterization of PAPFVBT nanoparticles was investigated with UV-Vis and fluorescence spectroscopies and compared with the polymer in THF and in solid state (Figure 2.33). For all three cases, there is a broad absorption band having maxima at 340 and 420 nm. When the polymer in THF was excited with 420 nm light, the emission maximum at 545 nm was observed. When nanoparticle dispersion in water were excited with 420 nm light, the emission maximum at 608 nm was observed which was 63 nm red shifted compared to the emission band of the polymer in THF. If the emission maximum of nanoparticles in water compared with the emission maximum of the polymer film (617 nm), it can be seen that only 9 nm red shift was observed for the polymer film indicating that optical properties of nanoparticles in water resembles to polymer's solid state properties.

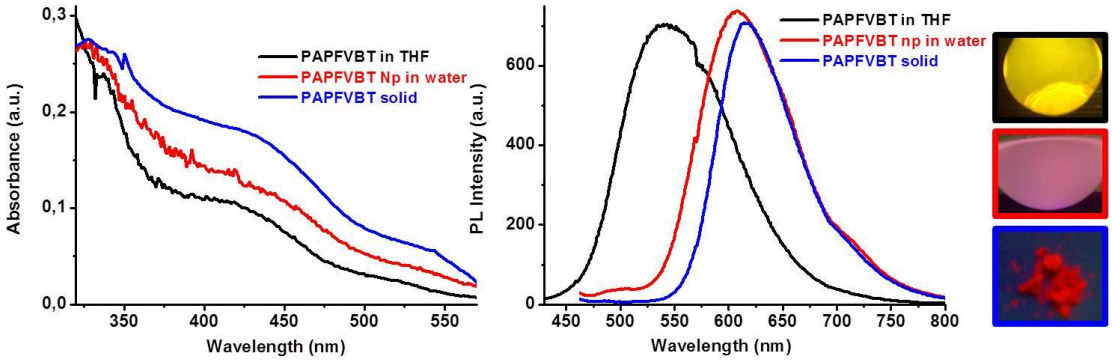

Figure 2.33. UV–vis absorption and fluorescence emission spectra of **PAPFVBT** in THF, as film and as dispersions of the nanoparticles in water ($\lambda_{exc.}$= 420 nm). Inset images represent real images of these three states under 366 nm UV light.

2.3.3.1. Cell Viability of PAPFVBT Nanoparticles

Through SRB assay, dose dependent *in vitro* cytotoxicity test of the blank PAPFVBT nanoparticles (~147 nm) against Huh7 cells were performed. The results were plotted as in Figure 2.34. and indicate that they are not toxic to the Huh7 cells up to 16 μM at the end of 72 h. Their higher percent viability results can be explained in a way that red emitting conjugated polymers have lower energy that make them better for biomedical applications without tissue damage. As a result, their convenience for further studies on cell imaging and the drug delivery was demonstrated.

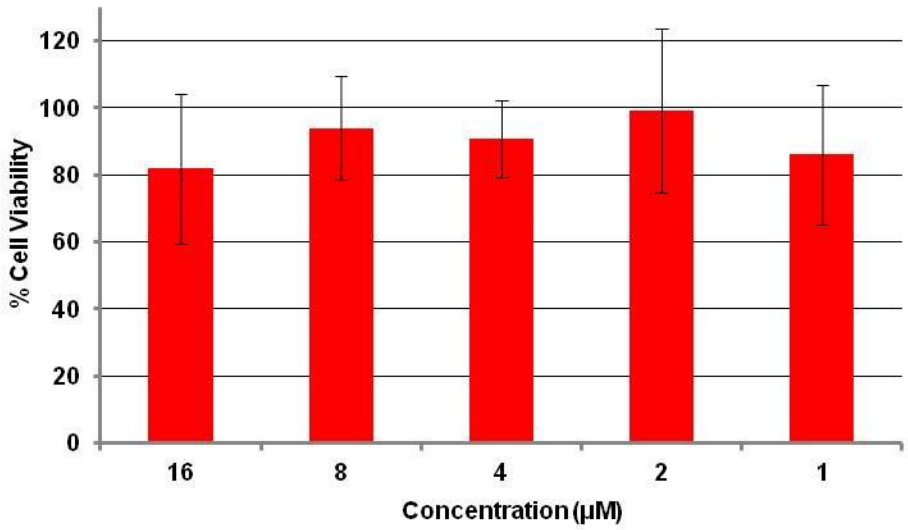

Figure 2.34. Percent cell viability results of **PAPFVBT** nanoparticles having concentrations of 16, 8, 4, 2, 1 µM after 72 h incubation.

2.3.4. Synthesis and Characterization of Camptothecin (CPT) - Loaded PAPFVBT Nanoparticles as a Drug Carrier

The synthetic conditions, in which the polymer to drug ratio was 25:1, were kept constant for drug loaded nanoparticles that would be used for cell studies. The size of the blank and CPT-loaded nanoparticles were determined by dynamic light scattering (DLS) measurements (Figure 2.35 a, b) and as 146.5 nm for blank nanoparticles and 152.2 nm for drug loaded nanoparticles. The morphologies of blank nanoparticles and CPT loaded nanoparticles were revealed by SEM (Figure 2.35 c, d) imaging technique. The zeta potential values were measured as -35.0 mV for blank nanoparticles and -42.0/-16.8 mV for CPT loaded nanoparticles (Figure 2.35 e, f), which indicate the formation of stable nanoparticle dispersion caused by the repulsion between the nanoparticles. As can be seen from the DLS measurements, no significant changes were observed in their diameters, indicating that the structural integrity of nanoparticles were not affected when they are loaded with drug.

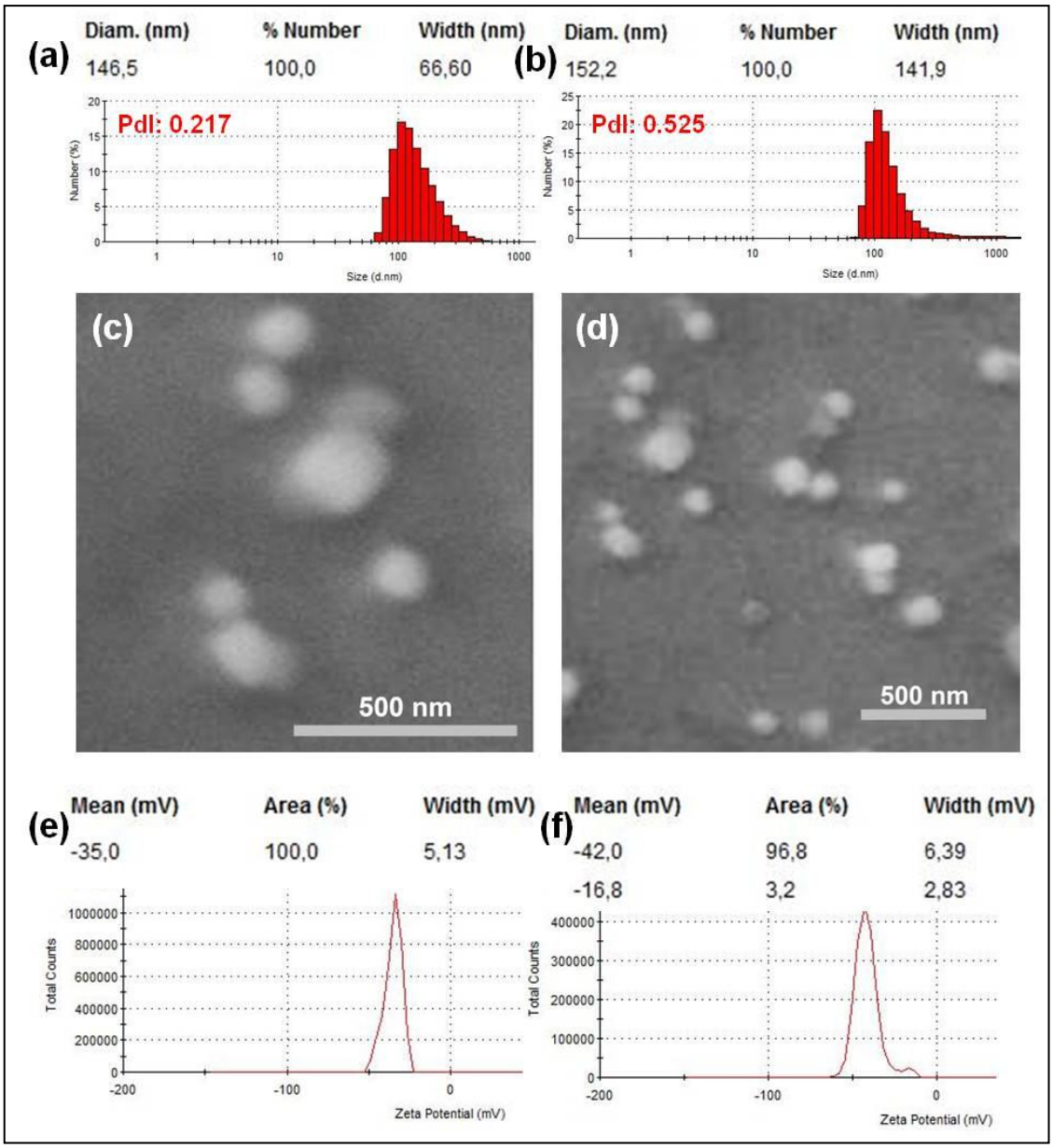

Figure 2.35. Size distribution histograms from DLS measurements of PPFBT nanoparticles **(a)** and CPT-loaded PPFBT nanoparticles **(b)**; SEM images of PPFBT nanoparticles **(c)** and CPT-loaded PPFBT nanoparticles **(d)**; Zeta potential measurements of PPFBT nanoparticles **(e)** and CPT-loaded PPFBT nanoparticles **(f)**

In Figure 2.36, dose dependent *in vitro* cytotoxicity tests of the blank CPNs, CPT loaded CPNs and free CPT against Huh7 cells were performed through SRB assay. Free CPT was used as a positive control and DMSO and blank CPNs were used as negative controls to CPT loaded CPNs. SRB test system is based on quantitative staining of cellular protein by SRB dye. Therefore, more purple color indicates more live cells like in the regions of I, IV and V. As expected, the regions of II and III belonging to the cells treated with CPT-loaded nanoparticles and free CPT are almost clear that this anticancer drug kills these cancer cells.

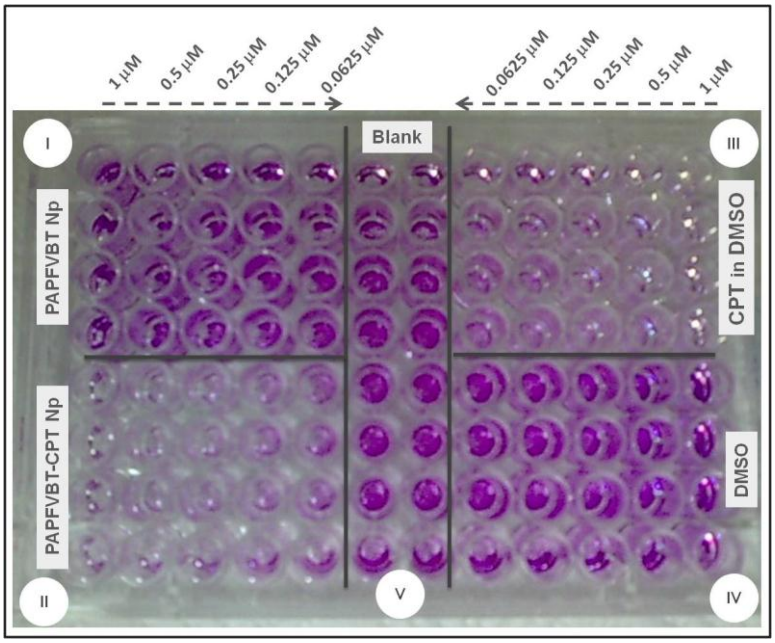

Figure 2.36. The image of 96-well plate with SRB dye after 72 h incubation.

The SRB results were plotted as in Figure 2.37. At the end of 72 h, IC_{50} of free CPT and CPT-loaded PAPFVBT Nps were calculated to be 0.03 µM and 0.1 µM respectively, corresponding to that CPT-loaded PAPFVBT Nps are 3.3 times less effective than free CPT. Having bigger size of PAPFVBT Nps is the main reason of not being effective as PPFBT Nps since they could be less efficiently taken up by the cells.

.

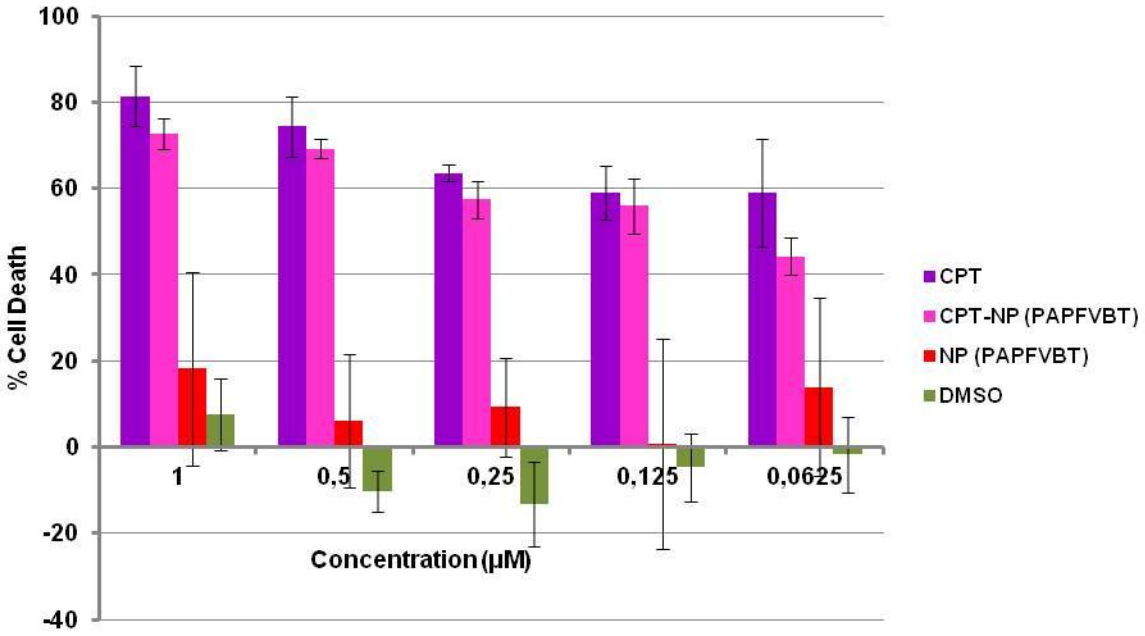

Figure 2.37. Percent cell death with CPT- loaded PAPFVBT Nps, PAPFVBT Nps, CPT and DMSO. Huh7 cells were inoculated in 24-well plates. All molecules and their DMSO controls were administered to the cells in triplicates with five different concentrations of CPT: 1, 0.5, 0.25, 0.125, and 0.0625 µM. After 72 h of incubation, SRB assays were generated and the cell death percentages were calculated.

CHAPTER 3. CONCLUSION

In conclusion, a new and simple approach for the combination chemotherapy was presented by incorporating a water-insoluble drug camptothecin into the conjugated polymer nanoparticles with very high loading efficiency because of the favorable non-covalent interactions (e.g. hydrophobic effect and π-π interactions) between the aromatic backbone of the polymer chains and the drug molecules. The blank and drug loaded nanoparticles are uniform in size, size distribution and surface charge.

		IC_{50} (48 h) (μM)	IC_{50} (72 h) (μM)
PPFBT (~ 25 nm) *Blank Nps are not toxic up to 25 μM*	**Free Drug (CPT)**	0.9	0.1
	CPT-Loaded Nps	0.1	0.008
PAPFVBT (~ 150 nm) *Blank Nps are not toxic up to 16 μM*	**Free Drug (CPT)**		0.03
	CPT-Loaded Nps		0.1

Table 2. Summary for IC_{50} values of free drug (CPT), CPT-loaded PPFBT and PAPFVBT Nanoparticles.

Time and dose dependent SRB assay results indicated that these nanoparticles assisted the delivery of water-insoluble anticancer drugs into cancer cells (Huh7 cells) in an efficient manner leading to effective apoptosis. As it can be seen in Table 2, at the end of 48 h, CPT-loaded PPFBT Nps were 9 times more effective than free CPT. However, at the end of 72 h, CPT-loaded PPFBT Nps are 12.5 times more effective than free CPT in inducing the apoptosis of Huh7 cells. This is certainly a very impressive finding as well as a highly desirable goal to be achieved in the chemotherapy. Noticeably, this new imaging-guided drug delivery system does not require a complicated design and synthetic methods, needing only one type of polymer which can be synthesized easily and acts both as a photostable fluorescent probe, and a matrix to encapsulate the drug molecules.

On the other hand, CPT-loaded PAPFVBT Nps are 3.3 times less effective than free CPT because of their bigger size compared to PPFBT Nps that resulted in less efficiently taken up by the cells.

CHAPTER 4. EXPERIMENTAL

All reagents were purchased from Sigma–Aldrich Chemical Co. and were used as received. 2,7-dibromo-9,9-bis(3-bromo-propyl)-9H-fluorene and 9,9-bis-(3-bromo-propyl)-2,7-divinyl-9H-fluorene and 2,7-dibromo-9,9-bis-(propenyl)-9H-fluorene were synthesized according to the procedure shown in the experimental section. Column chromatography with silica gel (Kieselgel 60, 0.063 – 0.200 nm) was used for the purification of these monomers. Thin layer chromatography (TLC) was performed by using the silica gel plates (Kieselgel 60 F254, 1 mm) to identify the product and the side products in the reaction mixture and to determine the purity of the desired product. For the structural characterization, nuclear magnetic resonance (NMR, Bruker Avance III 400 MHz spectrometer) and FT-IR (Bruker TENSOR 27) were performed. $CDCl_3$ and DMSO-d6 solvents were used for NMR measurements. In the process of FT-IR measurements, the polymer samples were prepared as KBr pellets and each sample of nanoparticle dispersions in water was dropped onto the silicon wafer. The data were recorded at 25^{o}C, in the spectral range of 4000–400 cm^{-1}, by accumulating 256 scans with a resolution of 4 cm^{-1}. For the optical characterization, a UV–vis spectrophotometer (Cary UV–Vis) and a fluorescence spectrophotometer (Cary Eclipse Fluorescent spectrophotometer) equipped with a xenon-lamp as the excitation source were used. The molecular weight determination of the polymers were done with the use of gel permeation chromatography (GPC, Agilent 1200) equipped with Evaporation-Light-Scattering Detector (ELSD). The column type was ZORBAX PSM 300S, 6.2x250 mm, 5 μm. The analysis was performed in tetrahydrofuran (THF) (GPC/HPLC grade) at a flow rate of 0.6 ml/min. All of the polystyrene samples were 1% solutions in THF with the instrument operating at 31^{o}C having automotic injection system. Mass-to-charge ratio was determined via a time measurement by time-of-flight liquid chromatography mass spectroscopy (TOF LC/MS, Agilent 1200/6210). Autoclaved ddH_2O was used to prepare the nanoparticles. The sizes of the nanoparticles were measured by dynamic light scattering (DLS, Zetasizer Nano-ZS). Measurements were carried out at 633 nm and the laser, as a light source, was used at room temperature. The average particle diameters were calculated by the Marquardt method. The DLS measurements were usually repeated at least three times and the average values were reported. Morphological characterization was done by atomic force microscope-PSIA

(AFM, XE-100E), transmission electron microscopy (TEM, FEI Tecnai G2 F30) and scanning electron microscope (SEM, Quanta 200 FEG).

Preparation of cells and culture: Human hepatocellular carcinoma cell line Huh7 was maintained in Dulbecco's Modified Eagle's Medium (DMEM) (Invitrogen GIBCO), with 10% fetal bovine serum (FBS) (Invitrogen GIBCO), nonessential amino acids, and 1% penicillin (Biochrome). Huh7 cells were incubated at 37 °C with 5% CO_2. DMSO (Sigma) was used as a solvent for Camptothecin (Calbiochem) at a concentration less than 1% in the cell culture medium.

4.1.Synthesis of 2,7-dibromo-9,9-bis(3-bromo-propyl)-9H-fluorene (M1)

2,7-dibromofluorene (3.0 g, 9.25 mmol) and (0.6 mg, 1.85 mmol) tetrabutylammoniumbromide (TBAB) in two-neck round bottom flask (capacity of 100 mL) were dried under vacuum for 30 min. To this mixture, degassed DMSO (15 mL), 50% (w/w) NaOH (15 mL) and 1,3-dibromopropene (13 mL, 90 mmol) were added respectively. The resulting mixture was stirred under argon for 2 h at room temperature. The reaction was exothermic and a bath of ice and water was used to keep it at room temperature during 2 h. At the end of 2 h, argon was removed and the final reaction mixture was taken to one-neck round bottom flask (capacity of 250 mL), then diethyl ether (120 mL) and deionized water (50 mL) were added and stirred for 15 min. By the help of seperatory funnel, the above organic layer was separated and washed with the order of deionized water (1x100 mL), 2 N HCl (1x100 mL), deionized water (1x100 mL), brine solution (3x100 mL) and deionize water (4x100 mL). The final washed diethyl ether layer was evaporated under reduced pressure and the resulting product was obtained as solid. It was dissolved in minimum amount of cyclohexane/chloroform and purified through silica packed column chromatography. Cyclohexane/chloroform (8:2) was used as the eluent. For further purification, the desired monomer was dissolved in minimum amount of chloroform and precipitated into cold methanol, filtered and dried under vacuum. Yield: 1.7227 g, 33 %.

^{1}H-NMR (400 MHz, $CDCl_3$, δ ppm): 7.5 (m, 6H), 3.14 (t, 4H), 2.17 (t, 4H), 1.17 (m, 4H).

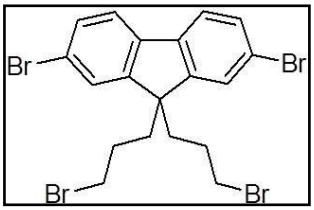

Scheme 4.1. The structure of 2,7-dibromo-9,9-bis(3-bromo-propyl)-9H-fluorene **(M1)**.

4.2. Synthesis of 9,9-bis-(3-bromo-propyl)-2,7-divinyl-9H-fluorene (M2)

2,7-dibromo-9,9-bis(3-bromo-propyl)-9H-fluorene (1.13 g, 2.0 mmol) and 2,6-di-tert-butylphenol (8 mg, 38 mmol) were dried under vacuum for 30 min. To this mixture, degassed toluene (20 mL) and tributylvinyltin (1.45 mL, 5.0 mmol) were added respectively. The catalyst, $PdCl_2(PPh_3)_2$ (56 mg, 0.09 mmol) was added quickly. The reaction mixture was stirred and heated at 100 ^oC in an oil bath for 24 h under argon. After cooling to room temperature, the mixture was diluted with diethyl ether and treated with 10% (w/w) NaF (20 mL). The resulting mixture was stirred for further 12 h at room temperature. At the end of 12 h, obtained insoluble solid was removed by filtration. After extraction with distelled water (4x100 mL) and it was dried over anhydrous Na_2SO_4. The solvent was evaporated under reduced pressure. The residue was dissolved in minimum amount of cyclohexane-chloroform mixture and purified through silica packed column chromatography. Cyclohexane/chloroform (8:2) was used as the eluent. For further purification, the desired monomer was dissolved in minimum amount of chloroform and precipitated into cold methanol, filtered and dried under vacuum. Yield: 0.2761 g, 30 %.

^{1}H-NMR (400 MHz, $CDCl_3$, δ ppm): 7.5 (m, 6H), 6.8 (m, 2H), 5.8 (d, 2H), 5.3 (d, 2H) 3.1 (t, 4H), 2.2 (t, 4H), 1.2 (m, 4H).

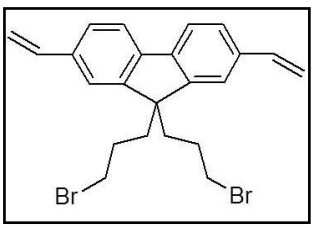

Scheme 4.2. The structure of 9,9-bis-(3-bromo-propyl)-2,7-divinyl-9H-fluorene **(M2)**.

4.3. Synthesis of 2,7-dibromo-9,9-bis-(propenyl)-9H-fluorene (M3)

2,7-dibromofluorene (3.0 g, 9.25 mmol) and tetrabutylammoniumbromide (TBAB) (0.6 g, 1.85 mmol) were dried under vacuum for 30 min. To this mixture, degassed DMSO (15 mL), 50% (w/w) NaOH (15 mL), allylbromide (16 ml, 90 mmol) were added respectively. The resulting mixture was stirred under argon for 2 h at room temperature. After 2 h, t-butyl methyl ether (125 mL) and deionized water (50 mL) were added into the mixture and stirred for 15 min. Organic layer was separated and subsequently washed with deionized water (50 mL), 2N HCl (50 mL), brine solution (50 mL) and deionized water (50 mL), respectively. After extraction, t-butyl methyl ether was evaporated under reduced pressure and the monomer was obtained. For the purification of the product, silica-packed column chromatography was used with cyclohexane as the eluent. The solid was further purified by dissolving in minimum amount of chloroform, precipitating into cold methanol. Colorless crystals were collected and dried under vacuum. Yield: 3.3 g, 89 %.

^{1}H-NMR (400 MHz, $CDCl_3$, δ ppm):7.52 (m, 6H), 5.21 (m, 2H), 4.89 (m, 4H), 2.68 (t, 4H)

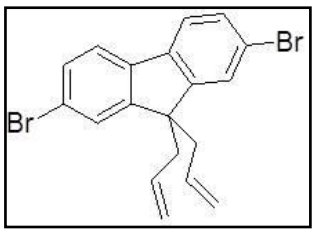

Scheme 4.3. The structure of 2,7-dibromo-9,9-bis-(propenyl)-9H-fluorene **(M3)**.

4.4. Synthesis of Poly[(9,9- bis{propenyl}fluorenyl-2,7-diyl))-co-(1,4-benzo-{2,1,3}-thiodiazole)] (PPFBT)

2,1,3-benzothiadiazole-4,7-bis (boronic acid pinocol ester) (573 mg, 1.47 mmol), 2,7-dibromo-9,9-bis-(propenyl)-9H-fluorene (M1) (500 mg, 1.47 mmol) and K_2CO_3 (2.04 g, 14.7 mmol) were dried under vacuum about 30 min. First the degassed solvents, THF (10 mL), water (10 mL) and toluene (10 mL) were added under Argon gas and then, catalyst tetrakis (triphenylphosphine) palladium (Pd $(PPh_3)_4$) was added quickly. After 3 h stirring of the mixture under argon at 80–90 °C, the phase transfer catalyst, tetra-n-butylammonium bromide (TBAB) was added. The stirring was continued for another

48h at 80–90 °C to complete the polymerization reaction. The mixture was evaporated under vacuum to obtain a solid residue, which was suspended in water; the water insoluble particles were collected by suction and dissolved in THF (20 mL) and the solution was precipitated into cold methanol (200 mL). The precipitates were collected by suction and dried under vacuum for 5 h. Yield: 646 mg, 60 %.

^{1}H-NMR (400 MHz, $CDCl_3$, δ ppm): 7.8-8.2 (m, 8H), 5.5 (m, 2H), 4.8-5.1 (m, 4H), 2.8 (t, 4H).

FT-IR: (KBr, pellet, $\upsilon_{max}(cm^{-1})$): 3074 (-CH, w), 2918 (-CH, s), 1455 (C=C-, w).

GPC: M_n= 4.5 x10^3 g/mol, M_w= 1.1 x 10^4 g/mol (Polystyrene as standard).

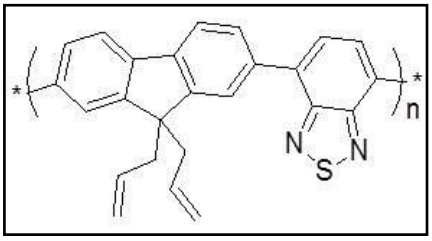

Scheme 4.4. The structure of poly[(9,9- bis{propenyl}fluorenyl-2,7-diyl))-co-(1,4-benzo-{2,1,3}-thiodiazole)] **(PPFBT)**.

4.5. Synthesis of Poly[(9,9-bis{3-bromo-propyl}fluorenyl-2,7-divinylene)-co-(1,4-benzo-{2,1,3}-thiodiazole)] (PBPFVBT)

9,9-bis-(3-bromo-propyl)-2,7-divinyl-9H-fluorene (M2) (98 mg, 0.212 mmol), 4,7-dibromo-2,1,3-benzothiodiazole (62 mg, 0.212 mmol), $Pd(OAc)_2$ (2 mg, 9 μmmol), PPh_3 (12.85 mg, 49 μmol) and K_2CO_3 (0.9919 g, 0.007 mol) was degassed with three vacuum-argon cycles to remove air. Then, degassed DMF (2 mL) and H_2O (0.5 mL) were added and the resulting mixture was frozen, evacuated, and thawed three times to further remove air. The reaction mixture was vigorously stirred and heated at 100 ^oC in an oil bath for 14 h under argon. After cooling to room temperature, the mixture was diluted with chloroform and water. The insoluble part was removed by filtering through glass filter funnel. Organic layer washed with deionized water and evaporated under reduced pressure. The solid product was dissolved in minimum amount of THF and the solution was precipitated into cold methanol (200 mL). The red precipitates were collected by suction and dried under vacuum. Yield: 65.527 mg, 52%

^{1}H-NMR (400 MHz, $CDCl_3$, δ ppm): 7.5-8.2 (m, 8H), 6.8 (m, 2H), 5.8 (m, 2H) 3.4 (t, 4H), 2.1 (m, 4H), 0.9 (m, 4H).

FT-IR: (KBr, pellet, $\upsilon_{max}(cm^{-1})$): 2961 (C-H, w), 1620 (C=C, w), 1431 (C-C, s), 822 (C-Br, s)

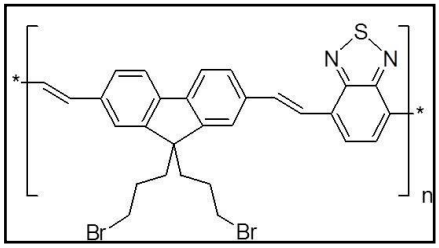

Scheme 4.5. The structure of poly[(9,9-bis{3-bromo-propyl}fluorenyl-2,7-divinylene)-co-(1,4-benzo-{2,1,3}-thiodiazole)] **(PBPFVBT)**.

4.6.Synthesis of Poly[(9,9-bis{3-azido-propyl}fluorenyl-2,7-divinylene)-co-(1,4-benzo-{2,1,3}-thiodiazole)] (PAPFVBT)

Poly[(9,9-bis{3-bromo-propyl}fluorenyl-2,7-divinylene)-co-(1,4-benzo-{2,1,3}-thiodiazole)] (PBPFVBT) (140 mg, 0.235 mmol) was dissolved in DMF (5 mL). Then, NaN_3 (38.28 mg, 0.589 mmol) was added in the solution. The reaction mixture was stirred and heated at 60 ^oC in an oil bath for 24 h under atmosphere. At the end of reaction, the solvent was evaporated under reduced pressure. The residue was dissolved in minimum amount of THF and the solution was precipitated into cold methanol (200 mL). The red precipitates were collected by suction and dried under vacuum. Yield: 101.2 mg, 83%.

FT-IR: (KBr, pellet, $\upsilon_{max}(cm^{-1})$): 2961 (C-H, w), 2020 (N_3, s), 1620 (C=C, w), 1431 (C-C, s), 822 (C-Br, s)

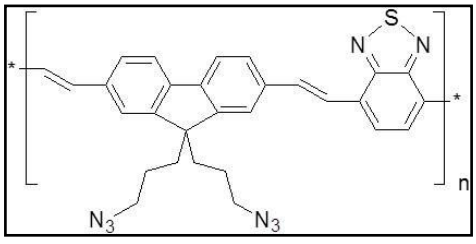

Scheme 4.6. The structure of poly[(9,9-bis{3-azido-propyl}fluorenyl-2,7-divinylene)-co-(1,4-benzo-{2,1,3}-thiodiazole)] **(PAPFVBT).**

4.7. Synthesis of PPFBT Nanoparticles

PPFBT (2.0 mg, 5.26 x 10^{-3} mmol) was dissolved in THF (5 mL). The resulting solution was sonicated for 30 min and then injected rapidly into autoclaved double distilled water (50 mL). It was stirred with sonication for further 30 min. THF was removed under reduced pressure. The resulting nanoparticle solution was concentrated by evaporating its water under reduced pressure to get the concentration of PPFBT as 0.75 mg / mL (1.98 x 10^{-3} mmol / mL).

4.8. Synthesis of Drug Loaded PPFBT Nanoparticles

For the drug loaded nanoparticles, the drug to polymer ratio was 1:25 (w/w). PPFBT (2.0 mg, 5.26 x 10^{-3} mmol) and CPT (0.08 mg, 0.23 x 10^{-3} mmol)) was dissolved in THF (5 mL). The resulting solution was sonicated for 30 min and then injected rapidly into autoclaved double distilled water (50 mL). It was stirred with sonication for further 30 min. THF was removed under reduced pressure. The resulting drug loaded nanoparticle solution was filtered through a 0.45 μm syringe filter to remove any free drug. Then, it was concentrated by evaporating its water under reduced pressure to get the final concentration of PPFBT as 1.98 x 10^{-3} mmol / mL (0.75 mg / mL) and the concentration of CPT as 0.86 x 10^{-4} mmol / mL (0.03 mg / mL).

4.9.Sulforhodamine B (SRB) Colorimetric Assay for Cytotoxicity Screening for Blank and Drug Loaded PPFBT Nanoparticles

Huh7 cells were inoculated (12000 cells/well in 500 μL) in 24-well plates. The next day, the media were refreshed and the CPT and CPT-loaded PPFBT nanoparticles were applied in concentrations between 1 and 0.0625 μM in parallel with DMSO-only and NP-only treated cells as negative controls. At the end of 48 and 72 hours of treatment Huh7 cells were fixed with 150 μL of 10% (w/v) trichloroacetic acid (TCA) and kept at +4 °C in the dark for one hour. TCA fixation was terminated by washing the wells with ddH_2O five times. Air-dried wells were stained with 0.4% sulphorhodamine B (SRB) dissolved in 1% acetic acid solution for 10 min in the dark, at room temperature. Unbound SRB dye was removed by five washes with 1% acetic acid, and protein-bound and dried SRB dye was then solubilized with 10 mM Tris-Base pH 8. The absorbance values were obtained at 515 nm in a microplate reader. The data normalized against DMSO-only and NP-only treated wells, which were used as controls in serial dilutions.

4.10. Hoechst Staining for Blank and Drug Loaded PPFBT Nanoparticles

Huh7 cells plated on coverslips and treated with CPT, CPT-loaded PPFBT nanoparticles, DMSO-only and PPFBT Nps-only for 48 h and 72h were MeOH (100%, ice-cold) fixed prior to staining with 1 μg/mL Hoechst 33258. Coverslips destained with ddH_2O were mounted on glass slides and examined under a fluoresence microscope (Nikon ECLIPSE 50i).

4.11. Synthesis of PAPFVBT Nanoparticles

PAPFVBT (1.0 mg, 1.93×10^{-3} mmol) was dissolved in THF (5 mL). The resulting solution was sonicated for 30 min and then injected rapidly into autoclaved double distilled water (50 mL). It was stirred with sonication for further 50 min. THF was removed under reduced pressure. The resulting nanoparticle solution was concentrated by evaporating its water under reduced pressure to get the concentration of PPFBT as 0.40 mg / mL (0.77×10^{-3} mmol / mL).

4.12. Synthesis of Drug Loaded PAPFVBT Nanoparticles

For the drug loaded nanoparticles, the drug to polymer ratio was 1:25 (w/w). PAPFVBT (1.0 mg, 1.93×10^{-3} mmol) and CPT (0.04 mg, 0.12×10^{-3} mmol)) was dissolved in THF (5 mL). The resulting solution was sonicated for 30 min and then injected rapidly into autoclaved double distilled water (50 mL). It was stirred with sonication for further 50 min. THF was removed under reduced pressure. The resulting drug loaded nanoparticle solution was filtered through a 0.45 μm syringe filter to remove any free drug. Then, it was concentrated by evaporating its water under reduced pressure to get the final concentration of PAPFVBT as 0.55×10^{-3} mmol / mL (0.29 mg / mL) and the concentration of CPT as 0.29×10^{-4} mmol / mL (0.011 mg / mL).

4.13. Sulforhodamine B (SRB) Colorimetric Assay for Cytotoxicity Screening for Blank and Drug Loaded PAPFVBT Nanoparticles

Huh7 cells were inoculated (2500 cells/well in 150 μL) in 96-well plates. The next day, the media were refreshed and the CPT and CPT-loaded PAPFVBT nanoparticles were applied in concentrations between 1 and 0.0625 μM in parallel with DMSO-only and PAPFVBT Nps-only treated cells as negative controls. At the end of 72 hours of treatment Huh7 cells were fixed with 50 μL of 10% (w/v) trichloroacetic acid (TCA) and kept at +4 °C in the dark for one hour. TCA fixation was terminated by washing the wells with ddH_2O five times. Air-dried wells were stained with 0.4% sulphorhodamine B (SRB) dissolved in 1% acetic acid solution for 10 min in the dark, at room temperature. Unbound SRB dye was removed by five washes with 1% acetic acid, and protein-bound and dried SRB dye was then solubilized with 10 mM Tris-Base pH 8. The absorbance values were obtained at 515 nm in a microplate reader. The data normalized against DMSO-only and NP-only treated wells, which were used as controls in serial dilutions.

REFERENCES

1. Friend, R., Conjugated polymers. New materials for optoelectronic devices. *Pure and Applied Chemistry* **2001,** *73* (3), 425-430.

2. Heeger, P. S.; Heeger, A. J., Making sense of polymer-based biosensors. *Proceedings of the National Academy of Sciences* **1999,** *96* (22), 12219-12221.

3. Nordén, B., Conductive Polymers. *The Nobel Prize in Chemistry 2000*.

4. Bäckvall, J.-E., Palladium-catalyzed Cross Couplings in Organic Synthesis *Scientific Background on the Nobel Prize in Chemistry 2010*.

5. Hoven, C. V.; Garcia, A.; Bazan, G. C.; Nguyen, T. Q., Recent Applications of Conjugated Polyelectrolytes in Optoelectronic Devices. *Adv. Mater.* **2008,** *20* (20), 3793-3810.

6. Bundgaard, E.; Krebs, F. C., Low-Band-Gap Conjugated Polymers Based on Thiophene, Benzothiadiazole, and Benzobis(thiadiazole). *Macromolecules* **2006,** *39* (8), 2823-2831.

7. Synthesis of Organic Semiconductors. <<http://photonicswiki.org/index.php?title=Synthesis_of_Organic_Semiconductors>>.

8. Colladet, K.; Fourier, S.; Cleij, T. J.; Lutsen, L.; Gelan, J.; Vanderzande, D.; Huong Nguyen, L.; Neugebauer, H.; Sariciftci, S.; Aguirre, A.; Janssen, G.; Goovaerts, E., Low Band Gap Donor−Acceptor Conjugated Polymers toward Organic Solar Cells Applications. *Macromolecules* **2006,** *40* (1), 65-72.

9. Sang, G.; Zou, Y.; Li, Y., Two Polythiophene Derivatives Containing Phenothiazine Units: Synthesis and Photovoltaic Properties. *The Journal of Physical Chemistry C* **2008,** *112* (31), 12058-12064.

10. Wakim, S.; Beaupre, S.; Blouin, N.; Aich, B.-R.; Rodman, S.; Gaudiana, R.; Tao, Y.; Leclerc, M., Highly efficient organic solar cells based on a poly(2,7-carbazole) derivative. *J. Mater. Chem.* **2009,** *19* (30), 5351-5358.

11. Pei, J.; Wen, S.; Zhou, Y.; Dong, Q.; Liu, Z.; Zhang, J.; Tian, W., A low band gap donor-acceptor copolymer containing fluorene and benzothiadiazole units: synthesis and photovoltaic properties. *New Journal of Chemistry* **2011,** *35* (2), 385-393.

12. Brabec, C. J.; Winder, C.; Sariciftci, N. S.; Hummelen, J. C.; Dhanabalan, A.; van Hal, P. A.; Janssen, R. A. J., A Low-Bandgap Semiconducting Polymer for Photovoltaic Devices and Infrared Emitting Diodes. *Adv. Funct. Mater.* **2002,** *12* (10), 709-712.

13. Blouin, N.; Michaud, A.; Leclerc, M., A Low-Bandgap Poly(2,7-Carbazole) Derivative for Use in High-Performance Solar Cells. *Adv. Mater.* **2007,** *19* (17), 2295-2300.

14. Agrawal, A. K.; Jenekhe, S. A., Electrochemical Properties and Electronic Structures of Conjugated Polyquinolines and Polyanthrazolines. *Chem. Mat.* **1996,** *8* (2), 579-589.

15. Cui, Y.; Zhang, X.; Jenekhe, S. A., Thiophene-Linked Polyphenylquinoxaline: A New Electron Transport Conjugated Polymer for Electroluminescent Devices. *Macromolecules* **1999,** *32* (11), 3824-3826.

16. Yasuda, T.; Sakai, Y.; Aramaki, S.; Yamamoto, T., New Coplanar (ABA)n-Type Donor−Acceptor π-Conjugated Copolymers Constituted of Alkylthiophene (Unit A) and Pyridazine (Unit B): Synthesis Using Hexamethylditin, Self-Organized Solid Structure, and Optical and Electrochemical Properties of the Copolymers. *Chem. Mat.* **2005,** *17* (24), 6060-6068.

17. Scherf, U.; List, E. J. W., Semiconducting Polyfluorenes—Towards Reliable Structure–Property Relationships. *Adv. Mater.* **2002,** *14* (7), 477-487.

18. Liu, B.; Yu, W.-L.; Lai, Y.-H.; Huang, W., Blue-Light-Emitting Fluorene-Based Polymers with Tunable Electronic Properties. *Chem. Mat.* **2001,** *13* (6), 1984-1991.

19. Cheng, Y.-J.; Yang, S.-H.; Hsu, C.-S., Synthesis of Conjugated Polymers for Organic Solar Cell Applications. *Chem. Rev.* **2009,** *109* (11), 5868-5923.

20. Shrotriya, V., Organic photovoltaics: Polymer power. *Nat Photon* **2009,** *3* (8), 447-449.

21. Huang, F.; Hou, L.; Shen, H.; Jiang, J.; Wang, F.; Zhen, H.; Cao, Y., Synthesis, photophysics, and electroluminescence of high-efficiency saturated red light-emitting polyfluorene-based polyelectrolytes and their neutral precursors. *J. Mater. Chem.* **2005,** *15* (25), 2499-2507.

22. Zhu, C.; Liu, L.; Yang, Q.; Lv, F.; Wang, S., Water-Soluble Conjugated Polymers for Imaging, Diagnosis, and Therapy. *Chem. Rev.* **2012**.

23. Pu, K.-Y.; Cai, L.; Liu, B., Design and Synthesis of Charge-Transfer-Based Conjugated Polyelectrolytes as Multicolor Light-Up Probes. *Macromolecules* **2009,** *42* (16), 5933-5940.

24. Duarte, A.; Pu, K.-Y.; Liu, B.; Bazan, G. C., Recent Advances in Conjugated Polyelectrolytes for Emerging Optoelectronic Applications†. *Chem. Mat.* **2010,** *23* (3), 501-515.

25. Chen, L.; McBranch, D. W.; Wang, H.-L.; Helgeson, R.; Wudl, F.; Whitten, D. G., Highly sensitive biological and chemical sensors based on reversible fluorescence quenching in a conjugated polymer. *Proceedings of the National Academy of Sciences* **1999,** *96* (22), 12287-12292.

26. Feng, X. L.; Liu, L. B.; Wang, S.; Zhu, D. B., Water-soluble fluorescent conjugated polymers and their interactions with biomacromolecules for sensitive biosensors. *Chem. Soc. Rev.* **2010,** *39* (7), 2411-2419.

27. Friend, R. H.; Gymer, R. W.; Holmes, A. B.; Burroughes, J. H.; Marks, R. N.; Taliani, C.; Bradley, D. D. C.; Santos, D. A. D.; Bredas, J. L.; Logdlund, M.; Salaneck, W. R., Electroluminescence in conjugated polymers. *Nature* **1999,** *397* (6715), 121-128.

28. Mwaura, J. K.; Pinto, M. R.; Witker, D.; Ananthakrishnan, N.; Schanze, K. S.; Reynolds, J. R., Photovoltaic Cells Based on Sequentially Adsorbed Multilayers of Conjugated Poly(p-phenylene ethynylene)s and a Water-Soluble Fullerene Derivative†. *Langmuir* **2005,** *21* (22), 10119-10126.

29. Miyaura, N.; Suzuki, A., Palladium-Catalyzed Cross-Coupling Reactions of Organoboron Compounds. *Chem. Rev.* **1995,** *95* (7), 2457-2483.

30. "The Nobel Prize in Chemistry 2010 - Illustrated Information." 19 Jul 2012. <<http://www.nobelprize.org/nobel_prizes/chemistry/laureates/2010/illpres.html>>.

31. Beletskaya, I. P.; Cheprakov, A. V., The Heck Reaction as a Sharpening Stone of Palladium Catalysis. *Chem. Rev.* **2000,** *100* (8), 3009-3066.

32. Amatore, C.; Jutand, A., Anionic Pd(0) and Pd(II) Intermediates in Palladium-Catalyzed Heck and Cross-Coupling Reactions. *Accounts of Chemical Research* **2000,** *33* (5), 314-321.

33. Stille, J. K., The Palladium-Catalyzed Cross-Coupling Reactions of Organotin Reagents with Organic Electrophiles [New Synthetic Methods (58)]. *Angewandte Chemie International Edition in English* **1986,** *25* (6), 508-524.

34. Transition Metal Reactions. <<http://www.ecompound.com/Reaction%20reference/reaction_reference_top.htm>>.

35. Stark, W. J., Nanoparticles in Biological Systems. *Angewandte Chemie International Edition* **2011,** *50* (6), 1242-1258.

36. Howes, P.; Green, M.; Bowers, A.; Parker, D.; Varma, G.; Kallumadil, M.; Hughes, M.; Warley, A.; Brain, A.; Botnar, R., Magnetic Conjugated Polymer Nanoparticles as Bimodal Imaging Agents. *J. Am. Chem. Soc.* **2010,** *132* (28), 9833-9842.

37. Wang, C.; Cheng, L. A.; Liu, Z. A., Drug delivery with upconversion nanoparticles for multi-functional targeted cancer cell imaging and therapy. *Biomaterials* **2011,** *32* (4), 1110-1120.

38. Manju, S.; Sreenivasan, K., Enhanced Drug Loading on Magnetic Nanoparticles by Layer-by-Layer Assembly Using Drug Conjugates: Blood Compatibility Evaluation and Targeted Drug Delivery in Cancer Cells. *Langmuir* **2011,** *27* (23), 14489-14496.

39. Michalet, X.; Pinaud, F. F.; Bentolila, L. A.; Tsay, J. M.; Doose, S.; Li, J. J.; Sundaresan, G.; Wu, A. M.; Gambhir, S. S.; Weiss, S., Quantum dots for live cells, in vivo imaging, and diagnostics. *Science* **2005,** *307* (5709), 538-544.

40. Medintz, I. L.; Clapp, A. R.; Mattoussi, H.; Goldman, E. R.; Fisher, B.; Mauro, J. M., Self-assembled nanoscale biosensors based on quantum dot FRET donors. *Nat. Mater.* **2003,** *2* (9), 630-638.

41. Green, M.; Howes, P.; Berry, C.; Argyros, O.; Thanou, M., Simple conjugated polymer nanoparticles as biological labels. *Proc. R. Soc. A-Math. Phys. Eng. Sci.* **2009,** *465* (2109), 2751-2759.

42. Moon, J. H.; McDaniel, W.; MacLean, P.; Hancock, L. E., Live-cell-permeable poly (p-phenylene ethynylene). *Angew. Chem.-Int. Edit.* **2007,** *46* (43), 8223-8225.

43. Moon, J. H.; McDaniel, W.; Hancock, L. F., PMSE 17-Conjugated polymer nanoparticles for live cell imaging. *Abstr. Pap. Am. Chem. Soc.* **2008,** *235*.

44. Wu, C.; Bull, B.; Szymanski, C.; Christensen, K.; McNeill, J., Multicolor Conjugated Polymer Dots for Biological Fluorescence Imaging. *ACS Nano* **2008,** *2* (11), 2415-2423.

45. Feng, X. L.; Yang, G. M.; Liu, L. B.; Lv, F. T.; Yang, Q.; Wang, S.; Zhu, D. B., A Convenient Preparation of Multi-Spectral Microparticles by Bacteria-Mediated Assemblies of Conjugated Polymer Nanoparticles for Cell Imaging and Barcoding. *Adv. Mater.* **2012,** *24* (5), 637-+.

46. Fernando, L. P.; Kandel, P. K.; Yu, J. B.; McNeill, J.; Ackroyd, P. C.; Christensen, K. A., Mechanism of Cellular Uptake of Highly Fluorescent Conjugated Polymer Nanoparticles. *Biomacromolecules* **2010,** *11* (10), 2675-2682.

47. Pu, K. Y.; Liu, B., Fluorescent Conjugated Polyelectrolytes for Bioimaging. *Adv. Funct. Mater.* **2011,** *21* (18), 3408-3423.

48. Wu, C. F.; Szymanski, C.; Cain, Z.; McNeill, J., Conjugated polymer dots for multiphoton fluorescence imaging. *J. Am. Chem. Soc.* **2007,** *129* (43), 12904-+.

49. Wu, C.; Szymanski, C.; McNeill, J., Preparation and Encapsulation of Highly Fluorescent Conjugated Polymer Nanoparticles. *Langmuir* **2006,** *22* (7), 2956-2960.

50. Ozel, I. O.; Ozel, T.; Demir, H. V.; Tuncel, D., Non-radiative resonance energy transfer in bi-polymer nanoparticles of fluorescent conjugated polymers. *Opt Express* **2010,** *18* (2), 670-684.

51. Park, E. J.; Erdem, T.; Ibrahimova, V.; Nizamoglu, S.; Demir, H. V.; Tuncel, D., White-Emitting Conjugated Polymer Nanoparticles with Cross-Linked Shell for Mechanical Stability and Controllable Photometric Properties in Color-Conversion LED Applications. *ACS Nano* **2011,** *5* (4), 2483-2492.

52. Ibrahimova, V.; Ekiz, S.; Gezici, O.; Tuncel, D., Facile synthesis of cross-linked patchy fluorescent conjugated polymer nanoparticles by click reactions. *Polym. Chem.* **2011,** *2* (12), 2818-2824.

53. Kietzke, T.; Neher, D.; Landfester, K.; Montenegro, R.; Guntner, R.; Scherf, U., Novel approaches to polymer blends based on polymer nanoparticles. *Nat Mater* **2003,** *2* (6), 408-412.

54. Kietzke, T.; Neher, D.; Kumke, M.; Montenegro, R.; Landfester, K.; Scherf, U., A Nanoparticle Approach To Control the Phase Separation in Polyfluorene Photovoltaic Devices. *Macromolecules* **2004,** *37* (13), 4882-4890.

55. Fisslthaler, E.; Blumel, A.; Landfester, K.; Scherf, U.; List, E. J. W., Printing functional nanostructures: a novel route towards nanostructuring of organic electronic devices via soft embossing, inkjet printing and colloidal self assembly of semiconducting polymer nanospheres. *Soft Matter* **2008,** *4* (12), 2448-2453.

56. Rahim, N. A. A.; McDaniel, W.; Bardon, K.; Srinivasan, S.; Vickerman, V.; So, P. T. C.; Moon, J. H., Conjugated Polymer Nanoparticles for Two-Photon Imaging of Endothelial Cells in a Tissue Model. *Adv. Mater.* **2009,** *21* (34), 3492-+.

57. Howes, P.; Green, M.; Levitt, J.; Suhling, K.; Hughes, M., Phospholipid Encapsulated Semiconducting Polymer Nanoparticles: Their Use in Cell Imaging and Protein Attachment. *J. Am. Chem. Soc.* **2010,** *132* (11), 3989-3996.

58. Wu, C.; Bull, B.; Christensen, K.; McNeill, J., Ratiometric Single-Nanoparticle Oxygen Sensors for Biological Imaging. *Angewandte Chemie International Edition* **2009,** *48* (15), 2741-2745.

59. Moon, J. H.; MacLean, P.; McDaniel, W.; Hancock, L. F., Conjugated polymer nanoparticles for biochemical protein kinase assay. *Chem. Commun.* **2007,** (46), 4910-4912.

60. Li, K.; Ding, D.; Huo, D.; Pu, K.-Y.; Thao, N. N. P.; Hu, Y.; Li, Z.; Liu, B., Conjugated Polymer Based Nanoparticles as Dual-Modal Probes for Targeted In Vivo Fluorescence and Magnetic Resonance Imaging. *Adv. Funct. Mater.* **2012**, n/a-n/a.

61. Li, K.; Liu, B., Polymer encapsulated conjugated polymer nanoparticles for fluorescence bioimaging. *J. Mater. Chem.* **2012,** *22* (4), 1257-1264.

62. Tuncel, D.; Demir, H. V., Conjugated polymer nanoparticles. *Nanoscale* **2010,** *2* (4), 484-494.

63. Pecher, J.; Mecking, S., Nanoparticles of Conjugated Polymers. *Chem. Rev.* **2010,** *110* (10), 6260-6279.

64. Ho Moon, J.; Deans, R.; Krueger, E.; Hancock, L. F., Capture and detection of a quencher labeled oligonucleotide by poly(phenylene ethynylene) particles. *Chem. Commun.* **2003,** (1), 104-105.

65. Landfester, K.; Montenegro, R.; Scherf, U.; Güntner, R.; Asawapirom, U.; Patil, S.; Neher, D.; Kietzke, T., Semiconducting Polymer Nanospheres in Aqueous Dispersion Prepared by a Miniemulsion Process. *Adv. Mater.* **2002,** *14* (9), 651-655.

66. Baier, M. C.; Huber, J.; Mecking, S., Fluorescent Conjugated Polymer Nanoparticles by Polymerization in Miniemulsion. *J. Am. Chem. Soc.* **2009,** *131* (40), 14267-14273.

67. Chen, K. J.; Tang, L.; Garcia, M. A.; Wang, H.; Lu, H.; Lin, W. Y.; Hou, S.; Yin, Q.; Shen, C. K. F.; Cheng, J. J.; Tseng, H. R., The therapeutic efficacy of camptothecin-encapsulated supramolecular nanoparticles. *Biomaterials* **2012,** *33* (4), 1162-1169.

68. Guo, Y.; Shi, D. L.; Cho, H. S.; Dong, Z. Y.; Kulkarni, A.; Pauletti, G. M.; Wang, W.; Lian, J.; Liu, W.; Ren, L.; Zhang, Q. Q.; Liu, G. K.; Huth, C.; Wang, L. M.; Ewing, R. C., In vivo imaging and drug storage by quantum-dot-conjugated carbon nanotubes. *Adv. Funct. Mater.* **2008,** *18* (17), 2489-2497.

69. Ferrari, M., Cancer nanotechnology: opportunities and challenges. *Nat Rev Cancer* **2005,** *5* (3), 161-171.

70. Allen, T. M.; Cullis, P. R., Drug Delivery Systems: Entering the Mainstream. *Science* **2004,** *303* (5665), 1818-1822.

71. Barreto, J. A.; O'Malley, W.; Kubeil, M.; Graham, B.; Stephan, H.; Spiccia, L., Nanomaterials: Applications in Cancer Imaging and Therapy. *Adv. Mater.* **2011,** *23* (12), H18-H40.

72. Liu, Y.; Miyoshi, H.; Nakamura, M., Nanomedicine for drug delivery and imaging: A promising avenue for cancer therapy and diagnosis using targeted functional nanoparticles. *International Journal of Cancer* **2007,** *120* (12), 2527-2537.

73. Cho, H. S.; Dong, Z. Y.; Pauletti, G. M.; Zhang, J. M.; Xu, H.; Gu, H. C.; Wang, L. M.; Ewing, R. C.; Huth, C.; Wang, F.; Shi, D. L., Fluorescent, Superparamagnetic Nanospheres for Drug Storage, Targeting, and Imaging: A Multifunctional Nanocarrier System for Cancer Diagnosis and Treatment. *ACS Nano* **2010,** *4* (9), 5398-5404.

74. Way, T. D.; Chang, C. J.; Lin, C. W., Bioconjugated Fluorescent Polymeric Nanoparticles for Imaging and Targeted Therapy of HER2-Overexpressing Cancer Cells. *J. Fluoresc.* **2011,** *21* (4), 1669-1676.

75. Aryal, S.; Hu, C. M. J.; Zhang, L. F., Polymeric Nanoparticles with Precise Ratiometric Control over Drug Loading for Combination Therapy. *Mol. Pharm.* **2011,** *8* (4), 1401-1407.

76. Traina, C. A.; Bakus, R. C.; Bazan, G. C., Design and Synthesis of Monofunctionalized, Water-Soluble Conjugated Polymers for Biosensing and Imaging Applications. *J. Am. Chem. Soc.* **2011,** *133* (32), 12600-12607.

77. Haag, R.; Kratz, F., Polymer therapeutics: Concepts and applications. *Angew. Chem.-Int. Edit.* **2006,** *45* (8), 1198-1215.

78. Feng, X. L.; Lv, F. T.; Liu, L. B.; Tang, H. W.; Xing, C. F.; Yang, Q. O.; Wang, S., Conjugated Polymer Nanoparticles for Drug Delivery and Imaging. *ACS Appl. Mater. Interfaces* **2010,** *2* (8), 2429-2435.

79. Choi, K. Y.; Liu, G.; Lee, S.; Chen, X., Theranostic nanoplatforms for simultaneous cancer imaging and therapy: current approaches and future perspectives. *Nanoscale* **2012,** *4* (2), 330-342.

80. Xie, J.; Lee, S.; Chen, X., Nanoparticle-based theranostic agents. *Adv. Drug Deliv. Rev.* **2010,** *62* (11), 1064-1079.

81. Mailänder, V.; Landfester, K., Interaction of Nanoparticles with Cells. *Biomacromolecules* **2009,** *10* (9), 2379-2400.

82. Chou, L. Y. T.; Ming, K.; Chan, W. C. W., Strategies for the intracellular delivery of nanoparticles. *Chem. Soc. Rev.* **2011,** *40* (1), 233-245.

83. Botella, P.; Abasolo, I.; Fernández, Y.; Muniesa, C.; Miranda, S.; Quesada, M.; Ruiz, J.; Schwartz Jr, S.; Corma, A., Surface-modified silica nanoparticles for tumor-targeted delivery of camptothecin and its biological evaluation. *Journal of Controlled Release* **2011,** *156* (2), 246-257.

84. Loh, X. J.; del Barrio, J.; Toh, P. P. C.; Lee, T.-C.; Jiao, D.; Rauwald, U.; Appel, E. A.; Scherman, O. A., Triply Triggered Doxorubicin Release From Supramolecular Nanocontainers. *Biomacromolecules* **2011,** *13* (1), 84-91.

85. Esser-Kahn, A. P.; Odom, S. A.; Sottos, N. R.; White, S. R.; Moore, J. S., Triggered Release from Polymer Capsules. *Macromolecules* **2011,** *44* (14), 5539-5553.

86. Pizzolato, J. F.; Saltz, L. B., The camptothecins. *The Lancet* **2003,** *361* (9376), 2235-2242.

87. Minko, T.; Paranjpe, P. V.; Qiu, B.; Lalloo, A.; Won, R.; Stein, S.; Sinko, P. J., Enhancing the anticancer efficacy of camptothecin using biotinylated

poly(ethyleneglycol) conjugates in sensitive and multidrug-resistant human ovarian carcinoma cells. *Cancer Chemotherapy and Pharmacology* **2002,** *50* (2), 143-150.

88. Conover, C. D.; Greenwald, R. B.; Pendri, A.; Gilbert, C. W.; Shum, K. L., Camptothecin delivery systems: enhanced efficacy and tumor accumulation of camptothecin following its conjugation to polyethylene glycol via a glycine linker. *Cancer Chemotherapy and Pharmacology* **1998,** *42* (5), 407-414.

89. Liu, Y. Q.; Dai, W.; Yang, L.; Li, H. Y., Design and synthesis of novel camptothecin/5-fluorouracil conjugates as cytotoxic agents. *Nat. Prod. Res.* **2011,** *25* (19), 1817-1826.

90. Feng, X. S.; Pinaud, J.; Chaikof, E. L.; Taton, D.; Gnanou, Y., Sequential Functionalization of Janus-Type Dendrimer-Like Poly(ethylene oxide)s with Camptothecin and Folic Acid. *J Polym Sci Pol Chem* **2011,** *49* (13), 2839-2849.

91. Morgan, M. T.; Nakanishi, Y.; Kroll, D. J.; Griset, A. P.; Carnahan, M. A.; Wathier, M.; Oberlies, N. H.; Manikumar, G.; Wani, M. C.; Grinstaff, M. W., Dendrimer-encapsulated camptothecins: increased solubility, cellular uptake, and cellular retention affords enhanced anticancer activity in vitro. *Cancer Res* **2006,** *66* (24), 11913-11921.

92. Schneider, T.; Zhao, H.; Jackson, J. K.; Chapman, G. H.; Dykes, J.; Hafeli, U. O., Use of Hydrodynamic Flow Focusing for the Generation of Biodegradable Camptothecin-Loaded Polymer Microspheres. *J. Pharm. Sci.* **2008,** *97* (11), 4943-4954.

93. Wang, X. Y.; Gurski, L. A.; Zhong, S.; Xu, X. A.; Pochan, D. J.; Farach-Carson, M. C.; Jia, X. Q., Amphiphilic Block Co-polyesters Bearing Pendant Cyclic Ketal Groups as Nanocarriers for Controlled Release of Camptothecin. *J. Biomater. Sci.-Polym. Ed.* **2011,** *22* (10), 1275-1298.

94. Weyermann, J.; Lochmann, D.; Zimmer, A., A practical note on the use of cytotoxicity assays. *International Journal of Pharmaceutics* **2005,** *288* (2), 369-376.

95. Keepers YP, P. P., Peters GJ, van Ark-Otte J, Winograd B, Pinedo HM, Comparison of the sulforhodamine B protein and tetrazolium (MTT) assays for in vitro chemosensitivity testing. *Eur J Cancer.* **1991,** *27(7)*, 897-900.

96. BioAntaresLLC, “Complete range of Fast, Efficient and Flexible Cytotoxicity assays” <<http://www.bioantares.com/uploads/Cyto_test.jpg>>.

97. Skehan, P.; Storeng, R.; Scudiero, D.; Monks, A.; McMahon, J.; Vistica, D.; Warren, J. T.; Bokesch, H.; Kenney, S.; Boyd, M. R., New Colorimetric Cytotoxicity Assay for Anticancer-Drug Screening. *Journal of the National Cancer Institute* **1990,** *82* (13), 1107-1112.

98. Voigt, W., Sulforhodamine B Assay and Chemosensitivity. 2005; Vol. 110, pp 39-48.

99. Vichai, V.; Kirtikara, K., Sulforhodamine B colorimetric assay for cytotoxicity screening. *Nat. Protocols* **2006,** *1* (3), 1112-1116.

100. Papazisis, K. T.; Geromichalos, G. D.; Dimitriadis, K. A.; Kortsaris, A. H., Optimization of the sulforhodamine B colorimetric assay. *Journal of Immunological Methods* **1997,** *208* (2), 151-158.

101. Caldwell GW, Y. Z., Lang W, Masucci JA., The IC50 Concept Revisited. *Curr Top Med Chem.* **2012,** *12(11)*, 1282-90.

102. Aryal, S.; Hu, C. M. J.; Zhang, L. F., Combinatorial Drug Conjugation Enables Nanoparticle Dual-Drug Delivery. *Small* **2010,** *6* (13), 1442-1448.

103. Ibrahimova, V., Synthesis and Characterization of Water Dispersible Conjugated Polymer Nanoparticles. *THESIS, MASTER OF SCIENCE* **2011**.

104. Marini, A.; Muñoz-Losa, A.; Biancardi, A.; Mennucci, B., What is Solvatochromism? *The Journal of Physical Chemistry B* **2010,** *114* (51), 17128-17135.

105. Davis, M. E.; Chen, Z.; Shin, D. M., Nanoparticle therapeutics: an emerging treatment modality for cancer. *Nat Rev Drug Discov* **2008,** *7* (9), 771-782.